**UNIVERSITE SAAD DAHLAB DE BLIDA 1**

**Faculté de Technologie**

**Département de Mécanique**

**THESE DE DOCTORAT (LMD)**

En Génie Mécanique

Spécialité : Construction Mécanique

# Contrôle actif des vibrations des plaques nano composites multicouches en utilisant des éléments piézoélectriques.

Par

**Mohamed Essedik LAZAR**

Devant le jury composé de :

| | | |
|---|---|---|
| M. TEMMAR | Pr, Univ. Blida1 | Président |
| M. BENTCHIKOU | Pr, Univ. Yahia Fares Médéa | Examinateur |
| N. AMOURA | MCA, ENP Alger | Examinateur |
| F. MADANI | MCA, Univ Blida 1 | Examinateur |
| R. TIBERKAK | Pr, Univ. Blida1 | Directeur de Thèse |
| M. EZZRAIMI | MCA, Univ. Blida1 | Co-directeur de Thèse |

Blida, 2025

## ملخص

في هذا العمل، يتم دراسة التحكم النشط بالاهتزاز للوحات المركبة البوليمرية المقوية بأنابيب نانوية من الكربون (CNTs) أو صفائح الجرافين (GPLs) ذات التدرج الوظيفي متعددة الطبقات والمغطاة بطبقات من المواد الكهرضغطية. تم تقوية اللوحات المركبة بتوزيع موحد (UD) للحشو النانوي في جميع طبقاتها، أو بتوزيع خطي أو غير خطي في اتجاه السماكة باستخدام قوانين القوى والأسس الأسية كأنواع التدرج الوظيفي X وO وA (FG-X، FG-O، وFG-A). نظرية اللوحة المستخدمة في هذا العمل هي نظرية التشوه القص الأولي (FSDT). وبالتالي، يُفترض أن الخصائص الميكانيكية للحشو النانوي تختلف عبر السماكة ويتم تقييمها باستخدام قاعدة خلط معدلة. تستخدم هذه الدراسة طريقة العناصر المحددة لدراسة سلوك لوحة مربعة تحت ظروف الحمل الثابتة والديناميكية. يتم تقسيم اللوحة المدروسة إلى عناصر تربيعية عقدية من تسع عقد، حيث تمتلك كل عقدة خمس درجات حرية. يتم حل المعادلات الديناميكية بواسطة طريقة تكامل نيومارك. تم تنفيذ برنامج مطور في برنامج Matlab للحصول على الحلول العددية والرسوم البيانية. في هذه الدراسة، ثبت أن استخدام الطبقات الكهرضغطية والدالة الأسيّة يؤدي إلى تخفيف الاهتزازات النشطة في الصفائح المركبة متعددة الطبقات والمكونة من البوليمر و المقواة بأنابيب الكربون النانوية (CNTs) أو صفائح الجرافين (GPLs).



الكلمات المفتاحية: طريقة العناصر المحدودة، أنابيب الكربون النانوية، صفيحات الجرافين النانوية، طريقة نيومارك بيتا، التحكم النشط في الاهتزاز، نظرية تشوه القص من الدرجة الأولى.



## ABSTRACT

This work investigates active vibration control of multilayer functionally graded carbon nanotubes (CNTs) or graphene platelets (GPLs) reinforced polymer composite plates, covered with piezoelectric layers. The composite plates is composed of multilayers, and reinforced with uniform distribution (UD) of nanofillers, and linearly or non-linearly distribution through the thickness direction using power and exponential laws, these are Functionally Graded types: X, O, and A (FG-X, FG-O, and FG-A). The plate theory used in this work was the first-order shear deformation theory (FSDT). Thus, the mechanical properties of the nanofillers are supposed to vary through the thickness and are evaluated using a modified rule of mixture. This study utilizes the finite element method to investigate the behavior of a square plate under both static and dynamic loading conditions. The studied plate is discretized into nine-node quadratic elements, with five degrees of freedom in each node. The dynamic equations are solved using the Newmark integration method. A developed code has been implemented in Matlab software to get the numerical and graphical solutions for the present work. In this study, it was proven that the use of piezoelectric layers

and exponential function leads to active vibration attenuation of polymer multilayer composite plates reinforced with functionally graded carbon nanotubes (CNTs) or graphene platelets (GPLs).

Keywords: Finite element method, Carbon Nanotubes, Graphene Nanoplatelets, Newmark $\beta$-method, Active vibration control, First order shear deformation theory.

## RESUME

Ce travail présente une étude de contrôle actif des vibrations de plaques composites multicouches en polymère renforcées par des nanotubes de carbone (CNTs) ou des plaquettes de graphène (GPLs) à gradient fonctionnel recouvertes de couches piézoélectriques. Les plaques composites sont composées de plusieurs couches, renforcées avec une distribution uniforme (UD) de nanomatériaux, ou avec des distributions linéaires ou non linéaires à gradient fonctionnel de type X, O et A (FG-X, FG-O et FG-A) à travers l'épaisseur par utilisation de lois de puissance et exponentielles. La théorie des plaques utilisée dans ce travail est la théorie de la déformation de cisaillement du premier ordre (FSDT). Ainsi, on suppose que les propriétés mécaniques des nanomatériaux varient à travers l'épaisseur, et sont évaluées à l'aide d'une règle de mélange modifiée. Cette étude utilise la méthode des éléments finis pour étudier le comportement d'une plaque carrée soumise à des charges statiques et dynamiques. La plaque étudiée est discrétisée en éléments quadratiques à neuf nœuds, chaque nœud possédant cinq degrés de liberté. Les équations non linéaires de la dynamique sont résolues par la méthode d'intégration de Newmark. Un code de calcul a été développé en Matlab pour obtenir les solutions numériques et graphiques du présent travail. Dans cette étude, il a été prouvé que l'utilisation des couches piézoélectriques et la fonction exponentielle conduit à une atténuation des vibrations active des plaques composites multicouches en polymère renforcées par des nanotubes de carbone (CNTs) ou des plaquettes de graphène (GPLs).

Mots clés : Méthode des éléments finis, Nanotubes de carbone, Nano-plaquettes de graphène, Méthode β de Newmark, Contrôle actif des vibrations, Théorie de la déformation par cisaillement du premier ordre.

# ACKNOWLEDGMENTs

First of all, I would like to thank **Allah** Almighty.

I express my sincere gratitude to the members of the jury for their interest in this work and for agreeing to examine it.

I want to thank mister president Pr. **Mustapha Temmar** and all the members of the arbitration committee, such as Pr. **Mohamed Bentchikou**, **Dr Nasereddine Amoura**, and Dr. **Fateh Madani** for their acceptance to arbitrate our work.

I would like to thank my thesis supervisors, Pr. **Rachid Tiberkak** and Dr. **Madjid Ezzraimi**, for their support throughout the entire period of this thesis.

On the other hand, I express my gratitude to the great Pr. **Tahar Chettibi** and my colleagues Dr. **Yasser Chiker** and Dr. **Billel Lounici** for their support and help throughout my doctoral career.

I would like to thank Mr. **Said Rechak** in particular for his help and for taking the time to correct and contribute to this work.

I would also like to express my sincere gratitude to all my undergraduate professors, and to all the staff of the Department of Mechanical Engineering. I would like to extend my warmest thanks to all my colleagues and friends.

I would like to thank everyone who has helped and supported me, whether directly or indirectly.

Thank you all very much.

# CONTENTs

# LIST OF FIGURES

# LIST OF TABLES

# LIST OF SYMBOLS

$E_C$: Young's modulus of ceramic material.

$E_m$: Young's modulus of metal material.

$z$: position of the $k^{th}$ layers relative to the average plane.

$h$: thickness of the plate.

$P_{in}$: power law index.

$\rho_C$: density of ceramic.

$\rho_m$: density of metal.

$f_r^{(k)}$ : volume fraction of reinforcement of the $k^{th}$ layers.

$f_m^{(k)}$ : volume fraction of matrix of the $k^{th}$ layers.

$N_{L:}$ total number of layers.

$w_i$: weight fraction of Nano fillers.

$E_{11:}$ longitudinal Young's modulus of carbon nanotube material.

$E_{22}$: transverse Young's modulus of carbon nanotube material.

$G_{12}^{CNT}$, $G_m$: are shear modulus of carbon Nano tube and matrix.

$v_{12}^{CNT}$, $v_m$: are poisson's ratio of carbon Nano tube and matrix.

$\xi_L$, $\xi_w$ : are the length by thickness fraction and width by thickness fraction.

$E_{GPL:}$ Young's modulus of graphene platelets.

$E_{eff}$: is the effective Young's modulus of the $k^{th}$ layers of the graphene platelets reinforced composite plate.

*U:* displacement of the plate in the X direction.

*V:* displacement of the plate in the Y direction.

*W:* Bending of the plate in the Z direction.

$\theta_{x,y}$ : rotation around the x and axes respectively.

$X$: global displacement.

[$L$]: operator for the localized translation and rotation variables.

[D]: membrane or bending or membrane-bending or shear Differential operator.

$Q_{ij}^{(k)}$ : are the elastics constants.

$\{\sigma\}$ : stress vector.

$\{\varepsilon\}$ : strain vector.

[$A$]: matrix of elastic constants due to the membrane effect.

[$B$]: matrix of elastic constants due to the bending effect.

[$D$]: matrix of elastic constants due to the membrane-bending effect.

[$F$]: matrix of elastic constants due to the shear effect.

$E_k$: kinetic energy.

$E_s$: strain energy.

$W$: work done by the external forces.

$h_c$: thickness of the composite layer.

$h_p$: thickness of the piezoelectric layer.

$\phi$ : is the electrical voltage.

$\{E\}$: electrical field vector.

$\{D\}$: electrical displacement vector.

[e] : piezoelectric constant matrix.

[d] : electrical permittivity constant matrix.

$a$: length of the plate.

$b$: width of the plate.

[$M$] : mass matrix.

$G_9$ : interpolation polynom.

$A_9$ : interpolation matrix.

$N_i$: interpolation functions vector.

$N_u$: nodal approximation for displacement.

$N_\phi$: nodal approximation for electrical potential.

[$J$]: Jacobin matrix.

$\rho_p$: density of piezoelectric layer.

$\rho_c$: density of composite layer.

$[K_{uu}]$: elastic stiffness matrix.

$[K_{u\phi}]$, $[K_{\phi u}]$: piezoelectric stiffness matrix.

$[K_{\phi\phi}]$: dielectric stiffness matrix.

$\{F_{mec}\}$: mechanical force.

$\{Q_{elec}\}$: electrical charge.

$\phi_a$: electrical potential given to the actuator.

$\phi_s$: electrical potential read from sensor.

$[C_{ad}]$: active damping matrix.

$[C_{sd}]$: structural damping matrix.

$\alpha_R$, $\beta_R$ : Rayleigh damping coefficient.

$\gamma_n$, $\beta_n$ : Newmark algorithm stability and accuracy parameters.

$G_v$: derivative control gain.

$G_d$: proportional control gain.

$x_0$: initial displacement.

$v_0$: initial speed.

$a_0$: initial acceleration.

$t_{n+1}$: previous time.

$t_n$: present time.

$\Delta t$ : period between $t_n$ and $t_{n+1}$.

$P$: predicted value.

# LIST OF ABREVIATIONS

CNT, CNTs: Carbon NanoTube, Carbon Nanotubes.

GPL, GPLs: graphene platelet, graphene platelets.

CNTRC: carbon nanotubes reinforced composite plate.

GPLRC: graphene platelets reinforced composite plate.

$( )^{T}$: transpose of vector or matrix.

inv: inverse of matrix.

UD: uniform distribution.

FG-X: X functionally graded configuration.

FG-O: O functionally graded configuration.

FG-A: A functionally graded configuration.

FG-V: V functionally graded configuration.

SWCNTs: single-walled carbon nanotubes.

DWCNTs: double-walled carbon nanotubes.

MWCNTs: multi-walled carbon nanotubes.

FG-CNTRC: functionally graded carbon nanotubes reinforced composite plate.

FG-GPLRC: functionally graded graphene platelets reinforced composite plate.

CLPT: classical laminated plate theory.

FSDT: first order shear deformation theory.

HSDT: high order shear deformation theory.

SSSS: simply supported plate on their four edges.

CCCC: clamped plate on their four edges.

CFFF: clamped plate on one edge and free on the other edges.

PZT: titano-zirconates of Plomb (lead).

# Introduction

Vibrations are a common occurrence in various engineering applications. Managing these vibrations is effectively crucial for the performance, the durability and the safety of different structures and different systems. These vibrations are an oscillatory movement with high amplitudes, which lead to structural fatigue, decreased operational efficiency, and even discomfort for users. Vibration control is employed in various industries and applications such as aerospace, automotive, civil engineering, manufacturing, and many others. Using vibration control can improve structural integrity, enhanced operational performance and can increase comfort for users. For example, it can be used to reduce vibrations in aircraft in order to enhance passenger comfort and protect sensitive equipment. In manufacturing, it helps maintain the precision of machining processes by minimizing machine tool vibrations. Actually, we have two kinds of controlling the vibrations: passive and active control. For example, We can use Rubber mounts, springs, or elastomeric dampers strategically between the vibrating source and its surroundings to absorb and dissipate a substantial amount of vibration energy. In another way, a strategically suspended mass placed on a spring system is tuned to resonate at the same frequency as the unwanted vibration in the structure. More than those cited, the creation of friction between surfaces in contact with a vibrational system could be used to dissipate vibrational energy. It is a simple control compared to active vibration control, which is a proactive and dynamic approach to managing vibrations, where technology actively responds to vibration data to ensure the safety, reliability, and performance of structures and systems. This kind of control uses a piezoelectric transducer. Piezoelectric materials exhibit a unique property that can generate an electrical charge in response to mechanical deformation and can be deformed when it is subjected to an electric field. This exceptional characteristic makes piezoelectric materials invaluable in the field of vibration control.

The sensors are responsible for detecting vibrations or oscillations in the structure or system. They can be accelerometers, strain gauges, piezoelectric sensors, or other types of sensors depending on the application. The control algorithms process is down from the sensors. Then the controller analyzes the vibration data and determines the necessary corrective actions to reduce or eliminate the vibrations. The algorithms are designed to be adaptive which means they can adjust their responses in real time based on changing vibration conditions. Actuators generate forces or motions in response to control signals

from the algorithms. In active vibration control, these actuators are strategically placed within the structure or system to apply forces or motions that counteract the undesired vibrations.

# CHAPTER 1: STATE OF THE ART

Smart composite plates refer to composite materials that incorporate advanced technologies and materials to enhance their properties and functionality. These plates are typically made by the combination of different materials, such as fibers (carbon, glass, or aramid) and a matrix (epoxy resin), to create a composite material that exhibits superior mechanical, thermal, and sometimes even electrical properties compared to traditional materials like metals or plastics. The term "smart" in this context implies that these composite plates have additional functionalities beyond their structural capabilities. Smart materials find applications in a wide range of fields and industries due to their unique properties and ability to respond to external stimuli. Some key areas where smart materials are used include aerospace, automotive, civil engineering and infrastructure, electronics, medical devices, energy, consumer electronics, defense and military, and robotics. Today carbon nanotubes (CNTs) and graphene platelets (GPLs) are some of the best smart materials used in the majority of industries due to their high performance. A Japanese physicist “Sumio Iijima” is credited with the discovery first studied carbon nanotubes in a research paper in 1991 [1]. He published a groundbreaking paper in the journal Nature in November 1991, describing the synthesis and characterization of carbon nanotubes. His work opened up a new field of nanotechnology and nanomaterial science, and carbon nanotubes have since been the subject of extensive research and have found numerous applications in various fields due to their unique properties (mechanical, electrical, and thermal) and structure (single, double or multi-walled). Due to these remarkable material properties, the mechanical analysis of CNT-reinforced composite (CNTRC) materials and structures has attracted a lot of researcher’s attention. For example, In 2009, Hui-Shen was the first researcher who investigate the CNT-based functionally graded material (FGM) polymer composite [2]. He illustrated the nonlinear distribution of nanotubes from the Power-law functionally graded material concept (P-FGM). In addition, he studied the nonlinear bending of simply supported, functionally graded Nano-composite plates reinforced by single-walled carbon nanotubes (SWCNTs) subjected to a transverse uniform or sinusoidal load in thermal environments. Their results show that the load-bending torque curves of the plate can be significantly increased because of a functionally graded reinforcement. They also confirm that the characteristics of nonlinear bending are significantly influenced by temperature rise, the character of in-plane boundary conditions, the transverse shear deformation, the plate

aspect ratio as well as the nanotube volume fraction. Kim and all fabricated and characterized Carbon fiber-reinforced epoxy composites modified with carbon nanotubes (CNTs) [3]. They used High-energy sonication to disperse CNTs in the resin, followed by an infiltration of fiber preform with the resin/CNT mixture, they showed a tendency to overestimate the properties and therefore may be utilized by the composite designers as a tool to obtain the upper bound. In order to strengthen the interface of a composite scarf joint. Faulkner and all investigated the benefits of using locally applied carbon nanotubes to reinforce a carbon fiber composite scarf joint [4]. Also, the effects of the waviness of the CNTs and the interfacial deboning between them and the matrix on the effective moduli of CNT-reinforced composites were studied by Shao and all [5]. After a modification was done on composites, which released the addition of multi-walled carbon nanotubes into the matrix material, the fracture energy of hybrid carbon fiber reinforced polymers was investigated by Karapappas and all [6]. The reinforcing effects of carbon nanotubes (CNTs) for aluminum matrix composites are investigated by Choi and all to achieve strong bonding between CNTs and the aluminum matrix using a controlled mechanical milling process in the composites [7]. In 2010, Formica and all studied the vibrational properties of carbon nanotube-reinforced composites by employing an equivalent continuum model based on the Eshelby–Mori–Tanaka approach [8]. Similarly, Ke and all investigate the nonlinear free vibration of functionally graded Nano-composite beams reinforced by single-walled carbon nanotubes (SWCNTs) based on Timoshenko beam theory and von Kármán geometric nonlinearity [8]. The material properties of functionally graded carbon nanotube-reinforced composites (FG-CNTRCs) are assumed to be graded in the thickness direction and estimated through the rule of mixture. Shen and all came back and presented the thermal buckling and post-buckling behavior for functionally graded Nano-composite plates reinforced by single-walled carbon nanotubes (SWCNTs) subjected to in-plane temperature variation [8].

Another study about the effective dispersion of different-length multiwall carbon nanotubes (MWCNTs) in water was achieved by applying ultrasonic energy and in combination with the use of a surfactant, the effects of ultrasonic energy and surfactant concentration on the dispersion of MWCNTs at an amount of 0.08 wt.% of cement were investigated by Konsta-Gdoutos and all [9]. Nano-composite reinforced with carbon nanotubes (CNTs/AZ91D) and magnesium matrix using mechanical stirring and Liu and all fabricated high-intensity ultrasonic dispersion processing. Their tensile fracture analysis shows that the damage mechanism of Nano-composite is still brittle fracture. However, the CNTs can prevent the local crack propagation to some extent [10]. Furthermore, Kwon and

all [11]fabricated a functionally graded CNT in-forced aluminum matrix composite by a powder metallurgy route [10]. The use of CNTs as an epoxy adhesive additive for adhesive joints between steel-composite interfaces and composite interfaces is explored. The effect of CNT functionalization to enhance CNT dispersion and, consequently, joint strength was also investigated by Burkholder and all [12]. Ayatollahi and all presented a Multi-scale modeling for the nonlinear properties of polymer/single wall carbon nanotube (SWNT) Nano-composite under tensile, bending, and torsional loading conditions [13]. A novel and simple approach was developed by Yang for overcoming the limits of traditional mixing methods and to obtain homogeneously dispersed carbon nanotube (CNT) reinforcement with good structure in Al powder. [14]. Thereafter, Khan and all studied Vibration damping characteristics of Nano-composites and carbon fiber-reinforced polymer composites (CFRPs) containing multiwall carbon nanotubes (CNTs) using the free and forced vibration tests. [14]. De Greef produced a composite using resin transfer molding and containing 0.25% weight of CNTs in the matrix to investigate the effect of carbon nanotubes (CNTs) on the initiation and development of damage in a woven carbon fiber/epoxy composite under quasi-static tensile loading. [14]. Yas and all assumed an aligned and straight with uniform layout SWCNTs to study the free vibrations and buckling analysis of Nano-composite Timoshenko beams reinforced by single-walled carbon nanotubes (SWCNTs) resting on an elastic foundation. [14]. Similarly, four types of distributions of the uniaxial aligned reinforcement material are considered. That are uniform and three kinds of functionally graded distributions of carbon nanotubes along the thickness direction of plates, which are proposed by Zhu and all to study the bending, and free vibration analyses of thin-to-moderately thick composite plates reinforced by single-walled carbon nanotubes using the finite element method based on the first order shear deformation plate theory. [14]. Thereafter, Sobhani Aragh and all assumed that the volume fractions of oriented, straight single-walled carbon nanotubes (SWCNTs) to be graded in the thickness direction to study the natural frequencies characteristics of a continuously graded carbon nanotube-reinforced (CGCNTR) cylindrical panels based on the Eshelby–Mori–Tanaka approach. [14]. Shen came back to the interface and presented the thermal post-buckling analysis for Nano-composite cylindrical shells reinforced by single-walled carbon nanotubes (SWCNTs) subjected to a uniform temperature rise. [14]. He assumed the SWCNTs to be aligned and straight by two kinds of carbon nanotube-reinforced composite (CNTRC) shells, namely, uniformly distributed (UD) and functionally graded (FG) reinforcements, with a uniform layout. Using a multi-scale simulation, Sevvas and all investigate in their study the effect of

interfacial shear strength (ISS) on the mechanical and damping properties of carbon nanotube-reinforced composites (CNT-RCs) [15]. The mechanical buckling of a functionally graded Nano-composite rectangular plate is reinforced by aligned and straight single-walled carbon nanotubes (SWCNTs) subjected to uniaxial and biaxial in-plane loadings. It is investigated by Jafari Mehrabadi and all [16]. They assumed the material properties of the Nano-composite plate to be graded in the thickness direction and vary continuously and smoothly according to two types of symmetric carbon nanotube volume fraction profiles. Lei and all used different types of distributions of uniaxially aligned SWCNTs, and the element-free kp-Ritz method to study the free vibration analysis of functionally graded Nano-composite plates reinforced by single-walled carbon nanotubes (SWCNTs). [17]. Rafiee and all follow them and present the large amplitude free vibration of functionally graded carbon nanotube reinforced composite (CNTRC) beams with surface-bonded piezoelectric layers subjected to a temperature change and an applied voltage. [18] . Similarly, Wattanasakulpong and all use an aligned single-walled CNTs distributed in the polymeric matrix to investigate the bending, buckling, and vibration behaviors of carbon nanotube-reinforced composite (CNTRC) beams. [19]. The beams resting on the Pasternak elastic foundation, including a shear layer and Winkler spring. Ke and all came back to carry out a dynamic stability analysis of functionally graded Nano-composite beams reinforced by single-walled carbon nanotubes (SWCNTs) based on the Timoshenko beam theory. [20]. Based on the three-dimensional theory of elasticity, the bending behavior of functionally graded carbon nanotube reinforced composite (FG-CNTRC) plate embedded in thin piezoelectric layers subjected to mechanical uniform load with simply supported boundary conditions is carried out by Alibeigloo and all [21]. Devalve and all investigate the damping effects of carbon nanotubes (CNTs) embedded in the matrix of fiber-reinforced composite materials. They analyzed composite materials using dynamic mechanical analysis and various modal analysis techniques to determine the damping characteristics of the composite as a function of strain, fiber volume fraction, and nanotube type and weight percentage loading. [22]. Deriving the stability equations using the adjacent equilibrium (Trefftz) buckling criterion and based on the first-order shear deformation theory (FSDT) of plates, Malekzadeh and all study the buckling behavior of quadrilateral laminated thin-to-moderately thick plates composed of perfectly bonded carbon nanotube reinforced composite (CNTRC) layers [23].

It is worth mentioning that Carbon nanotube applications are not limited to those reported in the scientific research mentioned in the above paragraph. It was aimed in

different articles of CNTs in those engineering fields are important for a mechanical engineer but not in all different applications of composites. In fact, the focus was on the major mechanics-based industries involved with composites. We can see when checking works that have been published by 2014, all research was processed on the buckling and post-buckling of CNTs reinforced composite, and a few research have been released on vibrations. The thing that the majority of researchers have not been able to address is the treatment of all types of vibrations related to nanotube-reinforced plates. However from 2014, some researchers began to address it. For example, Abdollahzadeh Shahrbabaki and all analyze the three-dimensional free vibration of carbon nanotube (CNT) reinforced composite rectangular plates with various boundary conditions by developing a set of orthogonal admissible functions used in the Ritz method [24] . Ansari and all study the forced vibration behavior of Nano-composite beams reinforced with single-walled carbon nanotubes (SWCNTs) based on the Timoshenko beam theory [25]. They considered carbon-nanotube reinforced composite (CNTRC) beams with uniform distribution (UD) and three types of functionally graded (FG) distribution patterns of SWCNT reinforcements. Based on the governing equations of the first-order shear deformation theory (FSDT), Malekzadeh and all present the study of free vibration behavior of quadrilateral laminated thin-to-moderately thick plates with carbon nanotube-reinforced composite (CNTRC) layers [26]. Lin and all investigate the free vibration of Nano-composite beams reinforced by single-walled carbon nanotubes (SWCNTs), where the distribution of the SWCNTs may vary through the thickness of a beam and are aligned along the beam's axial direction [27]. Hydarpour and all used composites reinforced by functionally graded carbon nanotube- (FG-CNTRCs) distribution to study the influences of centrifugal and Coriolis forces on the free vibration behavior of rotating carbon nanotube-reinforced composite (CNTRC) truncated conical shells [28]. Natarajan and all investigated the bending and free flexural vibration behavior of sandwich plates with carbon nanotube reinforced face sheets [29]. They used QUAD-8 shear flexible element developed based on higher-order structural theory. Fan and all investigate the large amplitude vibration behavior of a matrix-cracked laminated beam that contains carbon nanotube-reinforced composite (CNTRC) layers resting on an elastic foundation in thermal environments [30]. Wattanasakulpong investigate the static and dynamic behavior of carbon nanotube-reinforced composite plates resting on the Pasternak elastic foundation including the shear layer and Winkler springs [31]. In his work, he considered that the plates are reinforced by single-walled carbon nanotubes with four types of distributions of uniaxial aligned reinforcement material. Then, Shahriari and all used the

third-order shear deformation theory and the size parameter is taken into consideration by using Mindlin's strain gradient theory to investigate vibrations of functionally graded carbon nanotube-reinforced composite (FG-CNTRC) Nanoplates [32]. Mathematical modeled carbon nanotube-reinforced composite plate using higher-order shear deformation theory is presented by Mehar and all to study the free vibration behavior of functionally graded carbon nanotube-reinforced composite plate under an elevated thermal environment [32] . Zhang and all studied the free vibration characteristics of functionally graded Nano triangular plates reinforced by single-walled carbon nanotubes (SWCNTs) [32]. It employs the first-order shear deformation theory (FSDT) to account for the effect of transverse shear deformation of the plates and the element-free IMLS-Ritz method for numerical computation. Thomas and all study the vibration analysis of functionally graded carbon nanotube-reinforced composite (FG-CNTRC) shell structures [33]. Material properties of an FG-CNTRC shell are graded smoothly through the thickness direction of the shell according to uniform distribution and some other functionally graded (FG) distributions (such as FG-X, FG-V, FG-O, and FG-) of the volume fraction of the carbon nanotube, and the effective material properties are estimated by employing the extended rule of mixture. The multi-term Kantorovich-Galerkin method was proposed by Wang to investigate the buckling and free vibration behavior of thin carbon nanotube-reinforced composite plates with the classical plate theory [34]. First-order shear deformation theory of shell structure and Donnell-type kinematic assumptions for the investigation of free vibration characteristics of composite plates reinforced with single-walled carbon nanotubes. It was studied where the distribution of the carbon nanotubes through the thickness of the panel may be uniform or functionally graded. This case was studied by Mirzaei [35]. Kamarian and all took for their case a free vibration analysis of Carbon Nanotube-Reinforced Composite (CNTRC) conical shells performed by considering the agglomeration effect of Carbon Nanotubes (CNTs) [36]. They employ the Eshelby-Mori-Tanaka approach to estimate the material properties of the Nano-composite conical shell. They reveal that, frequencies of the panel are dependent to both, volume fraction of carbon nanotubes and their distribution pattern across the thickness. Also, while the volume fraction of carbon nanotubes increases, the frequencies of the panel increase too. Setoodeh and all solved geometrically nonlinear free vibration of functionally graded carbon nanotube-reinforced composite quadrilateral plates using a formulated differential quadrature (DQ) method in conjunction [37]. Fu and all studied the nonlinear dynamic stability of carbon nanotube-reinforced composite plates resting on an elastic foundation [38]. They aligned single-walled carbon nanotubes (SWCNTs) that are distributed in the form of uniformly

distributed (UD) and functionally graded (FG) in the composite. They found that the effect of a nonlinear factor on the boundary of the principle dynamic unstable regions is essential with the increase of amplitude. Wu and all studied the nonlinear vibration of imperfect shear deformable functionally graded carbon nanotube-reinforced composite (FG-CNTRC) beams based on the first-order shear deformation beam theory and von Kármán geometric nonlinearity [39]. They observed that whether the FG-CNTRC beam exhibits the "hard-spring" or "soft-spring" vibration behavior is largely dependent on the initial imperfection mode. Also, Wu and all observed that whether the FG-CNTRC beam exhibits the "hard-spring" or "soft-spring" vibration behavior is largely dependent on the initial imperfection mode, its amplitude as well as the vibration amplitude.

Later and with the appearance of graphene Nano-platelets with different dimensions, some researchers took the opportunity to study and compare this material with Carbon nanotubes and published many papers that discuss which one of them was the right choice for reinforcement. We can name Garcia-Macias and all [40]. He mentioned in his work the bending and the vibrational behavior of functionally graded graphene and carbon nanotube-reinforced composite flat plates. Also, Zhao and all used a modified Halpin-Tsai model and the rule of mixture [40] . They determined the effective material properties including Young's modulus, mass density, and Poisson's ratio of the Nano-composites. Their aim is to study the bending and vibration behaviors of a novel class of functionally graded trapezoidal plates reinforced with graphene Nano-platelets (GPLs) by employing the finite element method. They concluded that the bending and vibration behaviors of trapezoidal plates with such a distribution pattern are more sensitive to the GPL weight fraction and plate geometry compared to the other distribution patterns. Song and all presented the biaxial compressed buckling and post-buckling behaviors of functionally graded multilayer composite plates reinforced with a low content of graphene Nano-platelets that are randomly oriented and uniformly dispersed in the polymer matrix within each individual layer [41]. Feng and all studied the nonlinear free vibration of a multi-layer polymer Nano-composite beam reinforced by graphene platelets non-uniformly distributed along the thickness direction [41]. They used theoretical formulations of Hamilton's principle like the Timoshenko beam theory, and von Kármán nonlinear strain displacement relationship. They found that adding a very small amount of GPLs into the polymer matrix as reinforcements significantly increases the natural frequencies of the beam. Ahmadi and all analyzed the bending, buckling, and free vibration of hybrid polymer matrix composites reinforced by

carbon fibers and carbon nanotubes (CF/CNT-RP) [41]. They used a finite element-based multi-scale modeling approach. They found that bending was affected by reinforcement with both CF and CNT. In 2018, Guo and all employed the first-order shear deformation theory (FSDT) of the energy function to investigate on free vibration of graphene Nano-platelet reinforced laminated composite quadrilateral plates using the element-free IMLS-Ritz method [55]. After comparing with GPLRC with CNTRC, they found that GPLRC induces a dramatically higher natural frequency. Lin and all discussed the different GPL Nano-filler distribution patterns across the thickness [42]. They presented the vibration characteristics and nonlinear aero-elastic response of the functionally graded multilayer composite plate reinforced with graphene Nano-platelets. It was subjected to in-plane excitations and applied voltage using modified Halpin-Tsai model. Based on the Pasternak foundation, and the sinusoidal shear deformation theory, Arefi and all analyze the free vibration behavior of functionally graded (FG) polymer composite Nano plates reinforced with graphene Nano-platelets [43]. Their paper relates the sensitivity of the response to the Pasternak coefficient, an increased foundation stiffness yielding a meaningful increase in the composite structure's frequency. The modified Halpin-Tsai model is used to formulate the Material properties with gradient variation in the thickness aspect. It was presented by Wang and all to analyze the free vibration and static bending of functionally graded (FG) graphene Nano-platelet [44]. This reinforced composite doubly curved shallow shells with three distinguished distributions. Their numerical calculations revealed that an addition of a small quantity of GPLs can remarkably improve the fundamental frequency and cut down the static bending deflection of the shells. Garcia-Macias and all used the superior properties of graphene, as well as better dispersion and relatively low manufacturing cost. Also, and in that case, they noticed that the superior load-bearing capacity of graphene-reinforced composite plates for both fully aligned and randomly oriented filler configurations.

Our study showed that few articles worked worked on an active vibration control of Nano-composite plates. From 2019, a considerable number of papers was published in this field. Selim and all were among were the first who study the active vibration control of functionally graded multilayer graphene Nano-platelets reinforced composite plates integrated with piezoelectric layers [45]. Where the theoretical formulation of the composite plates with piezoelectric layers was developed utilizing the element-free improved moving least-squares Ritz (IMLS-Ritz) method in association with the higher-order shear deformation theory (HSDT). To provide a numerical solution to underlying problems,

Nguyen and all develop a computational approach based on a *C*° -HSDT polygonal finite element formulation (PFEM) to investigate the s free vibration and dynamic responses of smart FG metal foam plate structures reinforced by graphene platelets [46]. In their conclusion, they explained that the combination of advantages of both the metal foam architecture and GPL reinforcement into engineering material is a good idea to provide advanced ultra-light high-strength structures. Mirjavadi and all investigated on forced vibrational characteristics of a porous Nano-composite shell reinforced by graphene platelets under radial dynamic loads [47]. Material properties of the shell depend on uniform and non-uniform distributions of GPLs and porosities. After checking their results, they showed that the resonance frequency of a Nano-composite shell can be increased by increasing the GPL percentage. It was done by using the Halpin– Tsai model. Also, the rule of mixture determine the effective Young's modulus and to compute the effective Poisson's ratio and mass density respectively. Karami and all forced resonance vibration of graphene Nano-Platelets reinforced Functionally Graded Polymer Composite Nano-plates [48]. In 2020, Ma and all investigate the smart control and dynamic of a graphene Nano-platelets reinforced by a composite cylindrical shell surrounded [49]. A piezoelectric layer was used as actuator and sensor based on a numerical solution method called generalized differential quadrature method (GDQM). This was presented for the first time. In their outcomes, they found that the PD controller, viscoelastic foundation, slenderness factor, external voltage, and GPL's weight fraction have a considerable impact on the amplitude and vibration behavior of a GPLRC cylindrical shell. An active vibration control and vibration characteristics of a sandwich thin cylindrical shell whose intermediate layer is made of the graphene-reinforced composite that is bonded with integrated piezoelectric actuator and sensor layers at its outer and inner surfaces was presented by Dong and all [50]. They used a constant velocity feedback control algorithm and employing the Runge-Kutta method. They concluded that the results showed that the sandwich cylindrical shell with higher GPLs weight fractions and length-to-thickness ratio, lower temperature variation, and smaller thicknesses of piezoelectric layers has a higher natural frequency. In addition, the greater control gain makes the amplitude peak of the shell attenuate substantially faster. The vibration amplitude of the shell with active vibration control is insensitive to GPL distribution patterns. Similarly, Fadaee and all studied the vibration analysis of a beam-fluid coupled system and then, employing magnetostrictive layers, the vibration amplitude of the cantilever beam was controlled according to a closed-loop velocity proportional feedback control approach [51]. Results show that the vibration suppression times for a beam with various distributions of

the CNT are approximately the same. While increasing the location from the top of the cavity to the beam, the overshoot response, and the vibration suppression time of a beam submerged in a fluid cavity decrease. Mozafari and all gives an analytical solution for free vibration of a composite sandwich plate reinforced with graphene Nano-platelets enclosed by piezoelectric layers. They consider a multilayer functionally graded graphene platelets-reinforced composite plate [66].Their results show that the best way to predict the most effective reinforcement is to distribute more GPLs with a larger surface area near the top and bottom surfaces of the plate. Besides, adding a small amount of GPLs as reinforcing Nano-fillers can significantly improve the stiffness of the plate. Wang and all analyze the thermal vibration of functionally graded graphene platelets reinforced composite annular plate resting on an elastic foundation under the mechanical load framework of HSDT. [67]. Their results revealed that applying sinusoidal temperature rise and locating more square-shaped GPLs approximately to the top and bottom surface result in the highest natural frequency. In the same year, Y. Chiker and all investigated the influence of the linear and nonlinear distribution of Nano-fillers on the vibrational behavior of Nano-composite plates using a layer-wise formulation model, where the carbon nanotube is distributed inside a composite plate based on the power law distribution (P-FGM) [68]. They conclude that the best way to increase the reinforced composite plate stiffness is to disperse more Nano-fillers near composite lateral surfaces. In 2021, Abbaspour and all investigated the active control of vibrations of rectangular Nano-composite micro-plates reinforced with graphene platelets bonded with piezoelectric layers in a thermal environment regarding the structural damping. [51]. Results illustrate the effectiveness of the designed PD controller for X-GPL micro-plates with four clamped boundaries especially when the size dependency is incorporated into the formulation. Moreover, the PD controller performance boosts up at higher temperatures. Based on the Halpin–Tsai model and a modified rule of mixture, the effectiveness approximating material properties are represented by Shen and all [52]. Their use was to study the forced resonance vibration analysis of curved micro-size beams made of graphene Nano-platelets reinforced polymer composites. It was shown in their work that the resonance position is significantly affected by changing length scale coefficients, opening angle, weight fraction, and the total number of layers in GNPs on composite curved micro beams corresponding to different GPLs distribution parameters. Employing the first-order shear deformable theory, Moradi and all investigate the smart control and wave propagation examination of graphene Nano-platelets reinforced cylindrical micro-shell covered with piezoelectric layers as the sensor and actuator (PLSA) in the framework of an

analytical method [51]. As a result, they remarked that consideration of the PD controller leads to expanding the stable area and improving the dynamic behaviors of the smart system. Yu and all investigate the active control of free and forced vibration for piezoelectric-integrated functionally graded linear distribution of carbon nanotube reinforced composite plate using the finite element method (FEM) based on Hamilton's principle and the FSDT [53]. They derived the governing equations of the motion of a piezoelectric-integrated FG-CNTRC plate. They showed that the velocity feedback control method can achieve the dynamic response control of the piezoelectric FG-CNTRC plate with excellent control effect on both forced vibration and free vibration. Later, Liu and all studied the nonlinear transient response of fluid-conveying pipes made of graphene Nano-platelet (GPL)-reinforced composite (GPLRC) under blast loads and in a thermal environment [54]. Their numerical results showed that due to the fluid–structure interaction, the vibration amplitudes of the GPLRC pipes conveying fluid decay after the impact of blast loads. In order to evaluate the damped response, Ly and all derived a smoothie finite element model to simulate the laminated FG-CNTRC plate integrated with active constrained layer damping treatment patches consisting of 1-3 piezoelectric composite layer and a viscoelastic layer [55]. Moreover, the effect of CNT distribution, nanotube volume fraction, and CNT orientation on the damping behavior of FG-CNTRC plates are investigated. Additionally, the influence of symmetrical and asymmetrical damping treatment configuration for controlling the vibration is also carried out. Alnujaie and all examine the dynamics of thick rectangular plates reinforced with rectangular Nano-fillers known as graphene Nano-platelets (GNPs) utilizing the quasi-3D hyperbolic shear deformation theory (quasi-3D HSDT) [56]. He discovered that for a specific GNPs percentage, growth in the amount of agglomerated GNPs leads to lower natural frequencies and higher dynamic deflection. Meanwhile, for a specific mass fraction of the agglomerated GNPs, growth in the volume of clusters brings about higher natural frequencies and lower dynamic deflection. Ezzraimi and all [57] presented an examination of a carbon nanotube reinforced composite plate. This is the same plate that Chiker and all [58] studied. they considered that the composite plate is reinforced by nonlinear distributions of CNTs, where nonlinear distribution is based on power law functions in accordance to the work of Chiker and all [58].

According to these articles: Chiker and all [58], Yu and all [53], Chiker and all [59], we found that they do not propose the use of exponential functions in order to distribute carbon nanotubes inside composite plates and to study their effect. On the other hand, we

also found that few articles included the vibration control of functionally graded composite plates reinforced by linear distribution of CNTs or GPLs and covered with piezoelectric sensors and actuators, where the CNTs or GPLs are distributed based on the nonlinear power law function inside composite plates.

Our work aims to study and control the stiffness of this kind of plates during active vibration. We tried to investigate a free vibration analysis of functionally graded material 'FGM' plates reinforced with carbon nanotubes (CNTs), distributed using exponential law functions [60]. A comparative study was done between frequencies of plate reinforced by CNTs, distributed using a nonlinear power low function [58], and those obtained using the proposed exponential law distribution. The results showed a better distribution of CNTs through the thickness, which leads to an improved plate stiffness. After comparing natural frequencies, it was found that our results are higher than the one found in the following article "Free vibration analysis of multilayer functionally graded polymer nanocomposite plates reinforced with nonlinearly distributed carbon-based nanofillers using a layer-wise formulation model" [58]. This pushed us to study the vibration control of plates reinforced with a nonlinear distribution of carbon nanotubes or graphene nanoplatelets based on the exponential law functions, which gave unexpected positive results.

# CHAPTER 2: ACTIVE VIBRATION CONTROL FOR NANO COMPOSITE STRUCTURES USING PIEZOELECTRIC MATERIAL

## 2.1. Introduction

Driving on a smooth road is often a pleasant experience, providing a sense of comfort and stability. However, the presence of constant tremors in a car seat, often caused by engine vibrations, disrupts this comfort. Similarly, imagine a building swaying alarmingly during strong winds, both scenarios highlight the pervasive issue of unwanted vibrations. Vibration, defined as the rapid back-and-forth motion of an object, is a common phenomenon with diverse implications. While it can be advantageous in specific applications, such as moving materials efficiently on a vibrating conveyor belt, uncontrolled or excessive vibration can have serious consequences. In civil engineering, persistent vibrations can weaken structures, causing damage to buildings and bridges. In machinery, they reduce operational efficiency, accelerate wear, and increase the risk of mechanical failure. In vehicles, excessive vibration affects ride quality, contributes to component degradation, and diminishes passenger comfort. Furthermore, prolonged exposure to strong vibrations can negatively impact human health, leading to discomfort, fatigue, and even nerve damage. Because of these numerous drawbacks, engineers quickly recognized the critical need to control and manage vibrations effectively. For example, they use the active control of vibration to detect, analyze and attenuate vibrations. This consists mainly of controllers, piezoelectric sensors and actuators.

## 2.2. Piezoelectric Material

Piezoelectric materials are a fascinating class of materials with the unique ability to convert mechanical stress (pressure, vibration) into electrical energy, and vice versa. When a mechanical force is applied, it generates an electrical voltage. Conversely, applying a voltage can cause them to physically deform (Figure 2.1 [61])

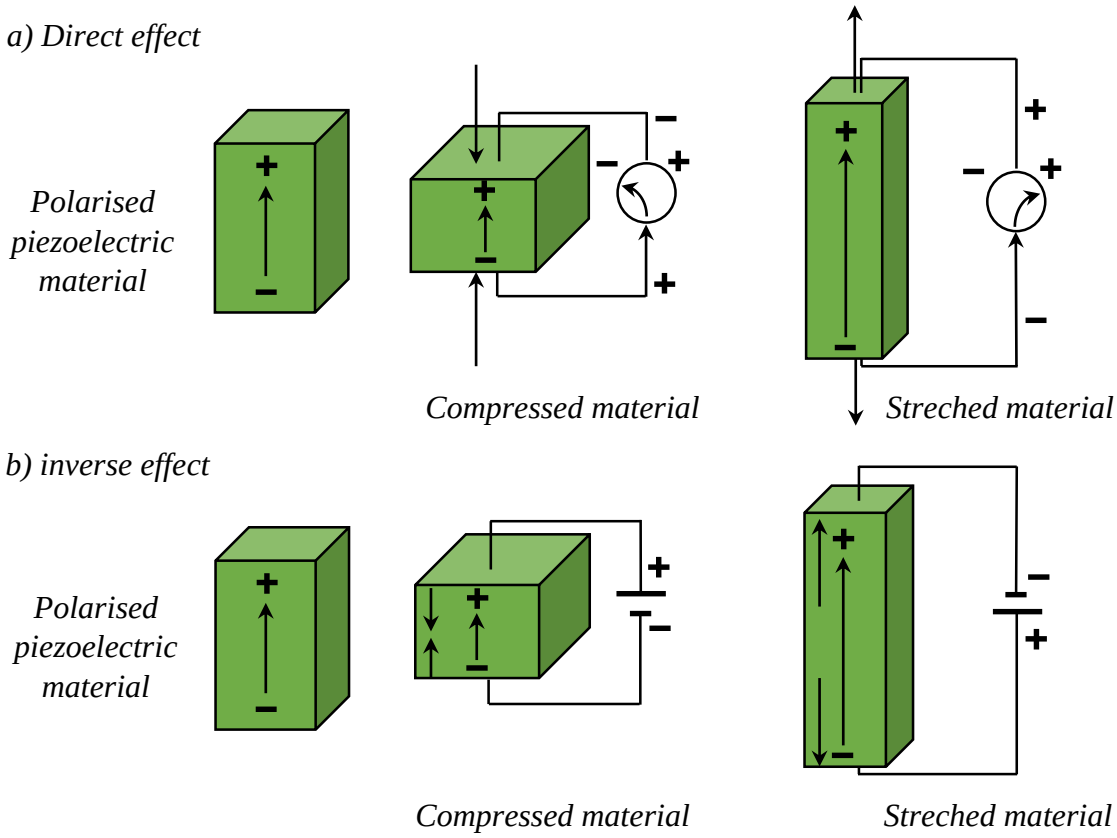


**Figure 2.1:** a) Direct and b) inverse, piezoelectricity effect.

## 2.3. Poling of Piezoelectric Material

The piezoelectric effect is strongly coupled with the existence of electric dipoles in the crystal structure of the ceramic. Generally, the raw material does not exhibit strong piezoelectric properties, because the electric dipoles in the material are pointing in random directions. Thus, the net dipole properties of the material are very small after the fabrication process. The orientation of the individual electric dipoles in a piezoelectric material must be aligned for the material to exhibit strong electromechanical coupling. The dipoles are oriented toward one another through a process called poling. Poling requires that the piezoelectric material placed in a strong electric field. The electric field produces an alignment of the dipoles along the direction of the electric field [83] as shown in Figure 2.2.

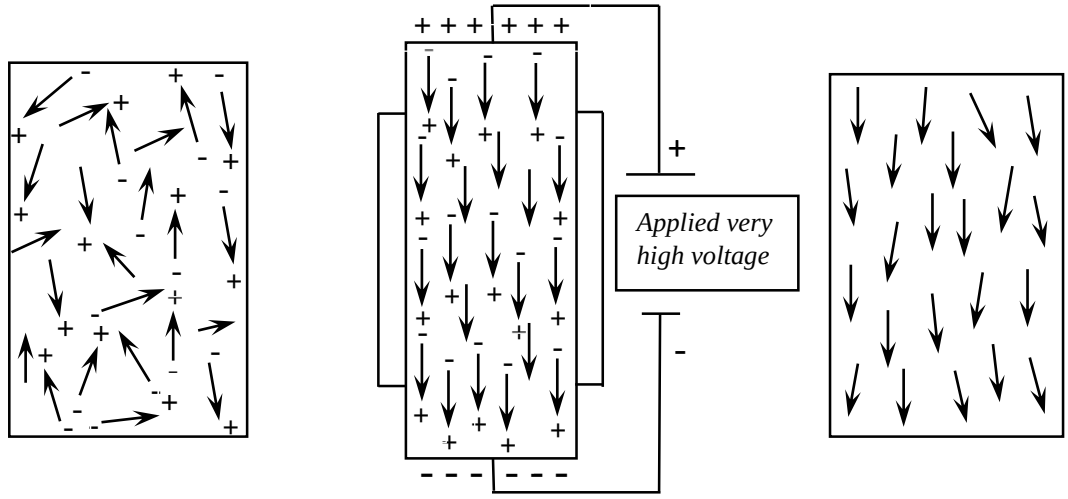


**Figure 2.2:** Process of poling a piezoelectric material.

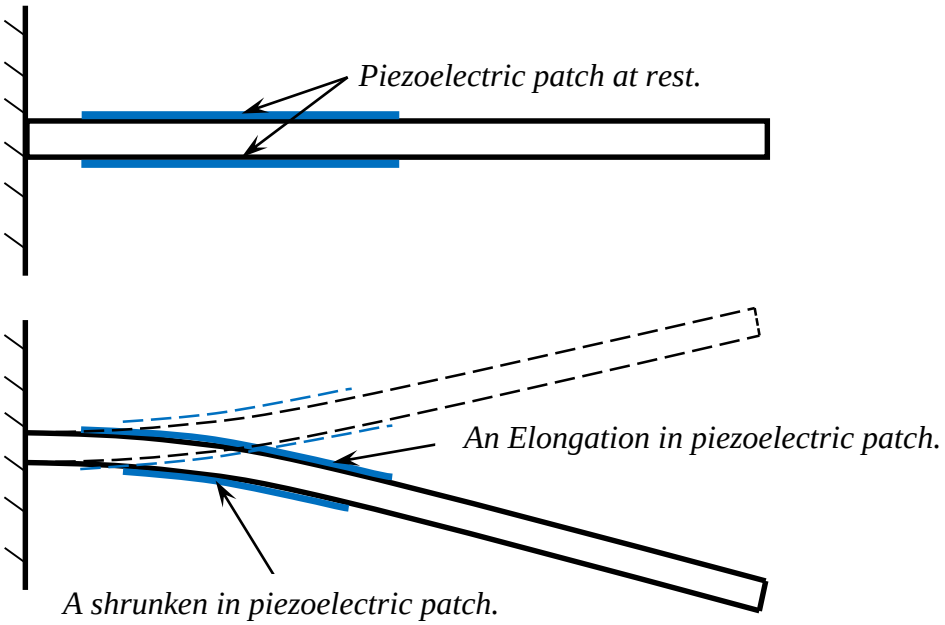


**Figure 2.3:** Structure bent under the elongation and shrunk of the top and bottom piezoelectric patches respectively.

## 2.4. Mechanism of Action in Structure

The bending of the isotropic or composite structures is the consequence of an interaction between opposing forces. Applying a voltage triggers the direct piezoelectric effect, causing the top patch to expand like a stretched spring with a positive voltage, while the bottom patch contracts like a squeezed sponge under a negative voltage. This creates an imbalance of forces on the structure, pushing it downwards from the top and pulling it downwards from the bottom [62]. Conversely, when inverse the voltage applied on the two piezoelectric patches. The structure will balance in the opposite way, pulling it upwards from the top by the top piezoelectric patch and pushing it upwards from the bottom by the bottom piezoelectric patch (Figure 2.3).

## 2.5. Vibration Control

Vibration control is a broad field of engineering concerned with reducing or eliminating unwanted vibrations in objects or systems. Vibrations can be caused by various factors such as:

- *Internal forces*, for example in machines, vibrations can arise from unbalanced rotors, misaligned gears, or engine imbalances.
- *External forces*, for example buildings experience vibrations due to earthquakes, wind, or traffic. Also, vehicles encounter vibrations from road imperfections or engine operation.

The importance of vibration control arises from its applications across diverse engineering fields. For instance, in civil engineering, vibration control ensures the safety and stability of structures like buildings and bridges under dynamic loads. In mechanical engineering, vibration control allows to:

- Improves the performance, lifespan, and noise characteristics of machinery.
- Enhances ride comfort, and reduces noise in vehicles.
- Counteract engine vibrations and enhance vehicle comfort by using active engine mounts.
- Reduce noise and vibration of transmission exhaust systems.

To mitigate these challenges, engineers have developed innovative techniques to manage and control vibration, ensuring the safety, reliability, and efficiency of various systems.

They can be categorized into two classes: Passive and active vibration control, (PVC) and (AVC) respectively.

## 2.6. Vibration Control Types

### 2.6.1. Passive Vibration Control

Passive control techniques like isolators and dampers have been used for many years. Passive vibration control offers a less complex and more economical way to manage unwanted vibrations in structures and machines. Unlike active control systems, it doesn't require external power or intricate electronics. Instead, it relies on clever design and material properties to absorb or isolate vibrations, preventing them from transferring or causing damage. However, they may not always be effective across a wide range of vibration frequencies or amplitudes.

#### *2.6.1.1. Vibration isolators*

The isolators are elements placed between the vibrating source and the structure you want to protect. They absorb vibration energy, reducing its transmission. (e.g., rubber mounts under a washing machine figure 2.4).


**Figure 2.4:** Washing machine vibration isolators [63].

#### 2.6.1.2. *Vibration damping materials*

Vibration damping materials are materials that absorb and dissipate the energy of vibrations. They are commonly used in various applications to reduce noise, improve comfort, and protect equipment from damage. (e.g., acoustic damping pads in car doors Figure 2.5).


**Figure 2.5:** Damping acoustic in car doors [64].

#### 2.6.1.3. *Tuned mass dampers*

**Figure 2.6:** Building vibration dampers [65].

These consist of a mass-spring system attached to the structure. They are tuned to resonate at the same frequency as the unwanted vibration, absorbing that specific frequency effectively. (e.g., dampers used to reduce wind sway in tall buildings Figure 2.6).

### 2.6.2. Active Vibration control

Active vibration control is a technology used to reduce unwanted vibrations in structures and machines. It is based on the idea of applying a force to the structure that is equal in magnitude but opposite in direction to the excitation force causing the vibration. Active vibration control use loop mechanisms, consisting mainly of controllers, sensors, and

actuators (figure 2.7). The latter are made of piezoelectric material because of the electromechanical properties of piezoelectricity.

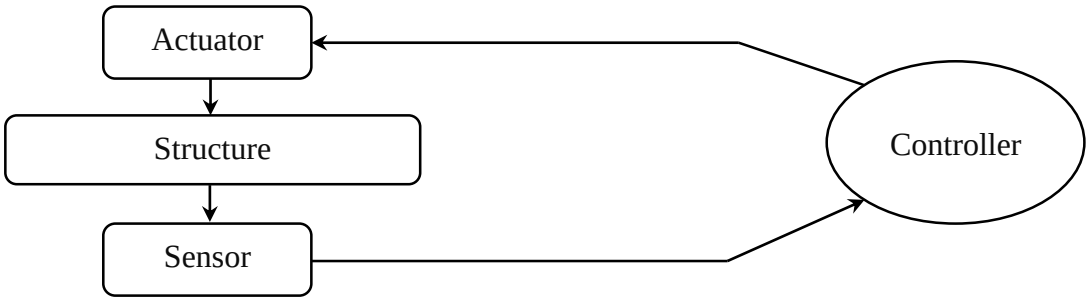


**Figure 2.7:** Active vibration control loop.

An interesting application field of vibration control lies in the field of aeronautics, where mitigating vibrations is essential for the comfort and well-being of pilots and passengers. Active Vibration Control is employed in aircraft and spacecraft to minimize structural vibrations, enhance ride comfort, and ensure operational efficiency. Additionally, vibration damping in airplane wings and helicopter rotor blades plays a critical role in improving stability, reducing noise, and enhancing overall performance. Figure 2.8 illustrates a test room for an airplane wing and fuselage covered by piezoelectric patches.

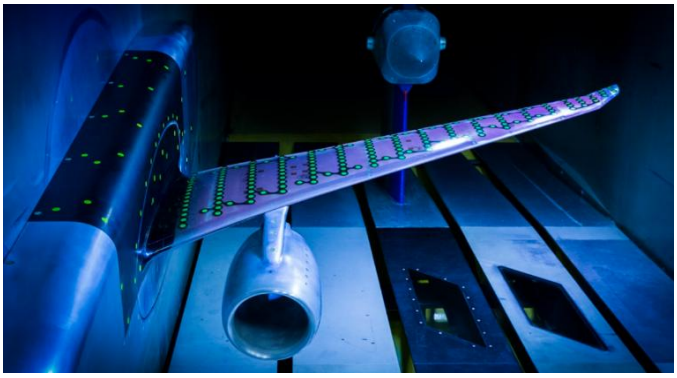

**Figure 2.8**: Vibration control for airplane ail using piezoelectric patches [66].

#### 2.6.2.1. *Piezoelectric Sensor*

In a vibration control loop, the piezoelectric sensor is attached to the vibrating structure. As the structure vibrates, it exerts a force on the piezoelectric material. This mechanical force creates a varying voltage within the sensor, acting like a fingerprint of the vibration itself. The greater the force (indicating a stronger vibration), the higher the voltage

generated. Similarly, the frequency of the vibration is reflected in the frequency of the voltage fluctuations the sensor picks up. This way, the piezoelectric sensor acts as a translator, converting the mechanical motion of the vibration into a corresponding electrical signal the control system can understand and use to counteract the unwanted movement.

#### 2.6.2.2. *Controller*

In Active Vibration Control, the controller serves as the central processing unit, orchestrating the entire system. It receives signals from sensors that provide detailed information about the vibration's amplitude and frequency. Using advanced algorithms, the controller interprets this data, effectively "decoding" the vibrations. Based on this analysis, it determines the optimal counteracting force and timing to mitigate the vibrations.

Control algorithms can range from straightforward, pre-programmed responses to adaptive systems that dynamically adjust in real time. Once the calculations are complete, the controller sends precise commands to the actuators, specifying the magnitude and timing of the force to be applied. This counteracting force neutralizes the vibrations, resulting in a more stable and balanced system.

#### 2.6.2.3. *Piezoelectric Actuator*

The controller serves as the conductor, orchestrating the actuator's movements. When it sends an electrical signal, the actuator doesn't simply receive a command, it undergoes a transformation. The signal generates an electric field across the piezoelectric material inside the actuator, which acts as a powerful nudge, causing the material to deform physically. This deformation depends on the material's intrinsic properties and the specific characteristics of the electrical signal. For instance, imagine a slender, plate-like structure made of piezoelectric material. When voltage is applied, the resulting electric field may cause the plate to bend in a precise manner. This bending is not random but carefully dictated by the actuator's design, translating into a directional force. The actuator uses this force to counteract unwanted vibrations effectively. In essence, the controller's electrical signal is converted into a deliberate physical movement through the synergy of the piezoelectric material and the actuator's engineered structure.

## 2.7. Nano fillers for the reinforcement of composite structures

Many structural components, including beams, plates, and shells made from isotropic or orthotropic materials, such as aircraft wings, bridge columns, girders, and vehicle frames, are often exposed to harmful vibrations. These vibrations can lead to structural fatigue-causing cracks and reducing their lifespan (Figure 2.9).


**Figure 2.9**: a) Crack in a pillar of a bridge [67] , b) Crack in house wall [68], and c) Crack in airplane wing [69].

In the order to repair these cracks and minimizing the cost and time, a novel composite material has been developed, offering superior properties compared to conventional materials. These composites incorporate nanoscale reinforcements to enhance their overall performance, earning them the name "nanocomposites." The primary advantage of using nanoscale elements lies in leveraging the exceptional properties of nanoparticles to strengthen a desired matrix, which can be metallic, polymeric, or other materials.

Polymeric matrices are the most commonly used, leading to the creation of polymeric nanocomposites. Additionally, a wide variety of nanoscale Fibers and particles can be utilized to improve matrix properties. Among the most renowned reinforcements are carbon nanotubes, cylindrical structures formed by rolling one or more layers of graphene (graphene

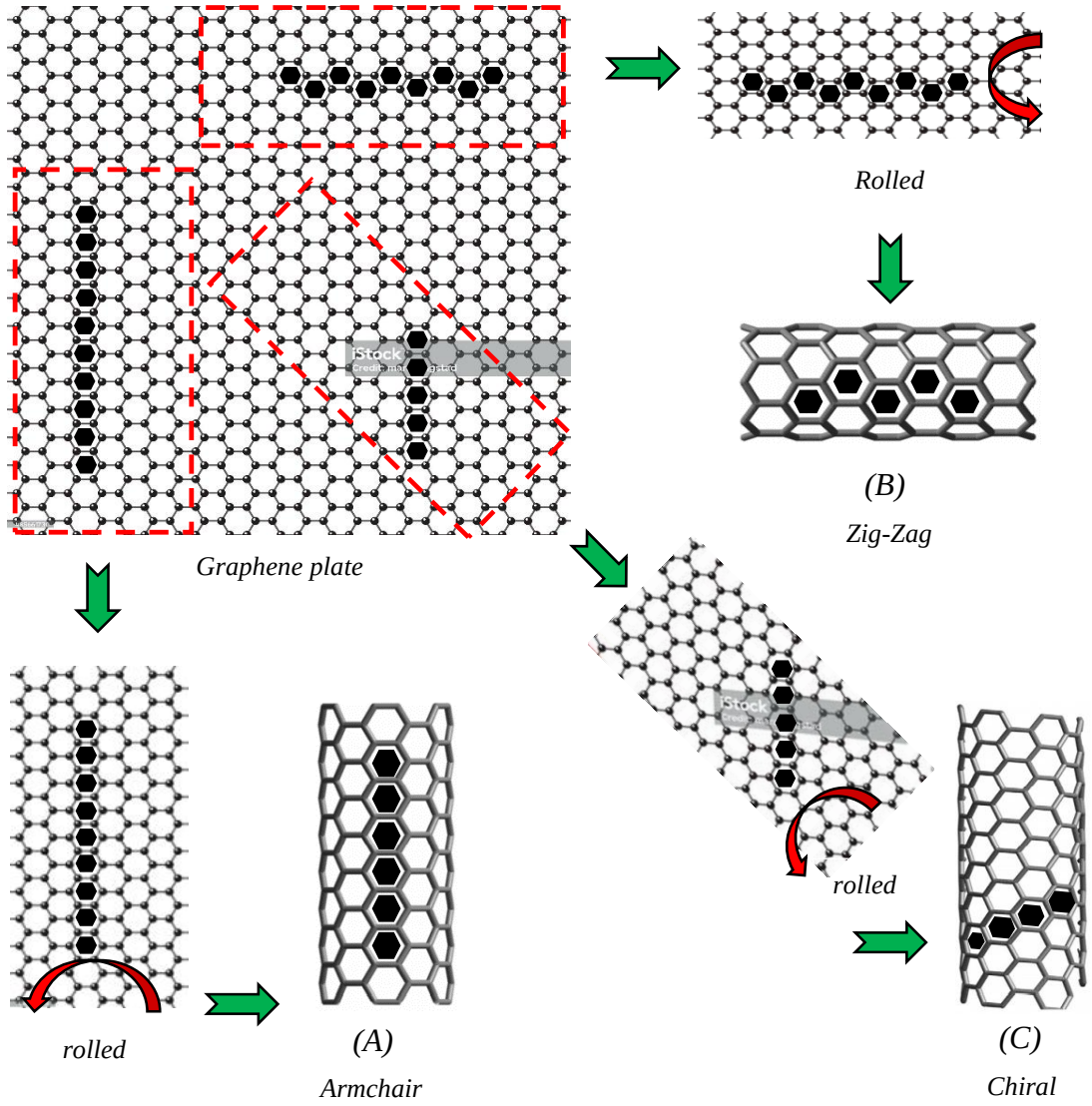


**Figure 2.10:** State to obtain single-walled carbon Nanotubes: (A) armchair, (B) Zig-zag, (C) Chiral.

platelets, or GPLs). These nanotubes are widely employed in the fabrication of polymeric nanocomposites due to their remarkable strength, stiffness, and unique properties.

All types of CNTs, namely single-walled CNTs (SWCNTs), double-walled CNTs (DWCNTs), and multi-walled (MWCNTs), can be implemented to enhance the material properties of a polymeric matrix. CNTs can support Young's moduli of Terra-Pascal (TPa)

order depending on their chiral, Zig-Zag, or armchair form (Figure 2.10). Hence, the remarkable stiffness of CNTs can improve the total stiffness of the Nano-composite properly [70].

### 2.7.1. Single-Walled CNTs

Single-Walled CNTs (SWCNT) consists of one layer of carbon sheet. The structure of a SWCNT can be conceptualized by wrapping a graphitic layer into a seamless cylinder (figure 2.11). A massive amount of SWCNTs is produced mainly by the chemical vaporization deposition (CVD) method. Most SWCNTs have a diameter close to one nanometer, with lengths extendable up to millimeter or even centimeter scales[71].

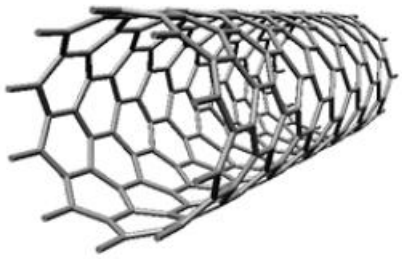

**Figure 2.11:** Single-walled Carbon Nanotube. [71]

### 2.7.2. Double–Walled CNTs

A double-walled carbon nanotube is a microscopic cylindrical structure composed of two

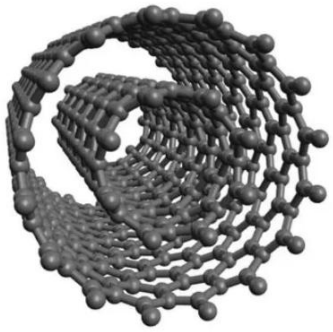

**Figure 2.12:** Double-walled Carbon Nanotube. [71]

sheets of graphene (a honeycomb structure of carbon atoms) wrapped around each other.(figure 2.12 [71]).

### 2.7.3. Multi-Walled CNTs

Multi-walled carbon nanotubes (MWCNTs) are made up of multiple graphene layers, and their description requires considering not only morphology and structure, as for single-walled carbon nanotubes (SWCNTs), but also texture and Nano-texture. One possible definition of MWCNTs is as "Nano-sized, hollow, carbon filaments whose wall is made up of more than one graphene (figure 2.13), with the inter-graphene distance being equal to the regular 0.34 nm van der Waals distance for turbo-stratic, poly-aromatic carbons [72]". However, this definition is not universally accepted, as some researchers prefer to restrict the use of the term "MWCNT" to concentric assemblies of two or more SWCNTs with increasing diameters [72].

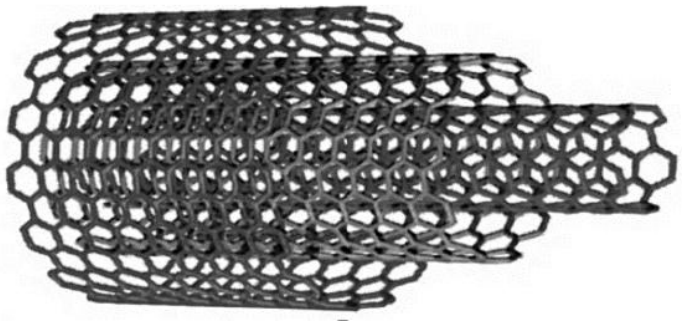

**Figure 2.13:** Multi-walled Carbon Nanotube. [72]

## 2.8. Functionally Graded Materials (FGMs)

Functionally graded materials (FGMs) are a class of advanced materials with a continuous variation of material properties from one surface to another (Figure 2.14). This variation in properties can be tailored to meet the specific needs of an application, resulting in a material that is more efficient and durable than traditional materials[72]. FGMs are typically made from two or more different materials, which are gradually mixed together to create a gradient in properties. For example, an FGM might be made with a metal on one side and a ceramic on the other, with a gradual transition from one material to the other in between. This gradation in properties (such as Young's modulus and density) is based on different functions of distribution, these are:

- ***The sigmoidal distribution*** [73]:

$$E^{(k)} = \left(1 - \frac{1}{2}\left(\frac{h/2 - z}{h/2}\right)^{P_{in}}\right)E_m + \left(1 - \left(1 - \frac{1}{2}\left(\frac{h/2 - z}{h/2}\right)^{P_{in}}\right)\right)E_c \qquad for \qquad 0 \le z \le h/2 \tag{2.1}$$

$$E^{(k)} = \left(\frac{1}{2}\left(\frac{h/2 + z}{h/2}\right)^{P_{in}}\right)E_m + \left(1 - \left(\frac{1}{2}\left(\frac{h/2 + z}{h/2}\right)^{P_{in}}\right)\right)E_c \qquad for \qquad -h/2 \le z \le 0 \tag{2.2}$$

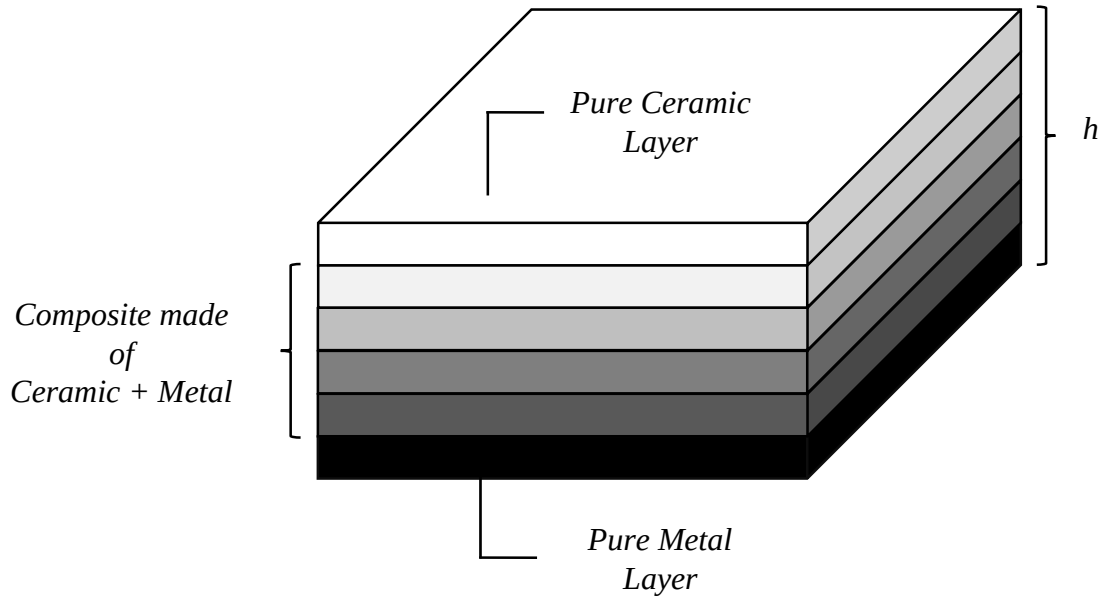


**Figure 2.14:** Functionally graded material (Ceramic/Metal).

- ***The power law distribution*** [74] [58]:

$$E^{(k)} = E_m + \left(E_c - E_m\right)\left(\frac{z}{h} + \frac{1}{2}\right)^{P_{in}} \tag{2.3}$$

$$\rho^{(k)} = \rho_m + \left(\rho_c - \rho_m\right)\left(\frac{z}{h} + \frac{1}{2}\right)^{P_{in}} \tag{2.4}$$

- ***The exponential law distribution*** [75]:

$$E\left(z\right) = E_C e^{-\delta\left(1 - \frac{2z}{h}\right)}, \qquad \delta = \frac{1}{2}\ln\left(\frac{E_c}{E_m}\right) \tag{2.5}$$

$$\rho\left(z\right) = \rho_C e^{-\delta\left(1 - \frac{2z}{h}\right)}, \qquad \delta = \frac{1}{2}\ln\left(\frac{\rho_c}{\rho_m}\right) \tag{2.6}$$

Where $P_{in}$ is the power law index and the superscripts $E_c$, $E_m$ signify, respectively, the Young's modulus on the top ceramic and the bottom metal surfaces of the structural element.

$\rho_c$, $\rho_m$ signify, respectively, the density of both ceramic and metal. ($z$) is the position of the considered layer, and $h$ is the thickness of the plate

### 2.9. Functionally Graded Nano Composite Materials

Functionally graded Nano-composite materials were first observed in early 2009, where Shen [2] was the first one who proposed four linear functionally graded distributions of carbon nanotubes inspired by the FGM concept. Namely: the uniform, the FG-X, the FG-O, and the FG-A distribution. Afterward, Chiker *et al* [59] followed them and proposed the nonlinear distribution of CNTs by using the following power law functions:

- UD : $$f_{UD}^{(k)} = f_r^* \tag{2.7.a}$$
- FG-X : $$f_{FG-X}^{(k)} = \left(1+P_{in}\right)\left(\frac{\left|2k-N_L-1\right|}{N_L}\right)^{P_{in}}.f_r^* \tag{2.7.b}$$
- FG-O : $$f_{FG-O}^{(k)} = \left(1+P_{in}\right)\left(1-\frac{\left|2k-N_L-1\right|}{N_L}\right)^{P_{in}}.f_r^* \tag{2.7.c}$$
- FG-A : $$f_{FG-A}^{(k)} = \left(1+P_{in}\right)\left(\frac{0.5-k+N_L}{N_L}\right)^{P_{in}}.f_r^* \tag{2.7.d}$$
- FG-V : $$f_{FG-V}^{(k)} = \left(1+P_{in}\right)\left(\frac{k-0.5}{N_L}\right)^{P_{in}}.f_r^* \tag{2.7.e}$$

In which $f_r^*$ is the volume fraction of carbon nanotubes or graphene Nano-platelets, $k^{th}$ is the number of layers, and $N_L$is the total number of layers. $P_{in}$ is an index and his variation gives the nonlinear distribution.

$$f_r^* = \frac{w_i}{w_i+(1-w_i)(\rho^i/\rho_m)}, \qquad i = CNTs, GPLs \tag{2.8}$$

$w_i$ is the weight fraction of the nano-fillers.

A new method of distribution is proposed by us in reference [60], it is based on the exponential law distributions, which is given as:

- UD : $$f_{UD}^{(k)} = f_r^* \tag{2.9.a}$$
- FG-X : $$f_{FG-X}^{(k)} = f_r^*.\frac{1.5}{N_L}e^{4\left|2\frac{(k-0.5)}{N_L}-1\right|} \tag{2.9.b}$$
- FG-O : $$f_{FG-O}^{(k)} = f_r^*.\frac{N_L+0.5}{5}e^{-4\left|2\frac{(k-0.5)}{N_L}-1\right|} \tag{2.9.c}$$

- FG-A : $$f_{FG-A}^{(k)} = f_r^* \cdot \frac{1}{2} e^{2\left(\frac{2(N_L+1-k)}{N_L}-1\right)} \quad (2.9.d)$$

- FG-V : $$f_{FG-V}^{(k)} = f_r^* \cdot \frac{1}{2} e^{2\left(\frac{2k}{N_L}-1\right)} \quad (2.9.e)$$

In Figure 2.15, we present the curve of power and exponential law distribution of the volume fraction from the $1^{st}$ to the last layer.

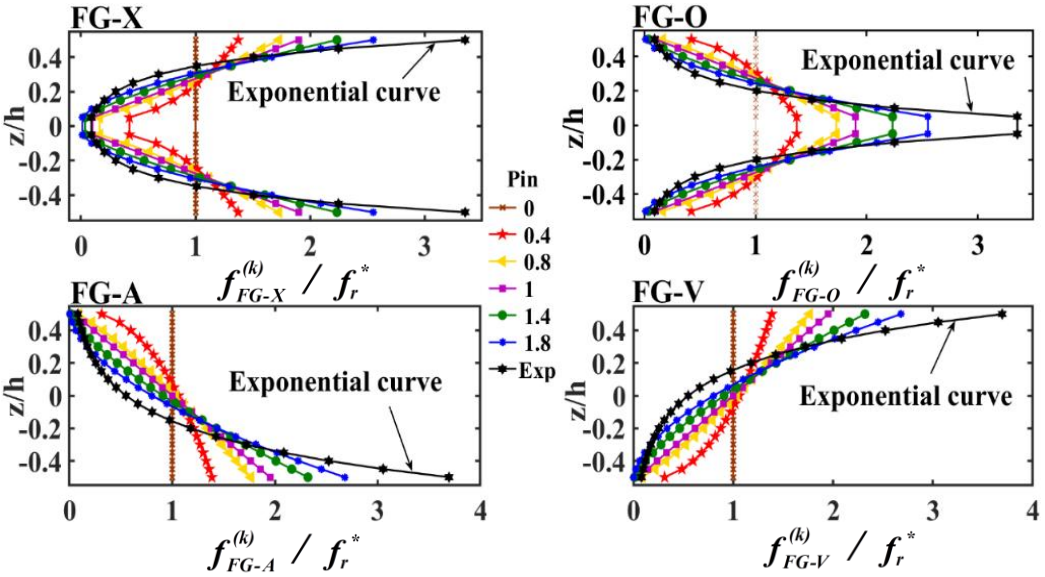


**Figure 2.15:** Volume fraction ratio $f_r{}^{(k)}/f_r^*$ along the plate thickness.

### 2.9.1. SWCNTs Reinforced Composite Plate Material Properties

In this section, we will implement the well-known rule of mixtures to predict the effective material properties of composites reinforced with carbon nanotubes (CNTs). This approach accounts for the small size of CNTs by using scale-dependent coefficients, which were derived by comparing experimental data with molecular dynamics simulations. According to this approach, the equivalent stiffness of the CNTR Nano-composite can be calculated for all layers using the following formula [76]:

$$E_{11}^{(k)} = k_1 f_r^{(k)} E_{11}^{CNT} + f_m^{(k)} E_m \quad (2.10)$$

$$E_{22}^{(k)} = \frac{k_2}{\frac{f_r^{(k)}}{E_{22}^{CNT}} + \frac{f_m^{(k)}}{E_m}} \quad (2.11)$$

$E_{11}^{CNT}$ , $E_{22}^{CNT}$ , and $E_m$ are the elastic young moduli of CNTs and matrix, respectively.

$$G_{12}^{(k)} = \frac{k_3}{\frac{f_r^{(k)}}{G_{12}^{CNT}} + \frac{f_m^{(k)}}{G_m}} \tag{2.12}$$

$G_{12}^{CNT}$ and $G_m$ are the shear moduli of CNT and matrix respectively.

Furthermore, the equivalent Poisson's ratio and mass density of the CNTR Nano-composites can be calculated using the following formula:

$$\nu_{12}^{(k)} = f_r^* \nu_{12}^{CNT} + f_m^{(k)} \nu_m \tag{2.13}$$

$\nu_{12}^{CNT}$ and $\nu_m$ are the Poisson's ratios of CNTs and matrix, respectively.

$$\rho^{(k)} = f_r^{(k)} \rho^{CNT} + f_m^{(k)} \rho_m \tag{2.14}$$

$\rho^{CNT}$, and $\rho_m$ are the densities of both CNT and matrix respectively. $k_1$, $k_2$, $k_3$ are the efficiency parameters. These coefficients vary as the volume fraction of the CNTs changes. They were determined by the comparison between the obtained results from the molecular dynamics simulation and the mixing law of CNT material properties. $f_m^{(k)}$ is the volume fraction of the matrix of the $k^{th}$ layer, which equals to $1 - f_r^{(k)}$.

### 2.9.2. GPLs Reinforced Composite Plate Material Properties

In this section, we are going to compute the effective material properties of graphene platelet-reinforced (GPLR) composites using the Halpin-Tsai micromechanical method. This method takes into account the small size and unique shape of the Nano-fillers to predict the material properties of the Nano-composite. According to this method, the equivalent stiffness of the GPLRC can be determined for all layers as follows [76]:

$$E_{eff}^{(k)} = \frac{5}{8}\underbrace{\left(\frac{1+\xi_w \eta_w f_r^{(k)}}{1-\eta_w f_r^{(k)}}\right)}_{E_T} + \frac{3}{8}\underbrace{\left(\frac{1+\xi_L \eta_L f_r^{(k)}}{1-\eta_L f_r^{(k)}}\right)}_{E_L} \tag{2.15}$$

Where $E_L$ and $E_T$ are longitudinal and transverse modules in x and y directions, respectively. Then:

$$\eta_w = \frac{\left(E_{GPL}/E_m\right)-1}{\left(E_{GPL}/E_m\right)+\xi_w}, \qquad \eta_L = \frac{\left(E_{GPL}/E_m\right)-1}{\left(E_{GPL}/E_m\right)+\xi_L} \tag{2.16}$$

In the previous equations, $E_{GPL}$ and $E_m$ denote the Young's moduli of GPLs and polymeric matrix, respectively. The Halpin-Tsai method includes the impact of the particular geometry of the reinforcements on the mechanical properties of the Nano-composite material. These geometrical parameters can be determined as follows:

$$\xi_w = 2\,w_{GPL}/h_{GPL} \quad , \qquad \xi_L = 2\,L_{GPL}/h_{GPL} \tag{2.17}$$

$L_{GPL}$, $w_{GPL}$, and $h_{GPL}$ are the average length, width, and thickness of the GPLs, respectively. Moreover, the terms, that are provided to account for the geometrical shape of the GPLs, are $\xi_L$ and $\xi_w$. Poisson's ratio and mass density of the GPLR Nano-composite material can be estimated via the simple form of the rule of the mixture as follows:

$$\nu_{eff}^{(k)} = f_r^{(k)}\nu^{GPL} + f_m^{(k)}\nu_m \tag{2.18}$$

$$\rho_{eff}^{(k)} = f_r^{(k)}\rho^{GPL} + f_m^{(k)}\rho_m \tag{2.19}$$

Where the subscript *eff* means effective.

## 2.10. Conclusion

In this chapter, we defined and explained the mechanism of action of piezoelectric materials and their application in the vibration control of structures. Additionally, we proposed a method for controlling composite plate structures reinforced with nanomaterials. This chapter sets the stage for a more in-depth exploration in the subsequent sections, which will focus on the advanced control of composite plates using piezoelectric sensors and actuators.

# CHAPTER 3: THEORY AND BEHAVIOR LAW FOR NANO COMPOSITE, PIEZOELECTRIC, AND SANDWICH PLATES

## 3.1. Introduction

In this chapter, the theoretical formulation will be presented to define kinetic, strain, and external forces for isotropic and orthotropic plates using the first-order shear deformation theory. Additionally, the relationship between stress and strain will be discussed.

## 3.2. Plate Deformation Theory

The First-order Shear Deformation Theory (FSDT) or Mindlin-Reissner theory is an advanced extension of the Classical Lamination Plate Theory (CLPT) that incorporates the effects of transverse shear strains. Following the Kirchhoff hypothesis, CPLT assumes that the sections perpendicular to the plate's mid-surface remain perpendicular after deformation (Figure 3.1). However, transverse shear strains are negligible in thin plates, like those made of piezoelectric materials. As we said, the FSDT is an extension of the CPLT were this take in consideration the effect of transverse shear strains, and said that sections perpendicular to the plate's mid-surface remain non-perpendicular after deformation for thick plates. The FSDT addresses this by modifying the displacement field of the CLPT to account for these strains, providing a more accurate description of plate deformation behavior [74][77][78], [79]:

$$\begin{cases} U(x,y,z,t) = u(x,y,t) - z.\theta_x(x,y,t) \\ V(x,y,z,t) = v(x,y,t) - z.\theta_y(x,y,t) \\ W(x,y,z,t) = w(x,y,t) \end{cases} \tag{3.1}$$

*U*, *V*, and *W* are the displacements in the *x*, *y*, and *z* directions, respectively. *u*, *v*, and *w* are the displacements of the mid-surface (z = 0), and $\theta_x$ and $\theta_y$ are the rotations of a transverse normal about the y and x axes, respectively:

CLPT: $\left( \theta_x^{CLPT} = \frac{\partial w}{\partial x} \quad , \quad \theta_y^{CLPT} = \frac{\partial w}{\partial y} \right)$, FSDT: $\left( \theta_x^{FSDT} = \theta_x^{CLPT} - \varphi_x \ , \ \theta_y^{FSDT} = \theta_y^{CLPT} - \varphi_y \right)$

Equation (3.1) can be rewritten in matrix form as follows:

$$\{X\} = \begin{Bmatrix} U \\ V \\ W \end{Bmatrix} = \underbrace{\begin{bmatrix} 1 & 0 & 0 & -z & 0 \\ 0 & 1 & 0 & 0 & -z \\ 0 & 0 & 1 & 0 & 0 \end{bmatrix}}_{[L]} \underbrace{\begin{Bmatrix} u \\ v \\ w \\ \theta_x \\ \theta_y \end{Bmatrix}}_{\{\overline{X}\}} \tag{3.2}$$

[$L$] is an operator for the localized translation and rotation variables. It can be expressed With another form as [78]:

$$\{X\} = \begin{Bmatrix} U \\ V \\ W \end{Bmatrix} = \underbrace{\begin{bmatrix} 1 & 0 & 0 & 0 & 0 \\ 0 & 1 & 0 & 0 & 0 \\ 0 & 0 & 1 & 0 & 0 \end{bmatrix}}_{[L_{tra}]} \begin{Bmatrix} u \\ v \\ w \\ \theta_x \\ \theta_y \end{Bmatrix} - z \underbrace{\begin{bmatrix} 0 & 0 & 0 & 1 & 0 \\ 0 & 0 & 0 & 0 & 1 \\ 0 & 0 & 0 & 0 & 0 \end{bmatrix}}_{[L_{rot}]} \begin{Bmatrix} u \\ v \\ w \\ \theta_x \\ \theta_y \end{Bmatrix} \tag{3.3}$$

[$L_{tra}$] and [$L_{rot}$] are the localized translation and rotation operator, respectively.

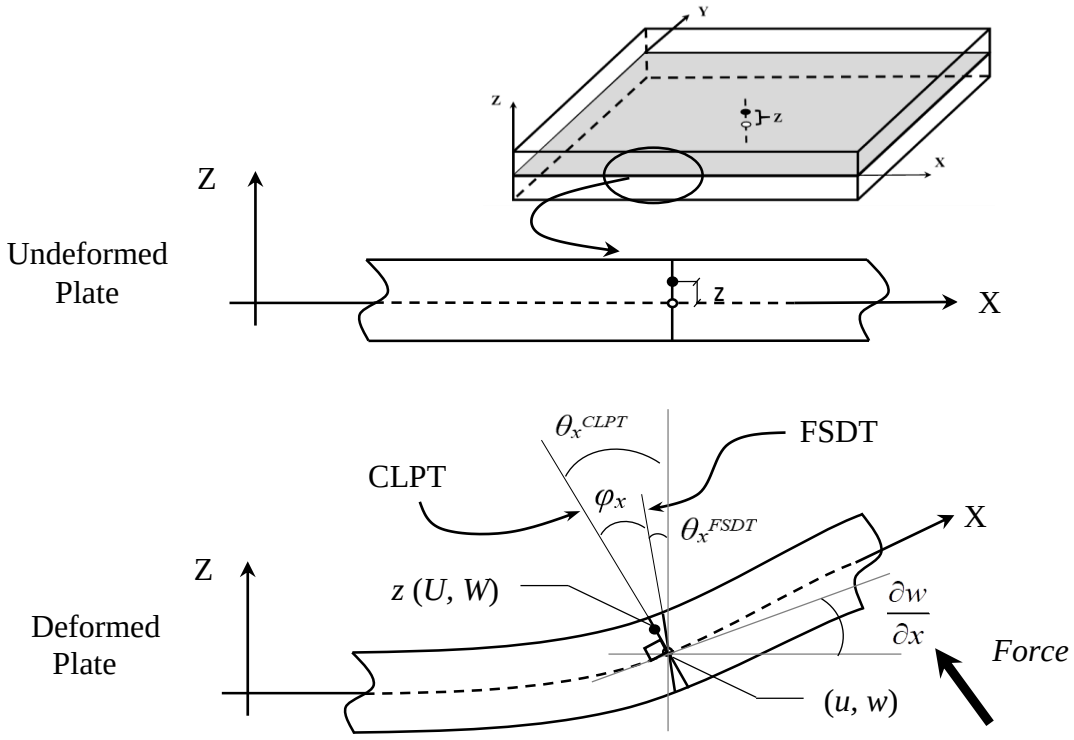


**Figure 3.1:** Deformation of plate according to FSDT and CLPT.

### 3.3. Strain-Displacement Relationship

The strain components in terms of displacement for a plate structure are given by the following relationships [80]:

$$\begin{Bmatrix} \varepsilon_x \\ \varepsilon_y \\ \varepsilon_z \\ \gamma_{xy} \\ \gamma_{xz} \\ \gamma_{yz} \end{Bmatrix} = \begin{Bmatrix} \dfrac{\partial u}{\partial x} + \mathrm{z}.\dfrac{\partial \theta_x}{\partial x} \\ \dfrac{\partial v}{\partial y} + \mathrm{z}.\dfrac{\partial \theta_y}{\partial y} \\ \dfrac{\partial w}{\partial z} = 0 \\ \dfrac{\partial u}{\partial y} + \dfrac{\partial v}{\partial x} + \mathrm{z}.\left( \dfrac{\partial \theta_x}{\partial y} + \dfrac{\partial \theta_y}{\partial x} \right) \\ \theta_x + \dfrac{\partial w}{\partial x} \\ \theta_y + \dfrac{\partial w}{\partial y} \end{Bmatrix} \tag{3.4}$$

The equation (3.4) can be rewritten with matrix form as follows:

$$\begin{Bmatrix} \varepsilon_x \\ \varepsilon_y \\ \varepsilon_z \\ \gamma_{xy} \\ \gamma_{xz} \\ \gamma_{yz} \end{Bmatrix} = \underbrace{\begin{bmatrix} \dfrac{\partial}{\partial x} & 0 & 0 & \mathrm{z}.\dfrac{\partial}{\partial x} & 0 \\ 0 & \dfrac{\partial}{\partial y} & 0 & 0 & z\dfrac{\partial}{\partial y} \\ 0 & 0 & 0 & 0 & 0 \\ \dfrac{\partial}{\partial y} & \dfrac{\partial}{\partial x} & 0 & \mathrm{z}.\dfrac{\partial}{\partial y} & \mathrm{z}.\dfrac{\partial}{\partial x} \\ 0 & 0 & \dfrac{\partial}{\partial x} & 1 & 0 \\ 0 & 0 & \dfrac{\partial}{\partial y} & 0 & 1 \end{bmatrix}}_{[D_{str}]} \underbrace{\begin{Bmatrix} u \\ v \\ w \\ \theta_x \\ \theta_y \end{Bmatrix}}_{\{\overline{X}\}}$$

Where the matrix [$D_{str}$], called the strain operator matrix, is composed of the three-operator below [78]

$$\{\beta\}=\underbrace{\begin{bmatrix}\frac{\partial}{\partial x} & 0 & 0 & 0 & 0\\ 0 & \frac{\partial}{\partial y} & 0 & 0 & 0\\ 0 & 0 & 0 & 0 & 0\\ \frac{\partial}{\partial y} & \frac{\partial}{\partial x} & 0 & 0 & 0\end{bmatrix}}_{[D_{mem}]}\underbrace{\begin{Bmatrix}u\\ v\\ w\\ \theta_x\\ \theta_y\end{Bmatrix}}_{\{\overline{X}\}} \quad , \quad \{\chi\}=\underbrace{\begin{bmatrix}0 & 0 & 0 & \frac{\partial}{\partial x} & 0\\ 0 & 0 & 0 & 0 & \frac{\partial}{\partial y}\\ 0 & 0 & 0 & 0 & 0\\ 0 & 0 & 0 & \frac{\partial}{\partial y} & \frac{\partial}{\partial x}\end{bmatrix}}_{[D_{ben}]}\underbrace{\begin{Bmatrix}u\\ v\\ w\\ \theta_x\\ \theta_y\end{Bmatrix}}_{\{\overline{X}\}}$$

$$\{\gamma\}=\underbrace{\begin{bmatrix}0 & 0 & \frac{\partial}{\partial x} & 1 & 0\\ 0 & 0 & \frac{\partial}{\partial y} & 0 & 1\end{bmatrix}}_{[D_{she}]}\underbrace{\begin{Bmatrix}u\\ v\\ w\\ \theta_x\\ \theta_y\end{Bmatrix}}_{\{\overline{X}\}} \tag{3.5}$$

We can reorganize the strain $\{\varepsilon\}$ vector as follows [78]:

$$\{\varepsilon\}=\begin{Bmatrix}\varepsilon_{mb}\\ \varepsilon_s\end{Bmatrix}=\begin{Bmatrix}\overset{\text{membrane deformation}}{\{\beta\}} + \overset{\text{bending deformation}}{z\{\chi\}}\\ \underset{\text{shear deformation}}{\{\gamma\}}\end{Bmatrix} \tag{3.6}$$

In which $\beta$, $\chi$ and $\gamma$ are the membrane, bending and shear deformation vectors, respectively. [$D_{mem}$], [$D_{ben}$] and [$D_{she}$] are the membrane, bending and shear operator's matrices, respectively. $\{\varepsilon_{mb}\}$ is the membrane-bending deformation vector and $\varepsilon_s$ is the shear deformation vector.

## 3.4. Theoretical Formulation for Composite Material

### 3.4.1. Stress- Strain Relationships

The constitutive equation for such a Nano-composite layer can be presented in the following form of the relationship between strain and stress [81]:

$$\{\sigma\}=\sum_{k=1}^{N}\left[Q_{ij}^{(k)}\right]\{\varepsilon\} \tag{3.7}$$

$$\begin{Bmatrix}\sigma_x\\ \sigma_y\\ \tau_{yz}\\ \tau_{xz}\\ \tau_{xy}\end{Bmatrix}=\begin{bmatrix}Q_{11}^{(k)} & Q_{12}^{(k)} & 0 & 0 & 0\\ Q_{21}^{(k)} & Q_{22}^{(k)} & 0 & 0 & 0\\ 0 & 0 & Q_{44}^{(k)} & 0 & 0\\ 0 & 0 & 0 & Q_{55}^{(k)} & 0\\ 0 & 0 & 0 & 0 & Q_{66}^{(k)}\end{bmatrix}\begin{Bmatrix}\varepsilon_x\\ \varepsilon_y\\ \gamma_{yz}\\ \gamma_{xz}\\ \gamma_{xy}\end{Bmatrix} \tag{3.8}$$

$Q_{ij}^{(k)}$ are the elastic constants. These are formulated for composite plates in equations (3.9) and (3.10) for both types of composite reinforced with CNTs and GPLs, respectively, as follows:

$$Q_{11}^{(k)}=\frac{E_{11}^{(k)}}{1-\nu_{12}\nu_{21}},Q_{22}^{(k)}=\frac{E_{22}^{(k)}}{1-\nu_{12}\nu_{21}},Q_{12}^{(k)}=\frac{E_{11}^{(k)}\nu_{21}}{1-\nu_{12}\nu_{21}},Q_{44}^{(k)}=G_{23}^{(k)},Q_{55}^{(k)}=G_{13}^{(k)},Q_{66}^{(k)}=G_{12}^{(k)} \tag{3.9}$$

$$Q_{11}^{(k)}=Q_{22}^{(k)}=\frac{E_{eff}^{(k)}}{1-\left(\nu_{eff}^{(k)}\right)^2},\quad Q_{12}^{(k)}=\frac{\nu_{eff}^{(k)}\,E_{22}^{(k)}}{1-\left(\nu_{eff}^{(k)}\right)^2},\quad Q_{44}^{(k)}=Q_{55}^{(k)}=Q_{66}^{(k)}=\frac{E_{eff}^{(k)}}{2\left(1+\nu_{eff}^{(k)}\right)} \tag{3.10}$$

If the fibers are oriented inside the composite plate the subscript equation, (3.7) can be rewritten as:

$$\{\sigma\}=\sum_{k=1}^{N}\left[\overline{Q_{ij}^{(k)}}\right]\{\varepsilon\} \tag{3.11}$$

In which $\overline{Q_{ij}^{(k)}}$ are determined as [81]:

$$\overline{Q_{11}^{(k)}}=Q_{11}^{(k)}C^4+2\left(Q_{12}^{(k)}+2\,Q_{66}^{(k)}\right)S^2\,C^2+Q_{22}^{(k)}\,S^4 \tag{3.12}$$

$$\overline{Q_{12}^{(k)}}=\left(Q_{11}^{(k)}+Q_{22}^{(k)}-4\,Q_{66}^{(k)}\right)S^2\,C^2+Q_{12}^{(k)}\left(S^4+C^4\right) \tag{3.13}$$

$$\overline{Q_{22}^{(k)}}=Q_{11}^{(k)}\;\;S^4+2\left(Q_{12}^{(k)}+2\,Q_{66}^{(k)}\right)S^2\,C^2+Q_{22}^{(k)}\,C^4 \tag{3.14}$$

$$\overline{Q_{13}^{(k)}}=\left(Q_{11}^{(k)}-Q_{12}^{(k)}+2\,Q_{44}^{(k)}\right)S\,C^3+\left(Q_{12}^{(k)}-Q_{22}^{(k)}+2\,Q_{44}^{(k)}\right)Q_{22}^{(k)}\,S^3\,C \tag{3.15}$$

$$\overline{Q_{23}^{(k)}}=\left(Q_{11}^{(k)}-Q_{12}^{(k)}-2\,Q_{44}^{(k)}\right)S^3\,C+\left(Q_{12}^{(k)}-Q_{22}^{(k)}+2\,Q_{44}^{(k)}\right)Q_{22}^{(k)}\,S\,C^3 \tag{3.16}$$

$$\overline{Q_{33}^{(k)}}=\left(Q_{11}^{(k)}+Q_{22}^{(k)}-2\,Q_{12}^{(k)}-2\,Q_{44}^{(k)}\right)S^2\,C^2+Q_{44}^{(k)}\left(S^4+C^4\right) \tag{3.17}$$

$$\overline{Q_{44}^{(k)}} = Q_{11}^{(k)}\ C^2 + Q_{66}^{(k)}\ S^2 \tag{3.18}$$

$$\overline{Q_{45}^{(k)}} = \left(Q_{66}^{(k)} - Q_{55}^{(k)}\right) C.S \tag{3.19}$$

$$\overline{Q_{55}^{(k)}} = Q_{55}^{(k)}\ S^2 + Q_{66}^{(k)}\ C^2 \tag{3.20}$$

The subscript *S* and *C* denote the sine and cosine.

### 3.4.2. Stress, Torque, and Shear Resultants for Composite Plate

Integrating the stresses in each lamina through the laminate thickness, the resultant forces *N*, Torques *M*, and shears $Q$ acting on a laminate cross section are defined as follows [82][83]:

$$N = \begin{Bmatrix} N_x \\ N_y \\ N_{xy} \end{Bmatrix} = \begin{bmatrix} A_{11} & A_{12} & A_{13} & B_{11} & B_{12} & B_{13} & 0 & 0 \\ A_{12} & A_{22} & A_{23} & B_{12} & B_{22} & B_{23} & 0 & 0 \\ A_{13} & A_{23} & A_{33} & B_{13} & B_{23} & B_{33} & 0 & 0 \end{bmatrix} \begin{Bmatrix} \varepsilon_{xx} \\ \varepsilon_{yy} \\ \varepsilon_{xy} \\ \kappa_{xx} \\ \kappa_{yy} \\ \kappa_{xy} \\ \gamma_{yz} \\ \gamma_{xz} \end{Bmatrix} \tag{3.21}$$

$$M = \begin{Bmatrix} M_x \\ M_y \\ M_{xy} \end{Bmatrix} = \begin{bmatrix} B_{11} & B_{12} & B_{13} & D_{11} & D_{12} & D_{13} & 0 & 0 \\ B_{12} & B_{22} & B_{23} & D_{12} & D_{22} & D_{23} & 0 & 0 \\ B_{13} & B_{23} & B_{33} & D_{13} & D_{23} & D_{33} & 0 & 0 \end{bmatrix} \begin{Bmatrix} \varepsilon_{xx} \\ \varepsilon_{yy} \\ \varepsilon_{xy} \\ \kappa_{xx} \\ \kappa_{yy} \\ \kappa_{xy} \\ \gamma_{yz} \\ \gamma_{xz} \end{Bmatrix} \tag{3.22}$$

$$Q = \begin{Bmatrix} Q_x \\ Q_y \end{Bmatrix} = \begin{bmatrix} 0 & 0 & 0 & 0 & 0 & 0 & F_{44} & F_{45} \\ 0 & 0 & 0 & 0 & 0 & 0 & F_{45} & F_{55} \end{bmatrix} \begin{Bmatrix} \varepsilon_{xx} \\ \varepsilon_{yy} \\ \varepsilon_{xy} \\ \kappa_{xx} \\ \kappa_{yy} \\ \kappa_{xy} \\ \gamma_{yz} \\ \gamma_{xz} \end{Bmatrix} \tag{3.23}$$

Where:

$N_{xx}$ and $N_{yy}$ represent the resultant normal forces in the *x* and *y* directions, respectively.

$N_{xy}$ denotes the shear force resultant.

$M_{xx}$ and $M_{yy}$ are the resultant bending Torques in the o*yz* and o*xz* planes, respectively. While $M_{xy}$ is the resultant twisting torque (torsion).

$Q_x$ and $Q_y$ are the resultant shear forces in the *x* and *y* direction, respectively.

With accumulate form:

$$\begin{Bmatrix} \{N_{x,y,xy}\} \\ \{M_{x,y,xy}\} \\ \{Q_{x,y}\} \end{Bmatrix} = \begin{bmatrix} [A_{ij}]_{ortho} & [B_{ij}]_{ortho} & 0 \\ [B_{ij}]_{ortho} & [D_{ij}]_{ortho} & 0 \\ 0 & 0 & [F_{ij}]_{ortho} \end{bmatrix} \begin{Bmatrix} \{\varepsilon_{xx,yy:,xy}\} \\ \{\kappa_{xx,yy,xy}\} \\ \{\gamma_{xz,yz}\} \end{Bmatrix} \tag{3.24}$$

Where, the subscript $A_{ij}$, $B_{ij}$, $D_{ij}$ refer to the membrane, membrane-bending (coupling) and bending stiffness matrices respectively, along with the shear stiffness matrix $F_{ij}$ for the orthotropic plates. These are expressed as:

$$A_{ij} = \sum_{k=1}^{N_L} \int_{z_k}^{z_{k+1}} Q_{ij}^{(k)}.dz\,, \qquad (i, j = 1,2,3) \tag{3.25}$$

$$B_{ij} = \sum_{k=1}^{N_L} \int_{z_k}^{z_{k+1}} Q_{ij}^{(k)}\ z.dz \qquad (i, j = 1,2,3) \tag{3.26}$$

$$D_{ij} = \sum_{k=1}^{N_L} \int_{z_k}^{z_{k+1}} Q_{ij}^{(k)}\ z^2.dz \qquad (i, j = 1,2,3) \tag{3.27}$$

$$F_{ij} = (5/6)\sum_{k=1}^{N_L}\int_{z_k}^{z_{k+1}} Q_{ij}^{(k)}.dz \qquad (i,j=4,5) \tag{3.28}$$

$Z_{k+1}$ and $Z_k$ are the positions of the top and bottom surfaces of the considered layer, respectively.

## 3.5. Theoretical Formulation for an Elastic Plate

### 3.5.1. Stress-Strain Relationships

The stress-strain relationship for homogeneous isotropic lamina is [84] [83][76]:

$$\begin{Bmatrix}\sigma_x\\ \sigma_y\\ \sigma_z\\ \tau_{xy}\\ \tau_{xz}\\ \tau_{yz}\end{Bmatrix} = \begin{Bmatrix}\frac{E}{1-\nu^2}\varepsilon_x + \frac{\nu E}{1-\nu^2}\varepsilon_y\\ \frac{E}{1-\nu^2}\varepsilon_y + \frac{\nu E}{1-\nu^2}\varepsilon_x\\ 0\\ \frac{E}{2(1+\nu)}\gamma_{xy}\\ \frac{E}{2(1+\nu)}\gamma_{xz}\\ \frac{E}{2(1+\nu)}\gamma_{yz}\end{Bmatrix} \tag{3.29}$$

Decomposed the equation (3.29), we can write the stress vector {σ} with following matrix form:

$$\begin{Bmatrix}\sigma_x\\ \sigma_y\\ \sigma_z\\ \tau_{xy}\\ \tau_{xz}\\ \tau_{yz}\end{Bmatrix} = \frac{E}{1-\nu^2}\underbrace{\begin{bmatrix}\overbrace{\begin{bmatrix}1 & \nu & 0 & 0\\ \nu & 1 & 0 & 0\\ 0 & 0 & 0 & 0\\ 0 & 0 & 0 & \frac{1-\nu}{2}\end{bmatrix}}^{C_{mb}} & \begin{matrix}0 & 0\\ 0 & 0\\ 0 & 0\\ 0 & 0\end{matrix}\\ \begin{matrix}0 & 0 & 0 & 0\\ 0 & 0 & 0 & 0\end{matrix} & \underbrace{\begin{bmatrix}\frac{1-\nu}{2} & 0\\ 0 & \frac{1-\nu}{2}\end{bmatrix}}_{C_s}\end{bmatrix}}_{[C]}\begin{Bmatrix}\varepsilon_{xx}\\ \varepsilon_{yy}\\ \varepsilon_{zz}\\ \gamma_{xy}\\ \gamma_{xz}\\ \gamma_{yz}\end{Bmatrix} \tag{3.30}$$

In which $\nu$ is the Poisson's ratio, and $E$ is the Young modulus of the isotropic material.

$[C]$ is the global elastic constants matrix.
$[C_{mb}]$ is the elastic constants matrix for membrane and bending deformation.
$[C_s]$ is the elastic constants matrix for shear deformation.

$$\begin{Bmatrix} \sigma_{mb} \\ \sigma_s \end{Bmatrix} = \begin{bmatrix} [C_{mb}] & 0 \\ 0 & [C_s] \end{bmatrix} \begin{Bmatrix} \varepsilon_{mb} \\ \varepsilon_s \end{Bmatrix} \tag{3.31}$$

$\{\sigma_{mb}\}$ and $\{\sigma_s\}$ are the membrane-bending and shear stress.

### 3.5.2. Stress, Torque, and Shear Resultants

The Mindlin plate theory assumes that the normal stresses in the thickness direction are negligible within the volume of the plate ($\sigma_z = 0$). For an isotropic material the stress, torque, and shear resultants are given by substitute equation (3.6) in (3.32), these are [85][79][86] [78]:

$$\begin{Bmatrix} N_x \\ N_y \\ N_{xy} \end{Bmatrix} = \int_{-h/2}^{h/2} \begin{Bmatrix} \sigma_x \\ \sigma_y \\ \tau_{xy} \end{Bmatrix} dz = \int_{-h/2}^{h/2} \{\sigma_{mb}\}\, dz = \int_{-h/2}^{h/2} [C_{mb}]\{\varepsilon_{mb}\}\, dz \tag{3.32}$$

$$= \int_{-h/2}^{h/2} [C_{mb}](\{\beta\} + z\{\chi\})\, dz$$
$$= \int_{-h/2}^{h/2} [C_{mb}]\{\beta\}\, dz + \int_{-h/2}^{h/2} z[C_{mb}]\{\chi\}\, dz$$
$$= [A]_{Elas}\{\beta\} + [B]_{Elas}\{\chi\}$$

The Torques resultants, $M_x$, $M_y$ and $M_{xy}$ are:

$$\begin{Bmatrix} M_x \\ M_y \\ M_{xy} \end{Bmatrix} = \int_{-h/2}^{h/2} z \begin{Bmatrix} \sigma_x \\ \sigma_y \\ \tau_{xy} \end{Bmatrix} dz = \int_{-h/2}^{h/2} z\{\sigma_{mb}\}\, dz = \int_{-h/2}^{h/2} z[C_{mb}]\{\varepsilon_{mb}\}\, dz$$

$$= \int_{-h/2}^{h/2} z[C_{mb}](\{\beta\} + z\{\chi\})\, dz \tag{3.33}$$

$$= \int_{-h/2}^{h/2} z[C_{mb}]\{\beta\}\, dz + \int_{-h/2}^{h/2} z^2[C_{mb}]\{\chi\}\, dz$$

$$= \quad [B]_{Elas}\{\beta\} \quad + \quad [D]_{Elas}\{\chi\}$$

The Shear resultants, $Q_x$, $Q_y$ are:

$$\begin{Bmatrix} Q_x \\ Q_y \end{Bmatrix} = \int_{-h/2}^{h/2} \begin{Bmatrix} \gamma_{xz} \\ \gamma_{yz} \end{Bmatrix} dz = \int_{-h/2}^{h/2} \{\sigma_s\}\, dz = \int_{-h/2}^{h/2} \left( [C_s]\{\varepsilon_s\} \right) dz \tag{3.34}$$

$$= \int_{-h/2}^{h/2} [C_s]\{\gamma\}\, dz$$

$$= \quad [F]_{Elas}\{\gamma\}$$

We can assemble the last three equations (3.32), (3.33) and (3.34) in the following resume equation [86] :

$$\begin{Bmatrix} N_{x,y,xy} \\ M_{x,y,xy} \\ Q_{x,y} \end{Bmatrix} = \begin{bmatrix} [A_{ij}]_{Elas} & [B_{ij}]_{Elas} & 0 \\ [B_{ij}]_{Elas} & [D_{ij}]_{Elas} & 0 \\ 0 & 0 & [F_{ij}]_{Elas} \end{bmatrix} \begin{Bmatrix} \varepsilon_{xx,yy,xy} \\ \kappa_{xx,yy,xy} \\ \gamma_{xz,yz} \end{Bmatrix} \tag{3.35}$$

Where $A_{ij}$, $B_{ij}$, $D_{ij}$, $F_{ij}$ are the membrane, bending, membrane-bending (coupling), and shear stiffness matrices for the elastic (*Elas*) plate, respectively.

### 3.6. Energy Conservation by Hamilton's Principle

Hamilton's principle is a universal principle that governs the motion of a wide range of mechanical systems. It states that the actual trajectory of a system between two points in time is the one that extremizes the time integral of the Lagrangian function. This is achieved if the variation of the time integral of the Lagrangian is set to zero [87][88][89]:

$$\delta \int_{t_0}^{t_1} \left( E_k - E_s + W \right) dt = 0 \tag{3.36}$$

$\delta$ is the variation operator.

Hamilton's principle can be used to derive the equations of motion and boundary conditions for a mechanical systems, given the strains $E_S$, external work $W$, and kinetic energy $E_k$. To accomplish this, the equations of these quantities are substituted into

Hamilton's principle equation, and the coefficients of the virtual displacements are set to zero. The Lagrangian for the three-dimensional elasticity problem is:

$$L = E_k - E_s + W \tag{3.37}$$

### 3.6.1. Kinetic Energy

The Lagrange is defined as the difference between the kinetic energy and potential energy of the system. For an isotropic plate, the kinetic energy is given by:

$$E_k = \frac{1}{2}\int_V \rho\, \dot{X}^2\, dV = \frac{1}{2}\int_V \rho\, \dot{X}^T \dot{X}\, dV \tag{3.38}$$

$\rho$ is the material density of the elastic considered plate and $V$ is the volume of the plate. Substituting equation (3.3) into equation (3.38), one obtains:

$$\begin{aligned} E_k &= \frac{1}{2}\rho\int_V \left( \left\{\overline{\dot{X}}\right\}^T \left[L_{tra}\right]^T - z\left\{\overline{\dot{X}}\right\}^T \left[L_{rot}\right]^T \right)\left( \left[L_{tra}\right]\left\{\overline{\dot{X}}\right\} - z\left[L_{rot}\right]\left\{\overline{\dot{X}}\right\} \right) dV \\ &= \frac{1}{2}\rho\int_V \left\{\overline{\dot{X}}\right\}^T \left( \left[L_{tra}\right]^T - z\left[L_{rot}\right]^T \right)\left( \left[L_{tra}\right] - z\left[L_{rot}\right] \right)\left\{\overline{\dot{X}}\right\} dV \\ &= \frac{1}{2}\rho\int_V \left\{\overline{\dot{X}}\right\}^T \left( \left[L_{tra}\right]^T \left[L_{tra}\right] - z\left( \left[L_{tra}\right]^T \left[L_{rot}\right] + \left[L_{rot}\right]^T \left[L_{tra}\right] \right) + z^2 \left[L_{rot}\right]^T \left[L_{rot}\right] \right)\left\{\overline{\dot{X}}\right\} dV \end{aligned} \tag{3.39}$$

Integrating the kinetic energy through the thickness direction between the born [*-h/2, h/2*], the equation (3.39) will be:

$$E_k = \frac{1}{2}\int_A \left\{\overline{\dot{X}}\right\}^T \underbrace{\rho\left( h_c \left[L_{tra}\right]^T \left[L_{tra}\right] + \frac{h_c^{\,3}}{12}\left[L_{rot}\right]^T \left[L_{rot}\right] \right)}_{\left[M\right]_{Elas}} \left\{\overline{\dot{X}}\right\} dA \tag{3.40}$$

Where $[M]_{Elas}$ is the mass matrix for the elastic plate and $A$ the area of plate. By replacing $[L_{tra}]$ and $[L_{rot}]$ mentioned in equation (3.3) with their matrices, the mass matrix will be:

$$[M]_{Elas} = \rho.\begin{bmatrix} h_c & 0 & 0 & 0 & 0 \\ & h_c & 0 & 0 & 0 \\ & & h_c & 0 & 0 \\ & sym & & \frac{h_c^3}{12} & 0 \\ & & & & \frac{h_c^3}{12} \end{bmatrix} \tag{3.41}$$

$h_c$ is the thickness of the plate.

### 3.6.2. Strain Energy

The strain energy was given as follow [90][88]:

$$E_s = \frac{1}{2}\int_V \{\varepsilon\}^T \underbrace{[C]\{\varepsilon\}}_{\{\sigma\}} dV \tag{3.42}$$

The integral of the strain energy density over the volume of the plate is given by substituting equations (3.6) and (3.30) in (3.42) [91]:

$$E_s = \frac{1}{2}\int_V \begin{Bmatrix} \{\beta\} + z\{\chi\} \\ \{\gamma\} \end{Bmatrix}^T \begin{bmatrix} [C_{mb}] & 0 \\ 0 & [C_c] \end{bmatrix} \begin{Bmatrix} \{\beta\} + z\{\chi\} \\ \{\gamma\} \end{Bmatrix} dV$$

$$E_s = \frac{1}{2}\int_V \left(\{\beta\} + z\{\chi\}\right)[C_{mb}]\left(\{\beta\} + z\{\chi\}\right) + \{\gamma\}[C_c]\{\gamma\}\, dV$$

$$E_s = \frac{1}{2}\int_V \underbrace{\{\beta\}^T[C_{mb}]\{\beta\}}_{Membrane} + \underbrace{\left(\{\beta\}^T[C_{mb}]z\{\chi\} + z\{\chi\}^T[C_{mb}]\{\beta\}\right)}_{Membrane-Bending} + \underbrace{z\{\chi\}^T[C_{mb}]z\{\chi\}}_{Bending} + \underbrace{\{\gamma\}^T[C_c]\{\gamma\}}_{Shear} dV \tag{3.43}$$

Where $[C_{mb}]$ and $[C_c]$ represent the elastic constant matrices for the membrane bending and shear effect, respectively.

As we have four sections of deformations, equation (3.43) may divide into the following parts:

3.6.2.1. *Membrane deformation*

$$\begin{aligned} E_s^m &= \frac{1}{2}\int_V \{\beta\}^T [C_{mb}]\{\beta\}\, dV \\ &= \frac{1}{2}\int_A \int_{-h/2}^{+h/2} \{\beta\}^T [C_{mb}]\{\beta\}\, dz.dA \\ &= \frac{1}{2}\int_A \{\beta\}^T \underbrace{h_c [C_{mb}]}_{[A]_{Elas}} \{\beta\}\, dA \end{aligned} \tag{3.44}$$

In which $[A]_{Elas} = h_c\,[C_{mb}]$.

3.6.2.2. *Bending deformation*

$$\begin{aligned} E_s^b &= \frac{1}{2}\int_V z.\{\chi\}^T [C_{mb}]\, z.\{\chi\}\, dV \\ &= \frac{1}{2}\int_A \int_{-h/2}^{+h/2} z^2 \{\chi\}^T [C_{mb}]\{\chi\}\, dz.dA \\ &= \frac{1}{2}\int_A \{\chi\}^T \underbrace{\frac{h_c^3}{12}[C_{mb}]}_{[D]_{Elas}} \{\chi\}\, dA \end{aligned} \tag{3.45}$$

In which $[D]_{Elas} = (h_c^3/12)\,[C_{mb}]$.

3.6.2.3. *Membrane-Bending deformation*

$$\begin{aligned} E_s^{m-b} &= \frac{1}{2}\int_V \{\beta\}[C_{mb}]\, z.\{\chi\} + z.\{\chi\}^T [C_{mb}]\{\beta\}\, dV \\ &= \frac{1}{2}\int_A \int_{-h/2}^{+h/2} z\left(\{\beta\}[C_{mb}]\{\chi\} + \{\chi\}^T [C_{mb}]\{\beta\}\right) dz.dA \\ &= 0 \end{aligned} \tag{3.46}$$

The membrane bending energy is equal to zero because of the symmetry of the structure by her mid-plan.

3.6.2.4. *Shear deformation*

$$\begin{aligned} E_s^s &= \frac{1}{2}\int_V \{\gamma\}^T [C_s]\{\gamma\}\, dV \\ &= \frac{1}{2}\int_A \int_{-h/2}^{+h/2} \{\gamma\}^T [C_s]\{\gamma\}\, dz.dA \\ &= \frac{1}{2}\int_A \{\gamma\}^T \underbrace{k\, h_c [C_s]}_{[F]_{Elas}} \{\gamma\}\, dA \end{aligned} \tag{3.47}$$

In which $[F]_{Elas} = k\, h_c\, [C_s]$, and $k$ is the shear correction factor.

3.6.3. External Forces Works

The work obtained due to the forces applied to the plate structure may depend on the type of force. It can be expressed in the following formulation forms [92]:

3.6.3.1. *Body load*

$$W_V = \int_V \{U\}^T \{F_V\}\, dV \tag{3.48}$$

3.6.3.2. *Surface load*

$$W_S = \int_S \{U\}^T \{F_S\}\, dS \tag{3.49}$$

3.6.3.3. *Concentrated load*

$$W_P = \{U\}^T \{F_P\} \tag{3.50}$$

## 3.7. Theoretical Formulation for Piezoelectric Plate

Most of the practical piezoelectric materials used in sensor and actuator applications are elastic and isotropic. They are poled in a specific direction. For our study, we suppose that it is poled throw its thickness direction. The behavior law of piezoelectricity, which relies upon the mechanical properties with electrical ones is given in the following [93]:

- *Direct Effect of Piezoelectricity:*

$$\begin{Bmatrix} D_x \\ D_y \\ D_z \end{Bmatrix} = \begin{bmatrix} \overbrace{\begin{bmatrix} 0 & 0 & 0 & 0 \\ 0 & 0 & 0 & 0 \\ e_{31} & e_{31} & e_{33} & 0 \end{bmatrix}}^{[e_{mb}]} & \underbrace{\begin{bmatrix} 0 & e_{15} \\ e_{15} & 0 \\ 0 & 0 \end{bmatrix}}_{[e_s]} \end{bmatrix} \begin{Bmatrix} \left.\begin{matrix} \varepsilon_x \\ \varepsilon_y \\ \varepsilon_z \\ \gamma_{xy} \end{matrix}\right\}\varepsilon_{mb} \\ \left.\begin{matrix} \gamma_{xz} \\ \gamma_{yz} \end{matrix}\right\}\varepsilon_s \end{Bmatrix} + \begin{bmatrix} d_{11} & 0 & 0 \\ 0 & d_{22} & 0 \\ 0 & 0 & d_{33} \end{bmatrix} \begin{Bmatrix} E_x \\ E_y \\ E_z \end{Bmatrix} \tag{3.51}$$

- *Inverse Effect of Piezoelectricity:*

$$\begin{Bmatrix} \sigma_x \\ \sigma_y \\ \sigma_z \\ \tau_{xy} \\ \tau_{xz} \\ \tau_{yz} \end{Bmatrix} = \begin{bmatrix} \overbrace{\begin{bmatrix} C_{11} & C_{12} & C_{13} & 0 \\ C_{21} & C_{22} & C_{23} & 0 \\ C_{31} & C_{32} & C_{33} & 0 \\ 0 & 0 & 0 & C_{66} \end{bmatrix}}^{[C_{mb}]} & 0 \\ 0 & \underbrace{\begin{bmatrix} C_{44} & 0 \\ 0 & C_{44} \end{bmatrix}}_{[C_s]} \end{bmatrix} \begin{Bmatrix} \left.\begin{matrix} \varepsilon_x \\ \varepsilon_y \\ \varepsilon_z \\ \gamma_{xy} \end{matrix}\right\}\varepsilon_{mb} \\ \left.\begin{matrix} \gamma_{xz} \\ \gamma_{yz} \end{matrix}\right\}\varepsilon_s \end{Bmatrix} - \begin{bmatrix} \overbrace{\begin{bmatrix} 0 & 0 & e_{31} \\ 0 & 0 & e_{31} \\ 0 & 0 & e_{33} \\ 0 & 0 & 0 \end{bmatrix}}^{[e_{mb}]^t} \\ \underbrace{\begin{bmatrix} 0 & e_{15} & 0 \\ e_{15} & 0 & 0 \end{bmatrix}}_{[e_s]^t} \end{bmatrix} \begin{Bmatrix} E_x \\ E_y \\ E_z \end{Bmatrix} \tag{3.52}$$

Where:

$\{D\}$ is the electric displacement array.

$[e_{mb}]$ and $[e_s]$ are the piezoelectric stress constants for membrane-bending and shear effects, respectively.

$[d]$ is the electrical permittivity for constant mechanical strain.

$\{E\}$ is the electrical field intensity.

### 3.8. Electrical Field Intensity

The electrical charge field witch penetrate the piezoelectric plate throw its thickness is distributed linearly through the thickness direction yields [93][94][95]. The electric field derive a potential [92][94]:

$$E_x = E_y = 0, \qquad E_z = -\frac{d\phi_z}{dz}$$

$$\phi_z = -\int_{-h_p/2}^{+h_p/2} E_z dz = -E_z.h_p \quad \Rightarrow \quad E_z = -\frac{\phi_z}{h_p} \tag{3.53}$$

Where $h_p$ is the thickness of the piezoelectric plate figure (3.2) and $\phi_z$ is the electrical voltage (potential) applied to the piezoelectric plate (piezo-plate).

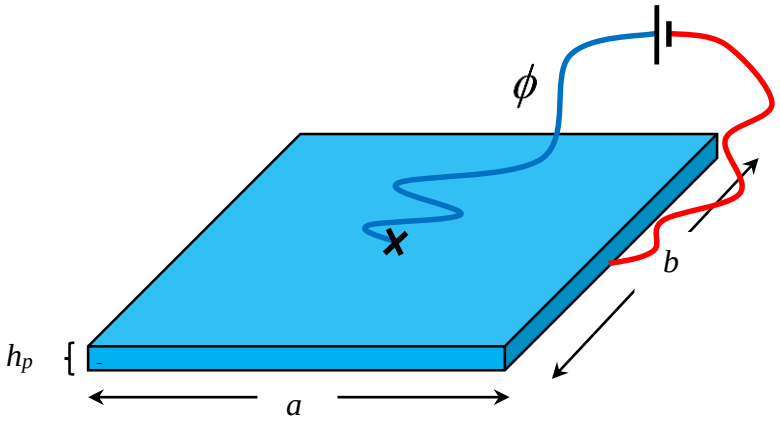


**Figure 3.2:** Piezoelectric plate.

We can write the equation (3.53) in matrix form as follow:

$$\{E\} = \begin{bmatrix} 0 & 0 & 0 \\ 0 & 0 & 0 \\ 0 & 0 & -1/h_p \end{bmatrix} \begin{Bmatrix} 0 \\ 0 \\ \phi_z \end{Bmatrix} = [D_\phi]\{\bar{\phi}\} \tag{3.54}$$

Where $D_\phi$ is the potential operator matrix, and $\bar{\phi}$ is the electrical potentials vector.

### 3.9. Kinetic Energy for Piezoelectric Plate

In the above, we say that piezoelectric plates are isotropic, so we can deduce the kinetic energy for piezoelectric plate from equation (3.40) as follow:

$$E_k = \frac{1}{2}\int_A \{\dot{\bar{X}}\}^T \underbrace{\rho_p \left( h_p [L_{tra}]^T [L_{tra}] + \frac{h_p^{\,3}}{12} [L_{rot}]^T [L_{rot}] \right)}_{[M]_{piezo}} \{\dot{\bar{X}}\} dA \tag{3.55}$$

$\rho_p$ is the density of the piezoelectric plate, and $[M]_{piezo}$ is the matrix of the piezoelectric plate:

$$[M]_{piezo} = \rho_p . \begin{bmatrix} h_p & 0 & 0 & 0 & 0 \\ & h_p & 0 & 0 & 0 \\ & & h_p & 0 & 0 \\ & sym & & \frac{h_p{}^3}{12} & 0 \\ & & & & \frac{h_p{}^3}{12} \end{bmatrix} \tag{3.56}$$

## 3.10. Strain Energy for Piezoelectric Plate

The strain energy for the piezoelectric plate is composed of an elastic strain energy and an electric strain energy [96][97]:

$$E_s = E_{Elas-s} - E_{Elec-s} = \underbrace{\frac{1}{2}\int_V \{\sigma\}^T \{\varepsilon\} dV}_{Elastic} - \underbrace{\frac{1}{2}\int_V \{D\}^T \{E\} dV}_{Electric} \tag{3.57}$$

Substituting the stress vector and electrical displacement vector (equation (1.1)) in equation (3.57) we get:

$$E_s = \frac{1}{2}\int_V \left([C]\{\varepsilon\} - [e]^T \{E\}\right)^T \{\varepsilon\} dV - \frac{1}{2}\int_V \left([e]\{\varepsilon\} + [d]^T \{E\}\right)^T \{E\} dV \tag{3.58}$$

Then, we substitute equation (3.51) and (3.52) in the above equation, we found [92]:

$$\begin{aligned} E_s = & \underbrace{\frac{1}{2}\int_V \begin{Bmatrix} \varepsilon_{mb} \\ \varepsilon_s \end{Bmatrix}^T \begin{bmatrix} C_{mb} & 0 \\ 0 & C_s \end{bmatrix} \begin{Bmatrix} \varepsilon_{mb} \\ \varepsilon_s \end{Bmatrix} dV}_{Elastic} - \underbrace{\frac{1}{2}\int_V \{E\}^T [d]\{E\} dV}_{dielectric} \\ & \underbrace{- \left( \frac{1}{2}\int_V \{E\}^T \begin{bmatrix} [e_{mb}] & [e_s] \end{bmatrix} \begin{Bmatrix} \varepsilon_{mb} \\ \varepsilon_s \end{Bmatrix} dV + \frac{1}{2}\int_V \begin{Bmatrix} \varepsilon_{mb} \\ \varepsilon_s \end{Bmatrix}^T \begin{bmatrix} [e_{mb}]^T \\ [e_s]^T \end{bmatrix} \{E\} dV \right)}_{piezoelectric} \end{aligned} \tag{3.59}$$

### 3.10.1. Elastic strain energy

The elastic energy for the piezoelectric plate is assumed to be equivalent to the elastic energy derived in section 3.4.2, with different elastic constants. This similarity is obtained because the piezoelectric material is considered isotropic in its thickness direction, and the shear effects within this material are not deemed significant, $\gamma_{yz} = \gamma_{xz} = 0$.

$$E_{s-elast} = \frac{1}{2}\int_V \{\varepsilon_{mb}\}^T [C_{mb}]\{\varepsilon_{mb}\}\, dV \tag{3.60}$$

3.10.2. Piezoelectric strain energy

$$E_{s-piezo} = -\frac{1}{2}\int_V \left(\{E\}^T [e_{mb}]\{\varepsilon_{mb}\} + \{\varepsilon_{mb}\}^T [e_{mb}]^T \{E\}\right) dV \tag{3.61}$$

Substitute $\{\varepsilon_{mb}\}$ by her expression mentioned in equation (3.6) in the previous equation:

$$E_{s-piezo} = -\frac{1}{2}\int_V \left(\{E\}^T [e_{mb}]\{\{\beta\} + z\{\chi\}\} + \{\{\beta\} + z\{\chi\}\}^T [e_{mb}]^T \{E\}\right) dV$$

$$E_{s-piezo} = -\frac{1}{2}\int_V \left(\{E\}^T [e_{mb}]\{\beta\} + \{E\}^T [e_{mb}] z\{\chi\} + \{\beta\}^T [e_{mb}]^T \{E\} + z\{\chi\}^T [e_{mb}]^T \{E\}\right) dV \tag{3.62}$$

By integrating of the equation (3.61) between [$-h_p/2 + h_p/2$] we found:

$$E_{s-piezo} = -\frac{1}{2} h_p \int_A \left(\{E\}^T [e_{mb}]\{\beta\} + \{\beta\}^T [e_{mb}]^T \{E\}\right) dA \tag{3.63}$$

3.10.3. Dielectric strain energy

$$\begin{aligned} E_{s-dielec} &= -\frac{1}{2}\int_V \{E\}^T [d]^T \{E\}\, dV \\ E_{s-dielec} &= \frac{1}{2} h_p \int_A \{E\}^T [d]^T \{E\}\, dA \end{aligned} \tag{3.64}$$

3.10.4. External Forces Works

The external forces that can be applied to the piezoelectric plate are both mechanical and electrical forces. The mechanical forces (volume, surface, and point forces) are described as in section 3.4.3, while the electrical force is expressed as follows [97]:

$$W_{electric} = -\int_A \{\bar{\phi}\}^T \{D\}\, dA \tag{3.65}$$

### 3.11. Theoretical Formulation for Piezoelectric Sandwich Plate

The objective of presenting the formulation of a piezoelectric sandwich plate is to prepare for active vibration control. A piezoelectric sandwich plate consists of a nanocomposite core reinforced by nanofillers, with two piezoelectric plates covering the top and bottom surfaces of the nanocomposite (Figure 3.3). The governing behavior laws of the piezoelectric sandwich plate, which link the piezoelectric plates to the nanocomposite core, are as follows:

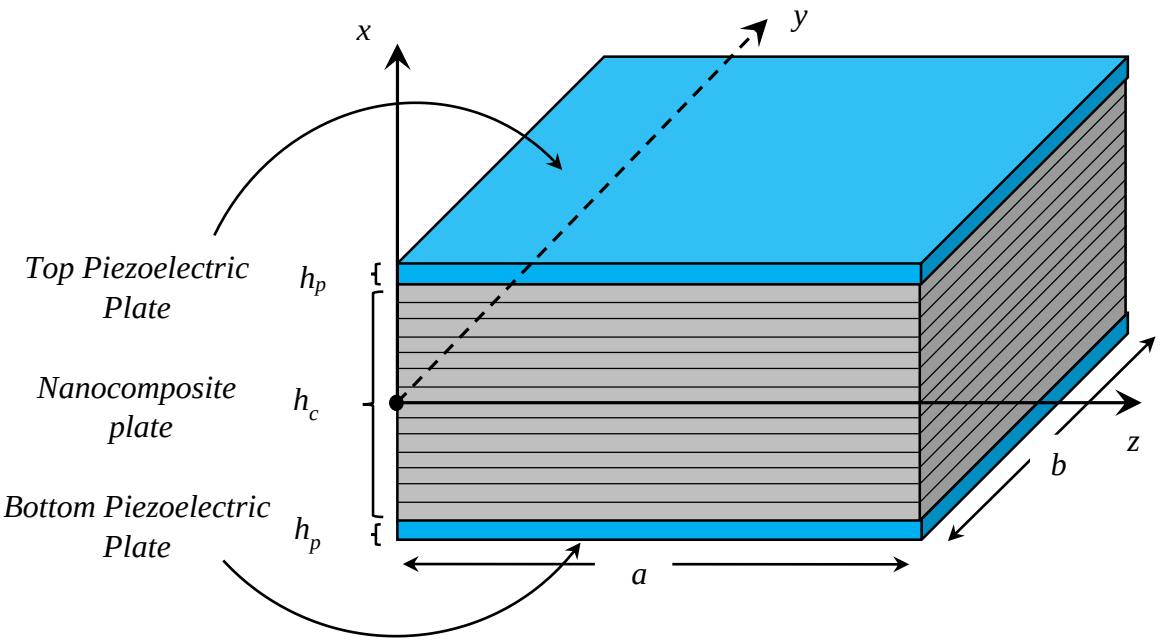


**Figure 3.3:** Sandwich plate made of composite in heart and covered by two piezoelectric plates.

#### 3.11.1. Kinetic Energy for Piezoelectric Sandwich Plate

The kinetic energy of the piezoelectric sandwich plate can be expressed as the sum of the kinetic energy of the elastic plate (as detailed in section 3.6.1) and the kinetic energy of the top and bottom piezoelectric plates. It is assumed that both piezoelectric plates have the same thickness, $h_p$. This can be formulated as follows:

$$E_k^{sandwich} = E_k^{Bottom-piezo} + E_k^{Nanocomposite} + E_k^{Top-piezo} \tag{3.66}$$

$$E_k^{sandwich} = \frac{1}{2}\int_A \left\{\dot{\overline{X}}\right\}^T \rho_p \left( \int_{-h_p-\frac{h_c}{2}}^{-\frac{h_c}{2}} \begin{pmatrix} \left[L_{tra}\right]^T\left[L_{tra}\right] - z\left(\left[L_{tra}\right]^T\left[L_{rot}\right] + \left[L_{rot}\right]^T\left[L_{tra}\right]\right) \\ + z^2\left[L_{rot}\right]^T\left[L_{rot}\right] \end{pmatrix} dz \right) \left\{\dot{\overline{X}}\right\} dA$$
$$+ \frac{1}{2}\int_A \left\{\dot{\overline{X}}\right\}^T \rho_c \left( \int_{-\frac{h_c}{2}}^{+\frac{h_c}{2}} \begin{pmatrix} \left[L_{tra}\right]^T\left[L_{tra}\right] - z\left(\left[L_{tra}\right]^T\left[L_{rot}\right] + \left[L_{rot}\right]^T\left[L_{tra}\right]\right) \\ + z^2\left[L_{rot}\right]^T\left[L_{rot}\right] \end{pmatrix} dz \right) \left\{\dot{\overline{X}}\right\} dA$$
$$+ \frac{1}{2}\int_A \left\{\dot{\overline{X}}\right\}^T \rho_p \left( \int_{+\frac{h_c}{2}}^{+\frac{h_c}{2}+h_p} \begin{pmatrix} \left[L_{tra}\right]^T\left[L_{tra}\right] - z\left(\left[L_{tra}\right]^T\left[L_{rot}\right] + \left[L_{rot}\right]^T\left[L_{tra}\right]\right) \\ + z^2\left[L_{rot}\right]^T\left[L_{rot}\right] \end{pmatrix} dz \right) \left\{\dot{\overline{X}}\right\} dA$$

(3.67)

After substituting equation (3.3) and integrating the expression through the thickness direction, the following mass system is obtained:

$$\left[M\right]^{sandwich} = \begin{bmatrix} M_1^{sandwich} & 0 & 0 & 0 & 0 \\ & M_1^{sandwich} & 0 & 0 & 0 \\ & & M_1^{sandwich} & 0 & 0 \\ & sym & & M_2^{sandwich} + M_3^{sandwich} & 0 \\ & & & & M_2^{sandwich} + M_3^{sandwich} \end{bmatrix} \quad (3.68)$$

$$M_1^{sandwich} = 2.\rho_p\, h_p + \rho_c\, h_c$$

$$M_2^{sandwich} = \rho_c \frac{h_c^3}{2}$$

$$M_3^{sandwich} = \frac{2}{3}\rho_p\left(\left(h_p + \frac{h_c}{2}\right)^3 - \left(\frac{h_c}{2}\right)^3\right)$$

With, $h_p$ and $h_c$ are the thickness of the piezoelectric and composite plate, respectively.

### 3.11.2. Strain Energy for Piezoelectric Sandwich Plate

The strain energy of the piezoelectric sandwich plate is composed of the strain energy of the two piezoelectric layers and the strain energy of the elastic core (nanocomposite). However, in this case, the integral of the strain energy for the piezoelectric layers is

calculated between the born of the bottom layer $\left[-h_p-\frac{h_c}{2},\ -\frac{h_c}{2}\right]$ and top layer $\left[+\frac{h_c}{2},\ +\frac{h_c}{2}+h_p\right]$.

$$E_s^{sandwich}=E_s^{Bottom-piezo}+E_s^{Nanocomposite}+E_s^{Top-piezo} \tag{3.69}$$

Omitting the shear effect, and due to the symmetry to the average plane of the sandwich plate, the components of equation (3.69) are [78]:

$$\begin{aligned}
&E_s^{Bottom-piezo}=E_{s-elastic}^{Bottom-piezo}+E_{s-piezoelectric}^{Bottom-piezo}+E_{s-dielectric}^{Bottom-piezo}\\
&E_{s-elastic}^{Bottom-piezo}=\frac{1}{2}\int_A\int_{-\frac{h_c}{2}-h_p}^{-\frac{h_c}{2}}\{\beta\}^T\left[C_{mb}\right]_{piezo}\{\beta\}\,dz\,dA+\frac{1}{2}\int_A\int_{-\frac{h_c}{2}-h_p}^{-\frac{h_c}{2}}z^2\{\chi\}^T\left[C_{mb}\right]_{piezo}\{\chi\}\,dz\,dA\\
&E_{s-eleastic}^{Bottom-piezo}=\frac{1}{2}\int_A\{\beta\}^T\underbrace{h_p\left[C_{mb}\right]_{piezo}}_{[A]_{Bottom-piezo}}\{\beta\}\,dA+\frac{1}{2}\int_A\{\chi\}^T\underbrace{\frac{1}{3}\left(\left(\frac{h_c}{2}+h_p\right)^3-\left(\frac{h_c}{2}\right)^3\right)\left[C_{mb}\right]_{piezo}}_{[D]_{Bottom-piezo}}\{\chi\}\,dA
\end{aligned} \tag{3.70}$$

$$\begin{aligned}
&E_{s-piezoelectric}^{Bottom-piezo}=-\left(\frac{1}{2}\int_V\{E\}^T\left[e_{mb}\right]\{\varepsilon_{mb}\}\,dV+\frac{1}{2}\int_V\{\varepsilon_{mb}\}^T\left[e_{mb}\right]^T\{E\}\,dV\right)\\
&E_{s-dielectric}^{Bottom-piezo}=-\frac{1}{2}\int_V\{E\}^T\left[d\right]^T\{E\}\,dV
\end{aligned}$$

$$E_{s-elastic}^{Nanocomp}=\frac{1}{2}\int_A\{\beta\}^T\underbrace{h_c\left[C_{mb}\right]}_{[A]_{Nanocomp}}\{\beta\}\,dA+\frac{1}{2}\int_A\{\chi\}^T\underbrace{\frac{h_c^3}{12}\left[C_{mb}\right]}_{[D]_{Nanocomp}}\{\chi\}\,dA+\frac{1}{2}\int_A\{\gamma\}^T\underbrace{k\,h_c\left[C_s\right]}_{[F]_{Nanocomp}}\{\gamma\}\,dA \tag{3.71}$$

$$\begin{aligned}
&E_s^{Top-piezo}=E_{s-elastic}^{Top-piezo}+E_{s-piezoelectric}^{Top-piezo}+E_{s-dielectric}^{Top-piezo}\\
&E_{s-elastic}^{Top-piezo}=\frac{1}{2}\int_A\int_{+\frac{h_c}{2}}^{+\frac{h_c}{2}+h_p}\{\beta\}^T\left[C_{mb}\right]_{piezo}\{\beta\}\,dz\,dA+\frac{1}{2}\int_A\int_{+\frac{h_c}{2}}^{+\frac{h_c}{2}+h_p}z^2\{\chi\}^T\left[C_{mb}\right]_{piezo}\{\chi\}\,dz\,dA\\
&E_{s-elastic}^{Top-piezo}=\frac{1}{2}\int_A\{\beta\}^T\underbrace{h_p\left[C_{mb}\right]_{piezo}}_{[A]_{Top-piezo}}\{\beta\}\,dA+\frac{1}{2}\int_A\{\chi\}^T\underbrace{\frac{1}{3}\left(\left(\frac{h_c}{2}+h_p\right)^3-\left(\frac{h_c}{2}\right)^3\right)\left[C_{mb}\right]_{piezo}}_{[D]_{Top-piezo}}\{\chi\}\,dA
\end{aligned} \tag{3.72}$$

$$\begin{aligned}
&E_{s-piezoelectric}^{Top-piezo}=-\left(\frac{1}{2}\int_V\{E\}^T\left[e_{mb}\right]\{\varepsilon_{mb}\}\,dV+\frac{1}{2}\int_V\{\varepsilon_{mb}\}^T\left[e_{mb}\right]^T\{E\}\,dV\right)\\
&E_{s-dielectric}^{Top-piezo}=-\frac{1}{2}\int_V\{E\}^T\left[d\right]^T\{E\}\,dV
\end{aligned}$$

From equations (3.70) (3.71) and (3.72), we can deduce the matrices of “membrane”, “bending”, “membrane-bending” (coupling), and “shear” stiffness for the sandwich plate as follows:

$$\begin{aligned}
[A]_{sandwich} &= [A]_{Bottom-piezo} + [A]_{Nanocomp} + [A]_{Top-piezo} \\
[B]_{sandwich} &= 0 \\
[D]_{sandwich} &= [D]_{Bottom-piezo} + [D]_{Nanocomp} + [D]_{Top-piezo} \\
[F]_{sandwich} &= [F]_{Nanocomp}
\end{aligned} \tag{3.73}$$

#### 3.11.3. External Forces Works

The external forces that can be applied on the piezoelectric sandwich plate are the same applied on piezoelectric, isotropic, and orthotropic plates (section 3.4.3).

## 3.12. Conclusion

In this chapter, we successfully presented the theoretical formulation for nanocomposite plates, piezoelectric plates, and sandwich plates. All the behavior laws, the relationship between strain and stress, kinetic energy, strain energy, forces works, and the laws of the electrical field, are involved in this part. This presentation was done to know how we are going to bring out the elementary matrices of mass and stiffness from a discretized medium, which will be presented in the next chapter. Having established the groundwork here, the next chapter will detail the steps to extract the elementary mass and stiffness matrices from a discretized medium.

# CHAPTER 4: FINITE ELEMENT METHOD FOR PLATES

## 4.1. Introduction

The Finite Element Method (FEM) is a powerful numerical technique used to solve a wide range of structural problems like displacement, static and dynamic analysis. This method consists of discretizing the domain into small subdomains to make the resolution of the problem easy and faster.

The problems tackled in the field of structural dynamics generally involve determining the magnitudes of displacement, velocity and acceleration of any point in the structure, in response to external excitations. These problems can be solved using a variety of approaches. In this chapter, we lay the foundations for the approach adopted in our thesis by rewriting the expressions for the deformation quantities and kinetic energy for the quadrilateral element under consideration. Newmark's integration method will also be presented in order to use it to solve the resulting problem.

## 4.2. Finite Element Method FEM

FEM involves discretizing the plate into small, interconnected elements. These elements typically take the form of triangles or quadrilaterals for 2$D$ structures. By analyzing the behavior of the plate over each element, the complex problem can be broken down into a series of simpler problems that are easier to solve. This makes FEM a valuable tool for engineers who need to understand and predict the behavior of complex structures.

The FEM-based structural analysis consists of four main phases [98]:

- Element choice and interpolation function generation.
- Discretization and transcription of the problem into a boundary value problem, this involves the calculation of element properties such as the mass and stiffness matrices through a variational method such as the Rayleigh-Ritz method.
- Transformation of the element mass, stiffness, and other characteristic matrices from an element-based reference frame to a global reference frame.

- Assembly of element equations into matrix format and obtaining a solution. The final step involves the solution of a large set of simultaneous algebraic equations.

### 4.2.1. Presentation of the chosen finite element

In our study, the plate is discretized into a considerable number of identical square elements, each of which contained nine nodes, every node has five degrees of freedom $\{u\ v\ w\ \theta_x\ \theta_y\}$. Figure 4.1 represents the geometrical characteristics of a representative element. Using this type of element with 9 nodes will allow to represent more precisely the curvatures and non-linear gradients of the displacement field.

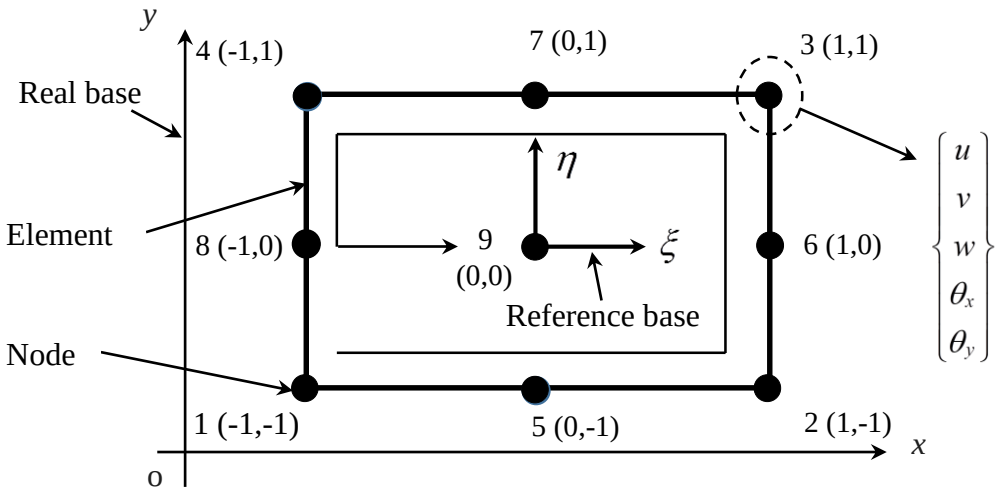


**Figure 4.1:** The representative nine-node element.

### 4.2.2. The Interpolation Polynom

The interpolation polynom used for the previous element with nine nodes is taken from Pascal's triangle as follows:

$$\{G_9\} = \{1 \quad \xi \quad \eta \quad \xi\eta \quad \xi^2 \quad \eta^2 \quad \xi^2\eta \quad \xi\eta^2 \quad \xi^2\eta^2\} \tag{4.1}$$

### 4.2.3. The Interpolation Matrix

In order to get the interpolation matrix [$A_9$], we just need to replace $\xi$ and $\eta$ by their values which are the natural coordinates:

$$[A_9]=\begin{bmatrix}1&-1&-1&1&1&1&-1&-1&1\\1&0&-1&0&0&1&0&0&0\\1&1&-1&1&-1&1&-1&1&1\\1&1&0&1&0&0&0&0&0\\1&1&1&1&1&1&1&1&1\\1&0&1&0&0&1&0&0&0\\1&-1&1&1&-1&1&1&-1&1\\1&-1&0&1&0&0&0&0&0\\1&0&0&0&0&0&0&0&0\end{bmatrix}$$

4.2.4. The Interpolation Functions

The interpolation functions for the nine nodes element are obtained by multiplying the inverse of the interpolation matrix by the interpolation polynomial [81] [99]:

$$N_i=\{G_9\}.[A_9]^{-1}=\begin{Bmatrix}N_1=\frac{1}{4}\xi(1-\xi)\eta(1-\eta)\\N_2=-\frac{1}{4}\xi(1+\xi)\eta(1-\eta)\\N_3=\frac{1}{4}\xi(1+\xi)\eta(1+\eta)\\N_4=-\frac{1}{4}\xi(1-\xi)\eta(1+\eta)\\N_5=-\frac{1}{2}(1-\xi)(1+\xi)\eta(1-\eta)\\N_6=\frac{1}{2}\xi(1+\xi)(1+\eta)(1-\eta)\\N_7=\frac{1}{2}(1+\xi)(1-\xi)\eta(1+\eta)\\N_8=-\frac{1}{2}\xi(1-\xi)(1-\eta)\eta\\N_9=(1-\xi^2)(1-\eta^2)\end{Bmatrix}^T \quad (4.2)$$

4.2.5. The Transformation of the Reference Element into a Real Element

The shape function matrices, denoted as [ $N_u$ ] and [ $N_\phi$ ] for displacement and electric potential, respectively, serve as fundamental tools in finite element analysis. They act as bridges between nodal variables (i.e. between the displacement $\{u_i\}$ or potential $\{\phi_i\}$ values

at the nodes of the discretized domain and the actual displacement { $\overline{X}$ } or potential { $\overline{\phi}$ } field throughout the domain) [81]:

$$\left\{\overline{X}\right\} = \left[N_u\right]\left\{u_i\right\} \ , \quad \left\{\overline{\phi}\right\} = \left[N_\phi\right]\left\{\phi_i\right\} \tag{4.3}$$

With,
$$\left[N_u\right] = \begin{bmatrix} N_i & 0 & 0 & 0 & 0 \\ 0 & N_i & 0 & 0 & 0 \\ 0 & 0 & N_i & 0 & 0 \\ 0 & 0 & 0 & N_i & 0 \\ 0 & 0 & 0 & 0 & N_i \end{bmatrix}, \qquad i=1, 2, 3\ldots.9$$

The integrals in the previous chapter were integrated into the global base in the *x* and *y* coordinates system. Since our plate is discretized into finite elements, the integrals will be integrated into the new base, $\xi$ and $\eta$ using the following transformation [100] [101][102]:

$$\frac{\partial N_i}{\partial \xi} = \frac{\partial N_i}{\partial x}\frac{\partial x}{\partial \xi} + \frac{\partial N_i}{\partial y}\frac{\partial y}{\partial \xi}$$
$$\frac{\partial N_i}{\partial \eta} = \frac{\partial N_i}{\partial x}\frac{\partial x}{\partial \eta} + \frac{\partial N_i}{\partial y}\frac{\partial y}{\partial \eta}$$

With the corresponding matrix form:

$$\begin{Bmatrix} \frac{\partial N_i}{\partial \xi} \\ \frac{\partial N_i}{\partial \eta} \end{Bmatrix} = \underbrace{\begin{bmatrix} \frac{\partial x}{\partial \xi} & \frac{\partial y}{\partial \xi} \\ \frac{\partial x}{\partial \eta} & \frac{\partial y}{\partial \eta} \end{bmatrix}}_{[J]} \begin{Bmatrix} \frac{\partial N_i}{\partial x} \\ \frac{\partial N_i}{\partial y} \end{Bmatrix} \tag{4.4}$$

$N_i$ is the interpolation function of the considered node, and [*J*] is the Jacobin matrix.

Therefore, the new area of integration is:

$$\int_A f \, \underline{dA} = \iint_{xy} f(x,y)\,\underline{dx\,dy} = \iint_{\xi\eta} f\left(x(\xi,\eta), y(\xi,\eta)\right)\underline{\det\left[J\right] d\xi\, d\eta} \tag{4.5}$$

### 4.3. Finite Element Formulation for the Piezoelectric Sandwich Plate

In order to formulate the expressions for the kinetic and deformation energies, as well as the work carried out by the external forces, it is recommended to follow the steps below

- Replace the actual displacement $\{\overline{X}\}$ with its nodal displacement approximation $\left[N_u\right]\{u_i\}$ (eq. (4.3)).
- The electrical filed $\{E\}$ with its $\left[D_\phi\right]\{\bar{\phi}\}$ (equation (3.54)).
- Replace the electrical potential $\{\bar{\phi}\}$ with its nodal approximation $\left[N_\phi\right]\{\phi_i\}$ (eq. (4.3)).
- Replace the integration domain $dA$ with the approximation (det $[J]$ $d\xi\, d\eta$) (eq. (4.5)).
- Replace $\{\varepsilon_{mb}\}$ by $\{\beta\}+z\{\chi\}$ (eq. (3.6)).
- Replace $\beta$ and $\chi$ by its matrix form (eq. (3.5)).

### 4.3.1. Kinetic Energy for the Sandwich Element

The expression of the approximated kinetic energy obtained after applying the previous first and third steps on equation (3.67) is as follows [78]:

$$E_k^{sandwich} = E_k^{Bottom-piezo} + E_k^{Nanocomp} + E_k^{Top-piezo}$$

$$E_k^{sandwich} =$$

$$\frac{1}{2}\int_A \{u_i\}^T \left[N_u\right]^T \rho_p \left( \int_{-h_p-\frac{h_c}{2}}^{-\frac{h_c}{2}} \begin{pmatrix} \left[L_{tra}\right]^T\left[L_{tra}\right] - z\left(\left[L_{tra}\right]^T\left[L_{rot}\right]+\left[L_{rot}\right]^T\left[L_{tra}\right]\right) \\ + z^2\left[L_{rot}\right]^T\left[L_{rot}\right] \end{pmatrix} dz \right) \left[N_u\right]\{u_i\}\, dA$$

$$+\frac{1}{2}\int_A \{u_i\}^T \left[N_u\right]^T \rho_c \left( \int_{-\frac{h_c}{2}}^{+\frac{h_c}{2}} \begin{pmatrix} \left[L_{tra}\right]^T\left[L_{tra}\right] - z\left(\left[L_{tra}\right]^T\left[L_{rot}\right]+\left[L_{rot}\right]^T\left[L_{tra}\right]\right) \\ + z^2\left[L_{rot}\right]^T\left[L_{rot}\right] \end{pmatrix} dz \right) \left[N_u\right]\{u_i\}\, dA$$

$$+\frac{1}{2}\int_A \{u_i\}^T \left[N_u\right]^T \rho_p \left( \int_{+\frac{h_c}{2}}^{+\frac{h_c}{2}+h_p} \begin{pmatrix} \left[L_{tra}\right]^T\left[L_{tra}\right] - z\left(\left[L_{tra}\right]^T\left[L_{rot}\right]+\left[L_{rot}\right]^T\left[L_{tra}\right]\right) \\ + z^2\left[L_{rot}\right]^T\left[L_{rot}\right] \end{pmatrix} dz \right) \left[N_u\right]\{u_i\}\, dA$$

(4.6)

We can notice that the obtained sandwich mass matrix is the same as it is founded in equation (3.68) but with nodal approximation.

### 4.3.2. Strain Energy for the Sandwich Element

The expression of the approximated strain energy obtained after applying all the previous steps on equations (3.70), (3.71), and (3.72) is as follows [78]:

$$
\begin{aligned}
E_s^{Bottom-piezo} &= E_{s-elastic}^{Bottom-piezo} + E_{s-piezoelectric}^{Bottom-piezo} + E_{s-dielectric}^{Bottom-piezo} \\
E_{s-elastic}^{Bottom-piezo} &= \frac{1}{2}\int_A \int_{-\frac{h_c}{2}-h_p}^{-\frac{h_c}{2}} \{\beta\}^T [C_{mb}]_{piezo} \{\beta\}\, dz\, dA + \frac{1}{2}\int_A \int_{-\frac{h_c}{2}-h_p}^{-\frac{h_c}{2}} z^2 \{\chi\}^T [C_{mb}]_{piezo} \{\chi\}\, dz\, dA \\
E_{s-eleastic}^{Bottom-piezo} &= \frac{1}{2}\int_A \{u_i\}^T [N_u]^T [D_{mem}]^T [A]_{Bottom-piezo} [D_{mem}][N_u]\{u_i\}\, dA \\
&\quad + \frac{1}{2}\int_A \{u_i\}^T [N_u]^T [D_{ben}]^T [D]_{Bottom-piezo} [D_{ben}][N_u]\{u_i\}\, dA \\
E_{s-piezoelectric}^{Bottom-piezo} &= -\left( \frac{1}{2}\int_A \int_{-\frac{h_c}{2}-h_p}^{-\frac{h_c}{2}} \{E\}^T [e_{mb}]\{\varepsilon_{mb}\}\, dz\, dA + \frac{1}{2}\int_A \int_{-\frac{h_c}{2}-h_p}^{-\frac{h_c}{2}} \{\varepsilon_{mb}\}^T [e_{mb}]^T \{E\}\, dz\, dA \right) \\
&= -\begin{pmatrix} \frac{1}{2} h_p \int_A \{\phi_i\}^T [N_\phi]^T [D_\phi]^T [e_{mb}][D_{mem}][N_u]\{u_i\}\, dA \\ + \frac{1}{2} h_p \int_A \{u_i\}^T [N_u]^T [D_{mem}]^T [e_{mb}]^T [D_\phi][N_\phi]\{\phi_i\}\, dA \end{pmatrix} \\
E_{s-dielectric}^{Bottom-piezo} &= -\frac{1}{2} h_p \int_A \{\phi_i\}^T [N_\phi]^T [D_\phi]^T [d]^T [D_\phi][N_\phi]\{\phi_i\}\, dA
\end{aligned}
\tag{4.7}
$$

$$
\begin{aligned}
E_{s-elastic}^{Nanocomp} &= \frac{1}{2}\int_A \{u_i\}^T [N_u]^T [D_{mem}]^T [A]_{Nanocomp} [D_{mem}][N_u]\{u_i\}\, dA \\
&\quad + \frac{1}{2}\int_A \{u_i\}^T [N_u]^T [D_{ben}]^T [D]_{Nanocomp} [D_{ben}][N_u]\{u_i\}\, dA \\
&\quad + \frac{1}{2}\int_A \{u_i\}^T [N_u]^T [D_{she}]^T [F]_{Nanocomp} [D_{she}][N_u]\{u_i\}\, dA
\end{aligned}
\tag{4.8}
$$

$$E_s^{Top-piezo} = E_{s-elastic}^{Top-piezo} + E_{s-piezoelectric}^{Top-piezo} + E_{s-dielectric}^{Top-piezo}$$

$$E_{s-elastic}^{Top-piezo} = \frac{1}{2}\int_A \int_{+\frac{h_c}{2}}^{+\frac{h_c}{2}+h_p} \{\beta\}^T \left[C_{mb}\right]_{piezo} \{\beta\}\, dz\, dA + \frac{1}{2}\int_A \int_{+\frac{h_c}{2}}^{+\frac{h_c}{2}+h_p} z^2 \{\chi\}^T \left[C_{mb}\right]_{piezo} \{\chi\}\, dz\, dA$$

$$E_{s-eleastic}^{Top-piezo} = \frac{1}{2}\int_A \{u_i\}^T \left[N_u\right]^T \left[D_{mem}\right]^T \left[A\right]_{Top-piezo} \left[D_{mem}\right]\left[N_u\right]\{u_i\}\, dA + \frac{1}{2}\int_A \{u_i\}^T \left[N_u\right]^T \left[D_{ben}\right]^T \left[D\right]_{Top-piezo} \left[D_{ben}\right]\left[N_u\right]\{u_i\}\, dA$$

$$E_{s-piezoelectric}^{Top-piezo} = -\left( \frac{1}{2}\int_A \int_{+\frac{h_c}{2}}^{+\frac{h_c}{2}+h_p} \{E\}^T \left[e_{mb}\right]\{\varepsilon_{mb}\}\, dz\, dA + \frac{1}{2}\int_A \int_{+\frac{h_c}{2}}^{+\frac{h_c}{2}+h_p} \{\varepsilon_{mb}\}^T \left[e_{mb}\right]^T \{E\}\, dz\, dA \right)$$

$$= -\left( \begin{array}{l} \frac{1}{2} h_p \int_A \{\phi_i\}^T \left[N_\phi\right]^T \left[D_\phi\right]^T \left[e_{mb}\right]\left[D_{mem}\right]\left[N_u\right]\{u_i\}\, dA \\ + \frac{1}{2} h_p \int_A \{u_i\}^T \left[N_u\right]^T \left[D_{mem}\right]^T \left[e_{mb}\right]^T \left[D_\phi\right]\left[N_\phi\right]\{\phi_i\}\, dA \end{array} \right)$$

$$E_{s-dielectric}^{Top-piezo} = -\frac{1}{2} h_p \int_A \{\phi_i\}^T \left[N_\phi\right]^T \left[D_\phi\right]^T \left[d\right]^T \left[D_\phi\right]\left[N_\phi\right]\{\phi_i\}\, dA \tag{4.9}$$

### 4.4. Elementary Mass Matrix

We can deduce the elementary mass matrix from the developed kinetic energy in equation (4.6) as follows [78]:

$$E_k^{sandwich} = \frac{1}{2}\{u_i\}^T \left[M_{Piezo-Bottom}\right]\{u_i\} + \frac{1}{2}\{u_i\}^T \left[M_{Nanocomposite}\right]\{u_i\} + \frac{1}{2}\{u_i\}^T \left[M_{Piezo-Top}\right]\{u_i\}$$

$$\left[M\right]_{elementary}^{sandwich} = \left[M_{Piezo-Bottom}\right] + \left[M_{Nanocomposite}\right] + \left[M_{Piezo-Top}\right] \tag{4.10}$$

### 4.5. Elementary Stiffness Matrices

We can also deduce the elementary elastic, piezoelectric, and dielectric stiffness matrices from the developed kinetic energy in equations (4.7), (4.8), and (4.9) as follows [78]:

4.5.1. Elastic Stiffness Matrix

$$
\begin{aligned}
\left[K_{uu}\right]^{sandwich}_{elastic-elem} = & \int_A \left[N_u\right]^T \left[D_{mem}\right]^T \left[A\right]_{Bottom-piezo} \left[D_{mem}\right]\left[N_u\right]\{u_i\}\,dA \\
& + \int_A \left[N_u\right]^T \left[D_{ben}\right]^T \left[D\right]_{Bottom-piezo} \left[D_{ben}\right]\left[N_u\right]dA \\
& + \int_A \left[N_u\right]^T \left[D_{mem}\right]^T \left[A\right]_{Nanocomp} \left[D_{mem}\right]\left[N_u\right]dA \\
& + \int_A \left[N_u\right]^T \left[D_{ben}\right]^T \left[D\right]_{Nanocomp} \left[D_{ben}\right]\left[N_u\right]dA \\
& + \int_A \left[N_u\right]^T \left[D_{she}\right]^T \left[F\right]_{Nanocomp} \left[D_{she}\right]\left[N_u\right]dA \\
& + \int_A \left[N_u\right]^T \left[D_{mem}\right]^T \left[A\right]_{Top-piezo} \left[D_{mem}\right]\left[N_u\right]dA \\
& + \int_A \left[N_u\right]^T \left[D_{ben}\right]^T \left[D\right]_{Top-piezo} \left[D_{ben}\right]\left[N_u\right]dA
\end{aligned}
\tag{4.11}
$$

The Piezo-Mechanical Coupling Stiffness Matrix is as follow:

$$
\left[K_{u\phi}\right]^{sandwich}_{piezo-elem} = -\int_A \begin{pmatrix}
2h_p\left[N_\phi\right]^T\left[D_\phi\right]^T\left[e_{mb}\right]\left[D_{mem}\right]\left[N_u\right]dA \\
+2h_p\left[N_u\right]^T\left[D_{mem}\right]^T\left[e_{mb}\right]^T\left[D_\phi\right]\left[N_\phi\right]dA \\
+h_p\left(h_p+h_c\right)\left[N_\phi\right]^T\left[D_\phi\right]^T\left[e_{mb}\right]\left[D_{ben}\right]\left[N_u\right]dA \\
+h_p\left(h_p+h_c\right)\left[N_u\right]\left[D_{ben}\right]\left[e_{mb}\right]^T\left[D_\phi\right]\left[N_\phi\right]dA
\end{pmatrix}
\tag{4.12}
$$

4.5.2. Permittivity Stiffness Matrix

$$
\left[K_{\phi\phi}\right]^{sandwich}_{dielect-elem} = -\left(2h_p\int_A \left[N_\phi\right]^T\left[D_\phi\right]^T\left[d\right]^T\left[D_\phi\right]\left[N_\phi\right]dA\right)
\tag{4.13}
$$

After determining all the elementary matrices, it is necessary to assemble them to get the global matrices. The accumulated form of the three stiffness components is as follows:

$$
\left[K\right]^{sandwich}_{piezo} = \begin{bmatrix} \left[K_{uu}\right] & \left[K_{u\phi}\right] \\ \left[K_{\phi u}\right] & \left[K_{\phi\phi}\right] \end{bmatrix}^{sandwich}_{piezo}
$$

Where the elementary stiffness $\left[K_{\phi u}\right]=\left[K_{u\phi}\right]^T$.

After integrating the previous equations and getting the elementary matrices, a code on Matlab software has been written to assemble these matrices to obtain the global mass and rigidity matrices $[M_{uu}]_{elastic}$, $[K_{uu}]_{elastic}$, $[K_{u\phi}]_{piezoelectric}$, $[K_{\phi\phi}]_{dielectric}$ of the sandwich plate. Then, it is possible to solve the resulting dynamic equation:

$$\begin{bmatrix} [M_{uu}] & [0] \\ [0] & [0] \end{bmatrix} \begin{Bmatrix} \ddot{X} \\ \ddot{\phi} \end{Bmatrix} + \begin{bmatrix} [C_{uu}] & [0] \\ [0] & [0] \end{bmatrix} \begin{Bmatrix} \dot{X} \\ \dot{\phi} \end{Bmatrix} + \begin{bmatrix} [K_{uu}] & [K_{u\phi}] \\ [K_{\phi u}] & [K_{\phi\phi}] \end{bmatrix} \begin{Bmatrix} X \\ \phi \end{Bmatrix} = \begin{Bmatrix} F_{mech} \\ Q_{elec} \end{Bmatrix} \quad (4.14)$$

In which, $F_{mech}$, and $Q_{elec}$ are the external mechanical force and electrical charge that can be applied to the plate. $X$ and $\phi$ are the mechanical displacement vector and the electrical potential vector obtained due to the applied external force and charge respectively. Where $\{X(t)\} = \{A'\} e^{i\omega t}$ and $\{\phi(t)\} = \{\varphi\} e^{i\omega t}$ are the solutions obtained from the dynamics equation.

**4.6. Modal Analysis** [92]

Modal analysis is a technique used in structural mechanics to study the dynamic behavior of structures. It focuses on determining the studied structure's natural frequencies, mode shapes. This process involves manipulating high-order matrices. The MATLAB software offers a large diversity of tools facilitating the accomplishment of this process, particularly computing eigenvalues, and the corresponding eigenvectors.

4.6.1. Eigenvalue problem analysis for nanocomposite plate

The equation of motion for the undamped and unforced plate is established as follows:

$$[M_{uu}]_{Nanocomp} \{\ddot{X}\} + [K_{uu}]_{Nanocomp} \{X\} = \{0\} \quad (4.15)$$

Equation (4.15) can be reduced to the following standard eigenvalue equation:

$$det\left([K_{uu}]_{Nanocomp} - \omega_i^2 [M_{uu}]_{Nanocomp}\right)\{X\} = 0 \quad (4.16)$$

Where: "*det*" refers to the determinant of the considered matrix, $\omega_i$ are the natural frequencies or proper values, and *X* is the mode shape vector or adequate vector.

### 4.6.2. Eigenvalue problem analysis for sandwich plate

The equation of motion for the undamped and unforced plate is:

$$\begin{aligned}\left[M_{uu}\right]_{sandwich}\left\{\ddot{X}\right\}+\left[K_{uu}\right]_{sandwich}\left\{X\right\}+\left[K_{u\phi}\right]_{piezo}\left\{\phi_a\right\}&=\left\{0\right\}\\ \left[K_{\phi u}\right]_{piezo}\left\{X\right\}+\left[K_{\phi\phi}\right]_{diele}\left\{\phi_s\right\}&=\left\{0\right\}\end{aligned} \tag{4.17}$$

Equation (4.17) can be reduced to a standard eigenvalue equation as follows:

$$det\left(\left[K_{eff}\right]_{sandwich}-\omega_i^2\left[M_{uu}\right]_{sandwich}\right)\begin{Bmatrix}X\\ \phi\end{Bmatrix}=0 \tag{4.18}$$

With $\left[K_{eff}\right]_{sandwich}=\left[K_{uu}\right]+G_d\left[K_{u\phi}\right]\left[K_{\phi\phi}\right]^{-1}\left[K_{\phi u}\right]$ is the effective rigidity.

$G_d$ is the proportional control gain.

## 4.7. Static Analysis

The equation of motion for the static undamped, forced and non-charged plate is:

$$\left[K_{uu}\right]_{sandwich}\left\{X\right\}+\left[K_{u\phi}\right]_{piezo}\left\{\phi_a\right\}=\left\{F\right\} \tag{4.19}$$

Were $\phi_a$ is the electrical potential of the actuator.

Since the load is constant, the velocity and acceleration of the plate are equal to zero, and the displacement field depends on the electrical potential and the applied uniform load.

## 4.8. Dynamic Analysis

Dynamic analysis of plates is an important field in structural dynamics, which aims to determine the behavior of plates under the action of dynamic loads. This involves calculating the deformations in the plate as a function of time. The equation of motion for the damped, forced, and non-electrically charged plate is as follows:

$$\begin{aligned}\left[M_{uu}\right]_{sandwich}\left\{\ddot{X}\right\}+\left[C_{uu}\right]_{sandwich}\left\{\dot{X}\right\}+\left[K_{uu}\right]_{sandwich}\left\{X\right\}+\left[K_{u\phi}\right]_{piezo}\left\{\phi_a\right\}&=\left\{F(t)\right\}\\ \left[K_{\phi u}\right]_{piezo}\left\{X\right\}+\left[K_{\phi\phi}\right]_{diele}\left\{\phi_s\right\}&=\left\{0\right\}\end{aligned} \tag{4.20}$$

Where: $F(t)$ is the variable load applied on the sandwich plate, which depends on time,

$[C_{uu}]_{sandwich}$ is the proportional damping matrix, given by

$$\left[C_{uu}\right]_{sandwich} = \left[C_{ad}\right] + \left[C_{sd}\right]$$

$[C_{sd}]$ is the structural damping matrix:

$$\left[C_{sd}\right] = \alpha_R \left[M_{uu}\right]_{sandwich} + \beta_R \left[K_{uu}\right]_{sandwich}$$

$\alpha_R$, and $\beta_R$ are Rayleigh's coefficients given by [103]:

$$\alpha_R = 2\frac{\sum_{i=1}^{N}\frac{\psi}{\omega_i}\sum_{i=1}^{N}\omega_i^2 - N\sum_{i=1}^{N}\psi\omega_i}{\sum_{i=1}^{N}\frac{1}{\omega_i^2}\sum_{i=1}^{N}\omega_i^2 - N^2}, \quad \beta_R = 2\frac{\sum_{i=1}^{N}\frac{1}{\omega_i^2}\sum_{i=1}^{N}\psi\omega_i - N\sum_{i=1}^{N}\frac{\psi}{\omega_i}}{\sum_{i=1}^{N}\frac{1}{\omega_i^2}\sum_{i=1}^{N}\omega_i^2 - N^2} \tag{4.21}$$

In eq. (4.21), $\psi$, $\omega_i$ and $N$ are the design values for the damping ratio, the $i^{th}$ natural frequency, and the number of modes contributing in the estimation of Rayleigh's coefficients, respectively.

Moreover, $[C_{ad}]$ is the active damping matrix produced by the proposed controller. It is formulated as follows:

$$\left[C_{ad}\right] = G_v\left[K_{u\phi}\right]\left[K_{\phi\phi}\right]^{-1}\left[K_{\phi u}\right]$$

Where $G_v$ is the velocity control gain or derivative control gain.

### 4.8.1. The Generated Electrical Potential by the Sensor

When a transverse external force bends the nanocomposite plate, the piezoelectric layer converts this deflection into an electric potential within the sensor layer $\phi_s$. Assuming no external electrical charge is present, this generated potential reads as:

$$\phi_s = -\left[K_{\phi\phi}\right]^{-1}\left[K_{\phi u}\right]\{X\} \tag{4.22}$$

### 4.8.2. The Actuator's Electrical Potential

The electrical potential ($\phi_s$) is transformed to a displacement and then given to the controller (The controller is based on Newmark's technique to achieve the dynamic time history response of the piezoelectric nanocomposite plate). The controller generates a new

displacement, which is then transformed into an electrical potential ($\phi_a$). This potential is assumed to be applied to the actuator layer (Figure 4.2). The electrical potential is thus given by:

$$\phi_a = G_v\,\dot{\phi}_s + G_d\,\phi_s \tag{4.23}$$

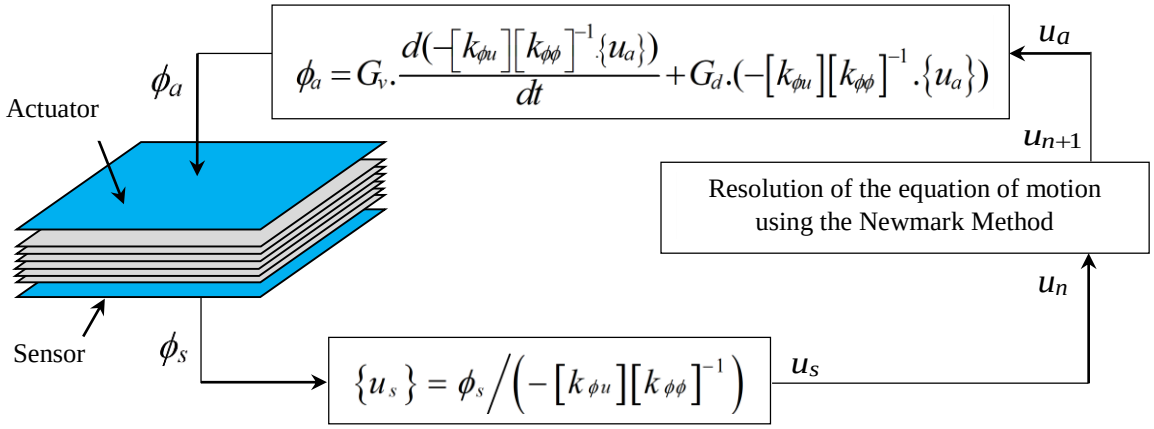


**Figure 4.2:** Control loop.

### 4.9. Newmark *β*-Method of Resolution

The Newmark direct integration method is one of the well-known and widely used methods in the resolution of the second-order equations of motion. It is based on the prediction of the solution and then corrects it [104] [95].

The principle of this method consists in determining, by using a limited development, the position and the speed at time $t_{n+1}$ from the same quantities at time $t_n$. This expansion contains a third-order error term proportional to the derivative of acceleration. Various hypotheses make it possible to replace this third derivative with the acceleration at the previous time by introducing two parameters $\gamma_n$ and $\beta_n$ [104] [95].

The Newmark Direct Integration Method involves multiple steps for each time step in dynamic analysis. In the following, we set the core steps [104] [95]:

I) ***Initialization***:

- Define the initial displacement $\{u_0\}$, velocity $\{v_0\}$ and load $\{F_0\}$.

- Choose appropriate values for $\beta$ and $\gamma$ (Newmark algorithm parameters) to balance the desired stability and accuracy.

II) ***Loop for each time step*** ($n+1$):

a) Calculate current accelerations ($a_n$) using the equation involving $\{u_0\}$, $\{v_0\}$, $\{F_0\}$, mass $[M]$, damping $[C]$, and stiffness $[K]$:

$$\{a_0\} = inv([M])\left(\{F_0\} - [C]\{v_0\} - [K]\{x_0\}\right)$$

b) Time increment:

$$t_{n+1} = t_n + \Delta t$$

c) Predict the displacement and velocity in the present step ($u^p_{n+1}$) and ($v^p_{n+1}$), using the displacement, velocity, and acceleration of the previous step:

$$\left\{u^p_{n+1}\right\} = \{u_n\} + \Delta t\,\{v_n\} + \left(\frac{1}{2} - \beta\right)\Delta t^2\,\{a_n\}$$

$$\left\{v^p_{n+1}\right\} = \{v_n\} + (1-\gamma)\,\Delta t\,\{a_n\}$$

d) Calculate the acceleration of the present step:

$$[S] = [M] + \gamma\,\Delta t[C] + \beta\,\Delta t^2[K]$$

$$\{a_{n+1}\} = [S]^{-1}\left(\{F_{n+1}\} - [C]\left\{v^p_{n+1}\right\} - [K]\left\{u^p_{n+1}\right\}\right)$$

e) Correct the displacement and velocity:

$$\{u_{n+1}\}^c = \left\{u^p_{n+1}\right\} + \beta\,\Delta t^2\,\{a_{n+1}\}$$

$$\{v_{n+1}\}^c = \left\{v^p_{n+1}\right\} + \gamma\,\Delta t\,\{a_{n+1}\}$$

f) Go back to step (b).

In which $u_n$, $u_{n+1}$, $v_n$, $v_{n+1}$, $a_n$, and $a_{n+1}$ are the displacement, velocity, and acceleration for the previous $n$ and present $n+1$ step. $P$ means the predicted value. $\Delta t$ is the period (seconds) between $n$ and $n+1$. The stability and accuracy parameters $\beta_n$ and $\gamma_n$ are token equals to 0.25 and 0.5 respectively, for the unconditionally stable system.

## 4.10. Conclusion

In this chapter, a brief presentation of the finite element method (FEM) was done, in order to achieve the approximate expressions for the kinetic, and strain energy of composite and sandwich plates. In addition, a presentation of the resolution method for the equations of motion of a free plate is well mentioned. In addition, The Newmark resolution method was also presented in order to compute the dynamic response of an unconditionally stable plate.

# CHAPTER 5: NUMERICAL RESULTS AND DISCUSSIONS

## 5.1. Introduction

This study focused on identifying the optimal control parameters, configurations, and distribution functions for nanofillers to achieve high performance and stiffness in plates.

At the beginning of this chapter, we present a validation study to demonstrate the high performance of the developed code and to illustrate the degree of accuracy in the results. First, a modal analysis was conducted to obtain the natural frequencies and modes of a composite plate and a piezoelectric sandwich plate under different boundary conditions, followed by a comparison with results from cited references. Second, a static control analysis was performed for clamped-free (CFFF) and simply supported (SSSS) sandwich plates, reinforced with various configurations using power and exponential laws, to identify the stiffest plate. Third, a dynamic analysis was carried out, where the identified stiffest plate was subjected to active vibration control. The Newmark prediction-correction method was employed to determine the dynamic response of the forced plate. The study concludes with promising and significant results.

## 5.2. Modal Analysis of Multilayer Nanocomposite Plates

In our work, a square multilayer polymer composite plate reinforced by carbon nanotubes (CNTs) is considered. The CNTs, specifically the armchair single-walled nanotubes, are chosen as the reinforcement for the plate, with the following geometrical dimensions: length $L$=9.26 *nm*, radius $R$=0.68 *nm*, and thickness $h$=0.067 *nm*. In the objective of studying the comparison between two different plates, the graphene platelets (GPLs) are also chosen as the reinforcement of the second composite plate. It is considered that the distribution of nano -reinforcement within each layer of the plate is either uniform or varies according to the power and exponential law functions as presented in equations (2.7) and (2.9), respectively, to form the configurations shown in Figure 5.1.

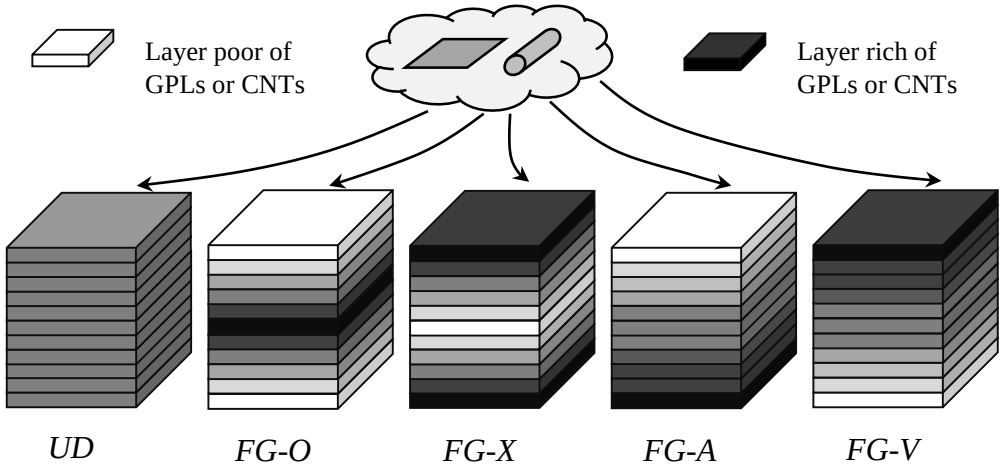


**Figure 5.1:** Different configurations of carbon nanotubes

The CNT properties are: longitudinal Young modulus $E_{11}^{CNT}$ = 5646.6 *GPa*, transversal modulus $E_{22}^{CNT}$ = 7080 *GPa*, density of $\rho^{CNT}$ = 1400 $kg/m^3$ shear modulus $G_{12}^{CNT}$ = 1944.5 *GPa*, and Poisons ratio $\nu_{CNT}$ = 0.175. The correction factors used in the mixing law are presented in Table 5.1.

**Table 5.1** The Correction coefficient used corresponds to volume fractions.

| $f_r^*$ | $\eta_1$ | $\eta_2$ | $\eta_3$ |
|---|---|---|---|
| 0.11 | 0.149 | 0.934 | 0.934 |
| 0.12 | 0.137 | 1.022 | 0.7 $\eta_2$ |
| 0.14 | 0.150 | 0.941 | 0.941 |
| 0.17 | 0.149 | 1.381 | 1.381 |
| 0.28 | 0.141 | 1.585 | 0.7 $\eta_2$ |

The graphene platelets properties are: Young modulus $E^{GPL}$ = 1010 *GPa*, density $\rho^{GPL}$ = 1060 $kg/m^3$, and Poisons ratio $\nu_{GPL}$ = 0.186. Their geometrical dimensions are $L$ = 2.5 $\mu m$ $W$ = 1.5 $\mu m$ and $h$=1.5 *nm*. The matrices used in the conception of plates are the [poly (m phenylene vinylene)-co-[(2,5-dioctoxy-p-phenylene) vinylene] PmPV matrix with the following properties: $E_m$ = 2.1 *GPa*, $\rho_m$ = 1150kg/m$^3$ and $\nu_m$ = 0.34, and the epoxy matrix with: $E_m$ = 3.0 *GPa*, $\rho_m$ = 1200kg/m$^3$ and $\nu_m$ = 0.34.

### 5.2.1. Validation study

Let us consider a square multilayer composite plate made of epoxy and graphene platelets, with the following geometrical characteristics: length $L$= 0.45 *m*, width $W$ = 0.45 *m*, and

thickness $h_{GPL/Epoxy}$ = 0.045 *m*. The plate is assumed to be divided into 10 layers, each with the same thickness $h_L$ =0.0045 *m*. In addition, each layer is designed to support a specified weight of graphene platelets (GPLs) as a form of a volume fraction ($f_r^*$). Similary, another square multilayer composite plate made of PmPV and carbon nanotubes with *L*= 1 *m*, *W* = 1 *m*, and thickness $h_{CNT/PmPV}$ = 0.1 *m* is considered. This plate is divided into 20 layers, each with a thickness $h_L$ = 0.005 *m*. Both plates are supposed to be simply supported (SSSS) along their four edges (see figure 5.2) and follow the conditions below:

$$\begin{cases} v = w = \theta_y = 0 \\ u = w = \theta_x = 0 \end{cases} \quad \text{at} \quad \begin{matrix} x = 0 \\ y = 0 \end{matrix}$$

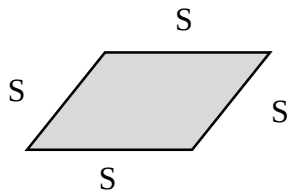


**Figure 5.2:** Boundary conditions.

Table 5.2 presents the first non-dimensional natural frequencies $\overline{\omega} = \omega\left(b^2 / h\right)\sqrt{\rho_m / E_m}$ for the CNTs / PmPV plate using volume fraction $f_r^*$ = 0.11, and those frequencies of Chiker et al 2020 [58] and Zhu et al 2012 [105]. The comparison of the obtained results with those from the references shows a close agreement.

**Table 5.2** non-dimensional first natural frequencies of a SSSS CNTs/ PmPV plate.

| *h* (m) | Source | $P_{in}$ = 1 | | | |
|---|---|---|---|---|---|
| | | UD | FG-X | FG-O | FG-V |
| 0.1 | Present method | 13.506 | 14.578 | 11.558 | 12.434 |
| | Chiker et al [58] | 13.532 | 14.653 | 11.593 | 12.478 |
| | Zhu et al [105] | 13.564 | 14.616 | 11.550 | 12.452 |

Table 5.3 presents the first non-dimensional natural frequencies $\overline{\omega} = \omega h\sqrt{\rho_m / E_m}$ for the GPLs / Epoxy plate using weigh fraction $w_t$ = 0.4%, and those frequencies of Chiker et al 2020 [58], Song et al [106] , and Reddy et al [107]. The obtained results with those from the references are in good agreement.

**Table 5.3** Non-dimensional first natural frequencies of a SSSS GPLs/ Epoxy plate.

| $h$ (m) | Source | $P_{in}$ = 1 | | | |
|---|---|---|---|---|---|
| | | UD | FG-X | FG-O | FG-V |
| 0.045 | Present method | 0.1216 | 0.1378 | 0.1020 | 0.1118 |
| | Chiker et al [58] | 0.1216 | 0.1378 | 0.1020 | 0.1118 |
| | Song et al [106] | 0.1216 | 0.1378 | 0.1020 | 0.1118 |
| | Reddy et al [107] | 0.1225 | 0.1420 | 0.0912 | 0.1080 |

One can observed in both tables 5.2 and 5.3, the FG-X configuration is the only one that exhibits high frequencies compared to the other configurations. This behavior may be attributed to the condensation of Nano-fillers at the top and bottom layers of the plate. In the next table (table 5.4), we present the results showing the effect of varying the parameter $P_{in}$ on the non-dimensional first natural frequencies. The finding results are as follows:

**Table 5.4** Effect of nonlinear distributions of both Nanofillers on the non-dimensional natural frequencies, with $W/h$ = 10, $P_{in}$ = 0 - 0.4 - 0.8 - 1 - 1.4 - 1.8, $f_r^*$ = 0.11, $w_t$ = 0.4%, SSSS.

| Reinfor -cement | Source | Configuration | $P_{in}$ | | | | | |
|---|---|---|---|---|---|---|---|---|
| | | | 0 | 0.4 | 0.8 | 1 | 1.4 | 1.8 |
| CNTs | Chiker et al [58] | FG-X | 13.564 | 14.141 | 14.512 | 14.653 | 14.879 | 15.054 |
| | Present method | FG-X | 13.506 | 14.074 | 14.439 | 14.578 | 14.801 | 14.974 |
| | Chiker et al [58] | FG-O | 13.564 | 12.735 | 11.950 | 11.593 | 10.954 | 10.405 |
| | Present method | FG-O | 13.506 | 12.687 | 11.911 | 11.558 | 10.925 | 10.381 |
| | Chiker et al [58] | FG-A | 13.564 | 13.165 | 12.706 | 12.478 | 12.045 | 11.646 |
| | Present method | FG-A | 13.506 | 13.113 | 12.659 | 12.434 | 12.007 | 11.612 |
| GPLs | Chiker et al [58] | FG-X | 0.0892 | 0.0945 | 0.0984 | 0.0999 | 0.1025 | 0.1045 |
| | Present method | FG-X | 0.0892 | 0.0945 | 0.0984 | 0.0999 | 0.1025 | 0.1045 |
| | Chiker et al [58] | FG-O | 0.0892 | 0.0834 | 0.0786 | 0.0766 | 0.0735 | 0.0712 |
| | Present method | FG-O | 0.0892 | 0.0834 | 0.0786 | 0.0766 | 0.0735 | 0.0712 |
| | Chiker et al [58] | FG-A | 0.0892 | 0.0869 | 0.0851 | 0.0850 | 0.0837 | 0.0833 |
| | Present method | FG-A | 0.0892 | 0.0869 | 0.0851 | 0.0850 | 0.0837 | 0.0833 |

The results given in Table 5.4 are in excellent agreement with those cited in reference [58]. After observing the results, one can conclude that increasing the $P_{in}$ index from zero to 1.8 may increase the frequencies for the FG-X configuration, whereas a decrease is observed with the other configurations. This behavior is attributed to the condensation of nanotubes on the lateral regions.

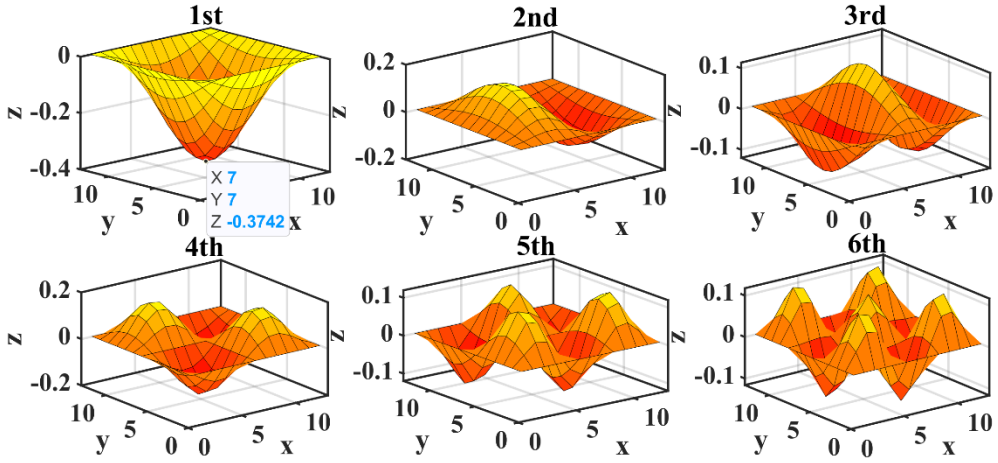


FG-X

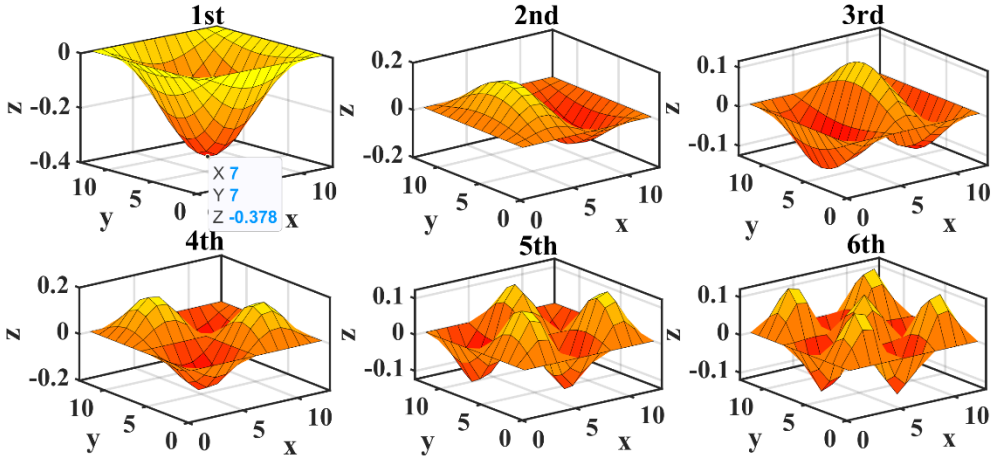


FG-O

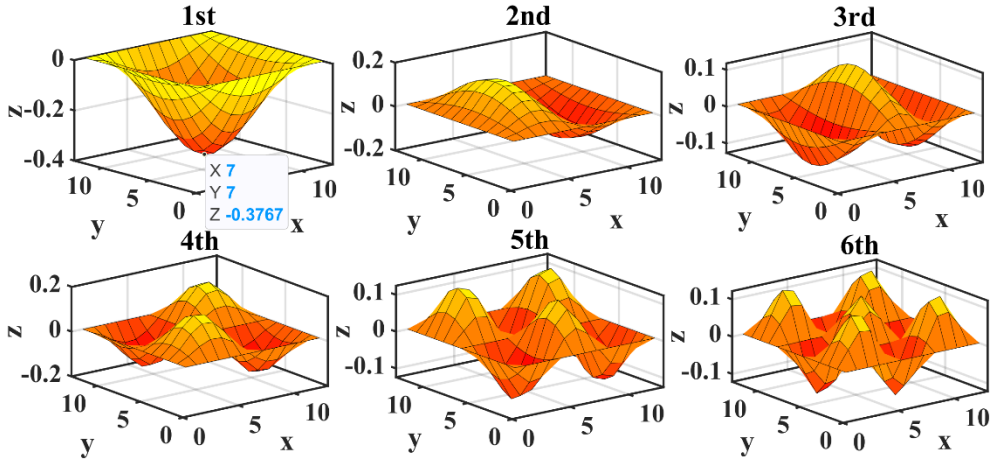


FG-A

**Figure 5.3:** First six modes for CCCC FG-(X, O, A) plates reinforced with CNTs based on exponential distribution approach with $f_r^* = 0.11$, $L/W = 1$, $W/h = 10$, $N_L = 20$.

### 5.2.2. Free vibrations analysis of FG-CNTRC and FG-GPLRC plates

In the previous chapter (Chapter 2), we presented a new distribution method, referred to as the exponential distribution, described by Equation (2.9). We found that this method could provide higher stiffness to the plate with an X form of distribution. This is due to the exponential function, which concentrates a significant high quantity of Nano-fillers on the lateral surfaces of the FG-X configuration.

**Table 5.5** Non-dimensional first five natural frequencies of an SSSS CNTs/PmPV and GPLs/ Epoxy plate using the novel exponential distribution.

| Reinfor -cement | Source | Configuration | *Mode* | | | | |
|---|---|---|---|---|---|---|---|
| | | | 1 | 2 | 3 | 4 | 5 |
| CNTs | Present method | FG-X | 15.205 | 19.213 | 19.213 | 19.613 | 28.942 |
| | Present method | FG-O | 10.070 | 15.256 | 19.256 | 19.615 | 25.542 |
| | Present method | FG-A | 11.880 | 16.919 | 19.919 | 19.621 | 27.397 |
| GPLs | Present method | FG-X | 0.1385 | 0.3235 | 0.3235 | 0.3651 | 0.3651 |
| | Present method | FG-O | 0.0647 | 0.1556 | 0.1556 | 0.2399 | 0.2479 |
| | Present method | FG-A | 0.0879 | 0.2096 | 0.2096 | 0.3011 | 0.30.11 |

Table 5.5 presents the natural frequencies obtained when using the novel method of distribution.

As first comment on the results obtained in Table 5.6 is that the decrease in the thickness of both plates led to a decrease in frequencies for the GPLs-reinforced composite plate, and an increase for the CNTs reinforced composite plate. Furthermore, the clamped plate frontiers (CCCC) give high frequencies. Figure 5.3 presents the first six 3D modes shape of the plate with CNTs reinforcement using the exponential distribution.

**Table 5.6** Non-dimensional first five natural frequencies for both CNTRC and GPLRC plates based on exponential distribution and using $L / W$=1, $W / h$ =20, $N_L$=20, $f_r^*$ = 0.11, $w_t$ = 0.4%.

| Nano filler | Boundary conditions | Configurations | *Mode number* | | | | |
|---|---|---|---|---|---|---|---|
| | | | 1 | 2 | 3 | 4 | 5 |
| CNTs | SSSS | FG-X | 21.433 | 25.120 | 35.376 | 39.226 | 39.226 |
| | | FG-O | 11.201 | 16.768 | 28.597 | 37.113 | 39.230 |
| | | FG-A | 14.006 | 19.370 | 31.443 | 39.245 | 39.245 |
| GPLs | SSSS | FG-X | 0.0359 | 0.0883 | 0.0883 | 0.1684 | 0.1716 |
| | | FG-O | 0.0165 | 0.0409 | 0.0409 | 0.0646 | 0.0806 |
| | | FG-A | 0.0259 | 0.0557 | 0.0557 | 0.0879 | 0.1095 |
| CNTs | CCCC | FG-X | 31.470 | 36.031 | 47.201 | 63.254 | 65.623 |
| | | FG-O | 21.267 | 27.081 | 39.358 | 47.952 | 51.417 |
| | | FG-A | 25.077 | 30.679 | 43.070 | 54.150 | 57.405 |
| GPLs | CCCC | FG-X | 0.2735 | 0.5017 | 0.5017 | 0.6868 | 0.7898 |
| | | FG-O | 0.1357 | 0.2594 | 0.2594 | 0.3627 | 0.4307 |
| | | FG-A | 0.1818 | 0.3429 | 0.3429 | 0.4757 | 0.5612 |
| CNTs | CFFF | FG-X | 1.0997 | 2.6916 | 6.8039 | 9.7221 | 13.315 |
| | | FG-O | 0.9889 | 2.4187 | 6.1279 | 8.7544 | 13.316 |
| | | FG-A | 1.0650 | 2.6027 | 6.5920 | 9.4094 | 13.311 |
| GPLs | CFFF | FG-X | 0.0309 | 0.0699 | 0.1383 | 0.1739 | 0.2231 |
| | | FG-O | 0.0142 | 0.0329 | 0.0826 | 0.0939 | 0.1054 |
| | | FG-A | 0.0194 | 0.0446 | 0.1116 | 0.1142 | 0.1422 |

### 5.2.3. CNTs /PmPV versus Carbon/PmPV plate

In the following section, we compare between the performance of a square nanocomposite plate (200x200x4 $mm^3$) reinforced with CNTs to that of a square composite plate made of Carbon/ PmPV. The Carbon/PmPV plate consists of four layers in which fibers have the same orientation as the nanocomposite plate. Both plates are simply supported along all four sides. Table 5.7 provides the properties of Carbon fibers.

**Table 5.7** Properties of Carbon Fibers.

| Properties | Carbon |
|---|---|
| $E_f\,(GPa)$ | 390 |
| $G_f\,(GPa)$ | 20 |
| ν | 0.35 |
| $\rho\ (kg/m^3)$ | 1800 |

The objective of this part of the study is to examine the natural frequencies of the Carbon/PmPV and those of the nanocomposite reinforced plate to address the following points:

- Ascertain the effect of the volume fraction (percentage) of carbon fibers on the natural frequencies.
- To determine the threshold volume fraction of carbon composite giving similar frequency to that of the nanocomposite.
- Compare the frequencies of carbon/PmPV with those of the nanocomposite.

**Table 5.8** First Natural frequencies for different volume fractions of Carbon/PmPV plate.

| Fiber volume fraction (%) | Carbon/PmPV | CNTs/PmPV |
|---|---|---|
| | UD | FGX |
| 11 | 462.70 | 544.82 |
| 15 | 484.55 | - |
| 20 | 509.36 | - |
| 25 | 531.84 | - |
| 28.11 | 544.81 | - |
| 30 | 552.36 | - |
| 35 | 571.19 | - |
| 40 | 588.56 | - |
| 45 | 604.66 | - |
| 50 | 619.61 | - |
| 55 | 633.56 | - |
| 60 | 646.58 | - |
| 65 | 658.77 | - |

Table 5.8 presents the fundamental natural frequencies of both Carbon/PmPV and Nanocomposite plates. Therefore, the Carbon fiber volume fraction that makes a Carbon/PmPV plate having the same rigidity as CNTs/PmPV is 28.11%.

### 5.3. Free vibration analysis of piezoelectric sandwich plate

Let us now consider a piezoelectric sandwich plates reinforcement in the heart with graphene platelets GPLs and Carbon Nanotubes CNTs. The plate is geometrically characterized by dimensions of $L\times W\times (h_c+2\times h_p) = 400\times 400\times (20+2\times 2)$ $mm^3$ as illustrated in figure 5.4. The composite plate is reinforced with different configurations for the distribution of nanofillers, and is covered by zirconate titanate (PZT-5A) piezoelectric material on both the top and bottom surfaces.

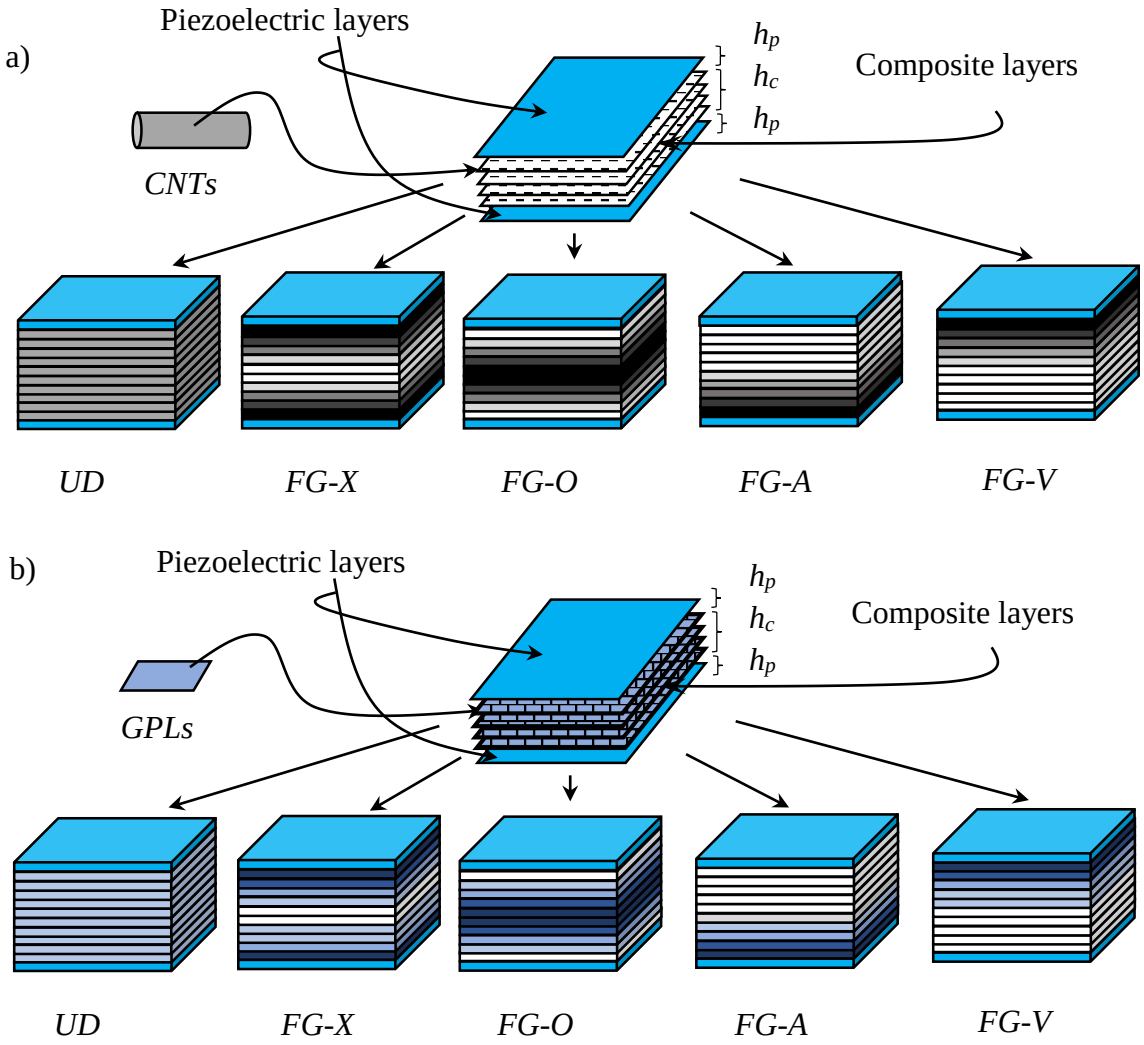


**Figure 5.4:** a) Piezoelectric sandwich plate made of CNTs.
b) Piezoelectric sandwich plate made of GPLs.

The properties of PZT-5A material are: Young's modulus $E^{PZT\text{-}5A} = 63\ GPa$, density $\rho^{PZT\text{-}5A} = 7750\ Kg/m^3$, Poisson's ratio $\nu^{PZT\text{-}5A} = 0.3$, $e_{31} = e_{32} = 6.1468\ C/m^2$, $d_{33} = 1.5\times 10^{-8}\ F/m$.

Table 5.9 presents the first three natural frequencies obtained from the developed code for the plates reinforced with CNTs, and those of Y Kiani [108]. The results look too close to each other. In Table 5.10, we present the first six natural frequencies for plates reinforced with GPLs. It is observed that the FG-X configuration is still giving high frequency. Additionally, it is noted that the frequencies obtained using GPLs as reinforcement are higher compared to those obtained with CNTs. This difference is obtained due to the geometrical characteristics of the reinforcement.

**Table 5.9** First three natural frequencies of piezoelectric sandwich plate reinforced with different configurations of CNTs using $P_{in} = 1$ and SSSS boundary conditions.

| $f_r^*$ | Configuration | Mode 1 | Ref [108] | Mode 2 | Ref [108] | Mode 3 | Ref [108] |
|---|---|---|---|---|---|---|---|
| 0.12 | UD | 581.26 | 581.68 | 1220.39 | 1223.51 | 1618.9 | 1637.4 |
| | FG-X | 618.98 | 620.82 | 1238.63 | 1242.20 | 1767.1 | 1794.4 |
| | FG-V | 576.55 | 558.17 | 1219.11 | 1215.31 | 1520.4 | 1530.4 |
| | FG-O | 539.65 | 538.47 | 1202.21 | 1204.68 | 1434.3 | 1442.3 |
| 0.17 | UD | 624.20 | 622.89 | 1264.04 | 1258.80 | 1784.5 | 1799.3 |
| | FG-X | 674.89 | 675.14 | 1292.45 | 1287.03 | 1967.7 | 1881.0 |
| | FG-V | 617.58 | 589.73 | 1263.03 | 1247.18 | 1652.7 | 1658.3 |
| | FG-O | 567.13 | 563.82 | 1236.77 | 1231.14 | 1546.5 | 1549.9 |
| 0.28 | UD | 685.52 | 685.16 | 1294.57 | 1288.05 | 2010.6 | 1892.7 |
| | FG-X | 756.78 | 757.99 | 1343.69 | 1335.17 | 2231.8 | 1904.7 |
| | FG-V | 676.32 | 636.50 | 1295.80 | 1271.29 | 1840.1 | 1849.0 |
| | FG-O | 603.06 | 599.89 | 1251.32 | 1244.46 | 1708.5 | 1713.1 |

**Table 5.10** First six natural frequencies of piezoelectric sandwich plate reinforced with different configurations of GPLs.

| $f_r^*$ | Configuration | Mode 1 | Mode 2 | Mode 3 | Mode 4 | Mode 5 | Mode 6 |
|---|---|---|---|---|---|---|---|
| 0.12 | UD | 905.177 | 2217.14 | 3475.99 | 4312.38 | 4313.11 | 5486.53 |
| | FG-X | 1045.45 | 2551.07 | 3985.27 | 4932.81 | 4933.41 | 6256.83 |
| | FG-V | 865.155 | 2004.71 | 3169.45 | 3906.08 | 3934.16 | 4992.15 |
| | FG-O | 736.774 | 1811.57 | 2851.14 | 3546.09 | 3547.03 | 4526.73 |
| 0.17 | UD | 1028.55 | 2521.71 | 3956.27 | 4910.45 | 4911.10 | 6251.21 |
| | FG-X | 1203.24 | 2938.56 | 4593.43 | 5687.83 | 5688.36 | 7218.27 |
| | FG-V | 975.321 | 2243.33 | 3553.92 | 4376.51 | 4412.16 | 5600.80 |
| | FG-O | 815.208 | 2006.73 | 3160.98 | 3933.66 | 3934.52 | 5025.24 |
| 0.28 | UD | 1259.57 | 3091.56 | 4854.28 | 6028.27 | 6028.81 | 7679.69 |
| | FG-X | 1496.46 | 3657.58 | 5722.08 | 7089.15 | 7089.58 | 9002.95 |
| | FG-V | 1182.70 | 2697.24 | 4283.84 | 5269.98 | 5317.78 | 6754.77 |
| | FG-O | 966.409 | 2382.04 | 3755.73 | 4676.67 | 4677.43 | 5979.45 |

## 5.4. Static analysis of piezoelectric sandwich plate

In this section of the study, we managed to identify the stiffest plate among the five types of configurations: UD, FG-X, FG-O, FG-A, and FG-V, each is covered with piezoelectric layers (PZT G1195-N) on the top acting as actuators. The plates are initially subjected to a uniform load of 100 Pa, and then charged by an electrical potential equal to 150 volts to their piezoelectric layers. It is assumed that the plates have the same length and width as the plate described in the previous section, but with different thickness of layers ($L=W=$ 400 $mm$, $h_c=$ 1 $mm$, $h_p=$ 0.1 $mm$). The plates are supposed to be clamped on one edge and free on the other three edges (CFFF) or simply supported on their four edges (SSSS).

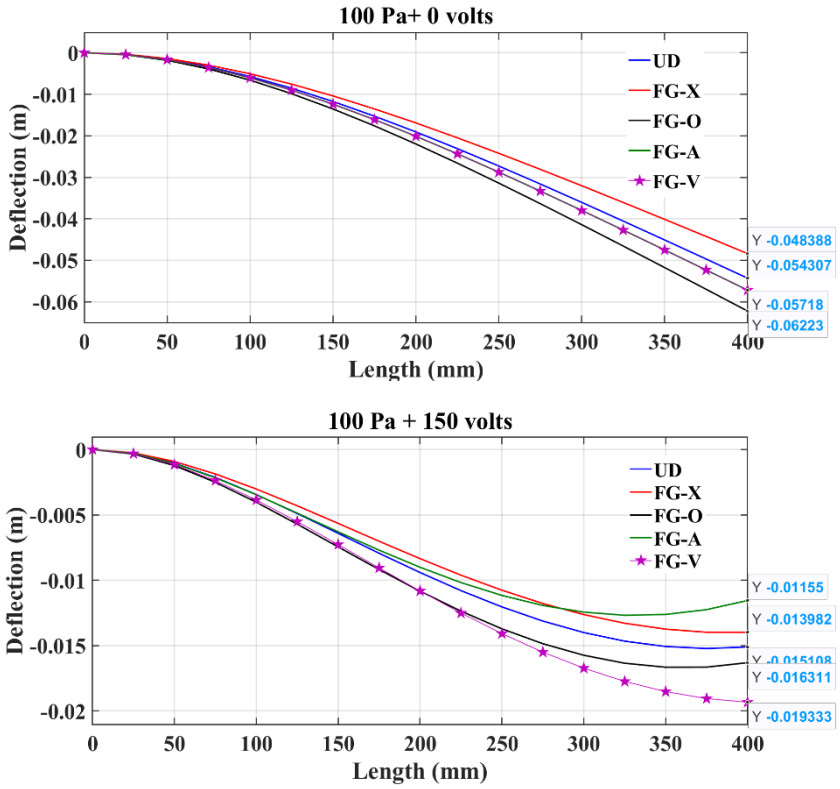


**Figure 5.5:** Deflection of plates reinforced with different FG-CNTs configurations, under a load of 100 Pa, with 0 and 150 voltage applied, stacking sequences $[-45°/45°]_{20}$ and CFFF boundary conditions.

The effect of applied an electrical potential ($\phi_a$) on the piezoelectric layers, makes the forced sandwich plate turn back to the original position (horizontal position). As observed in Figure 5.5, the stiffest plate before the application of the electrical potential is the one reinforced with FG-X configuration, and after the application of the electrical potential, this plate still give the high stiffest. Additionally, it is noted that the deflection of the FG-A and FG-V is

the same deflection before the application of the potential. However, after the electrical potential is applied, the deflections of both configurations differ. This discrepancy can be explained by the boundary conditions (CFFF) that are applied to each configuration and the position of the piezoelectric layer on the top of both FG-A and FG-V plates. This difference was caused by the approach of the piezoelectric layer to the upper layers of the composite of the FG-A configuration that contains fewer nanofillers. This mismatch of nanofiller in the nanocomposite makes the piezoelectric layer deflecting the system easy. Conversely, in the FG-V configuration, where the composite contains a higher concentration of nanofillers, the piezoelectric layer faces more resistance, making it harder to deflect the system (refer Figure 5.6). In contrast, Figure 5.7, which corresponds to the SSSS boundary condition, shows a distinct behavior compared to the CFFF boundary conditions in figure 5.5, where nothing happens to the plates with FG-V and FG-A after electrifying them, they deflected naturally. Additionally, the distribution following an exponential law affects the plate by reducing the

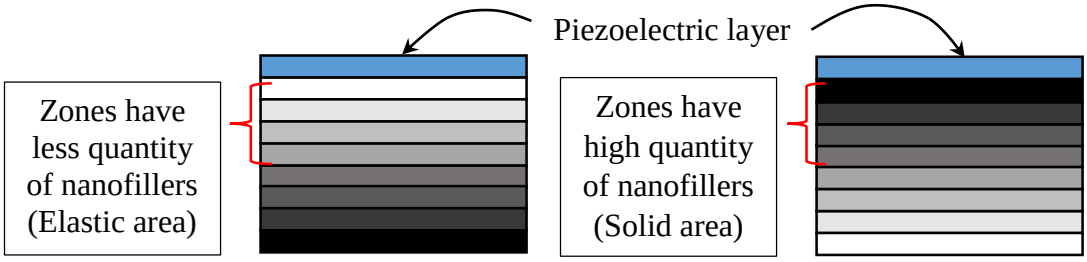


bending of the FG-X plate while increasing the bending of FG-O, FG-A or FG-V plates.

**Figure 5.6:** Explanation of the zones closes to piezoelectric layer, having less and high quantities of nanofillers.

Figure 5.8 shows the effect of varying the $P_{in}$ index of the power law and the use of exponential law function in the distribution of Nanofillers on the deflection of the centerline of a sandwich plate reinforced with oriented $[-45°/45°]_{20}$ CNTs using the FG-X configuration, subjected to a uniform load of 100 Pa and electrified with 190 volts. Therefore, the curve with discontinuous line represents the plate reinforced with FG-X configuration and oriented $[-45°/45°]_{20}$ CNTs, showing the least deflection. The other curves were bending decreases progressively are curves obtained due to the increases in $P_{in}$ index.

To compare the stiffness of plates reinforced with GPLs, CNTs, and oriented CNTs, the FG-X configuration was chosen for all three plates. Moreover, each of these plates is either clamped on one side and free on the other side, or simply supported on their four sides. All plates are subjected to a uniform load of 100 Pa.

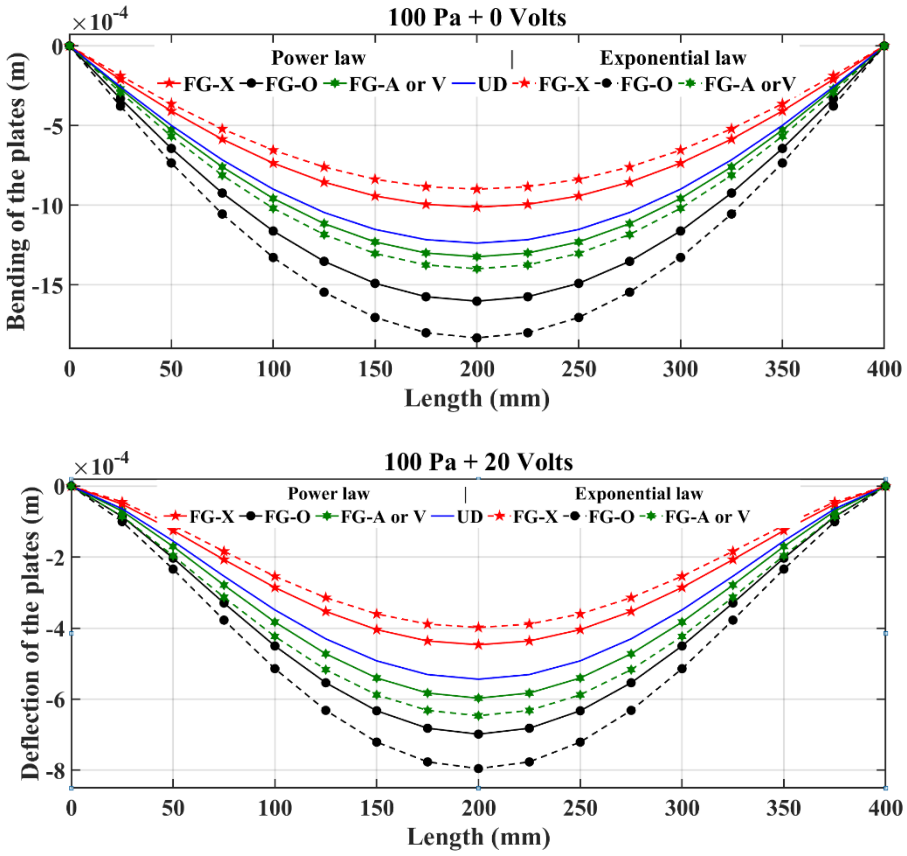


**Figure 5.7:** Deflection of plates reinforced with different FG-CNTs configurations, under a load of 100 Pa with 0 and 20 voltage applied, with SSSS boundary conditions.

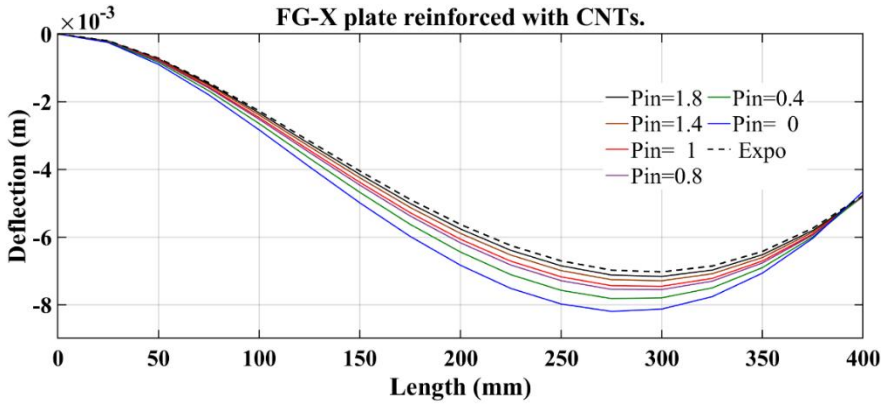


**Figure 5.8:** Deflection of CFFF FG-X plates reinforced with oriented CNTs and reinforced with nonlinear distribution (using power and exponential law).

Figures 5.9 and 5.10 illustrate the bending and deflection behavior of the sandwich plates reinforced with FG-X configuration based on the exponential distribution of reinforcements, and the consideration of an applied load under CFFF and SSSS boundary conditions

respectively. From the results given in Figure 5.9, one can say clearly that the plate reinforced with GPLs exhibits the least bending while it need 210 v to turn it back to the horizontal position. In opposite, the plates reinforced with oriented or non-oriented CNTs need less electrical potential (200 Volt and 170 Volt respectively). This is due to the

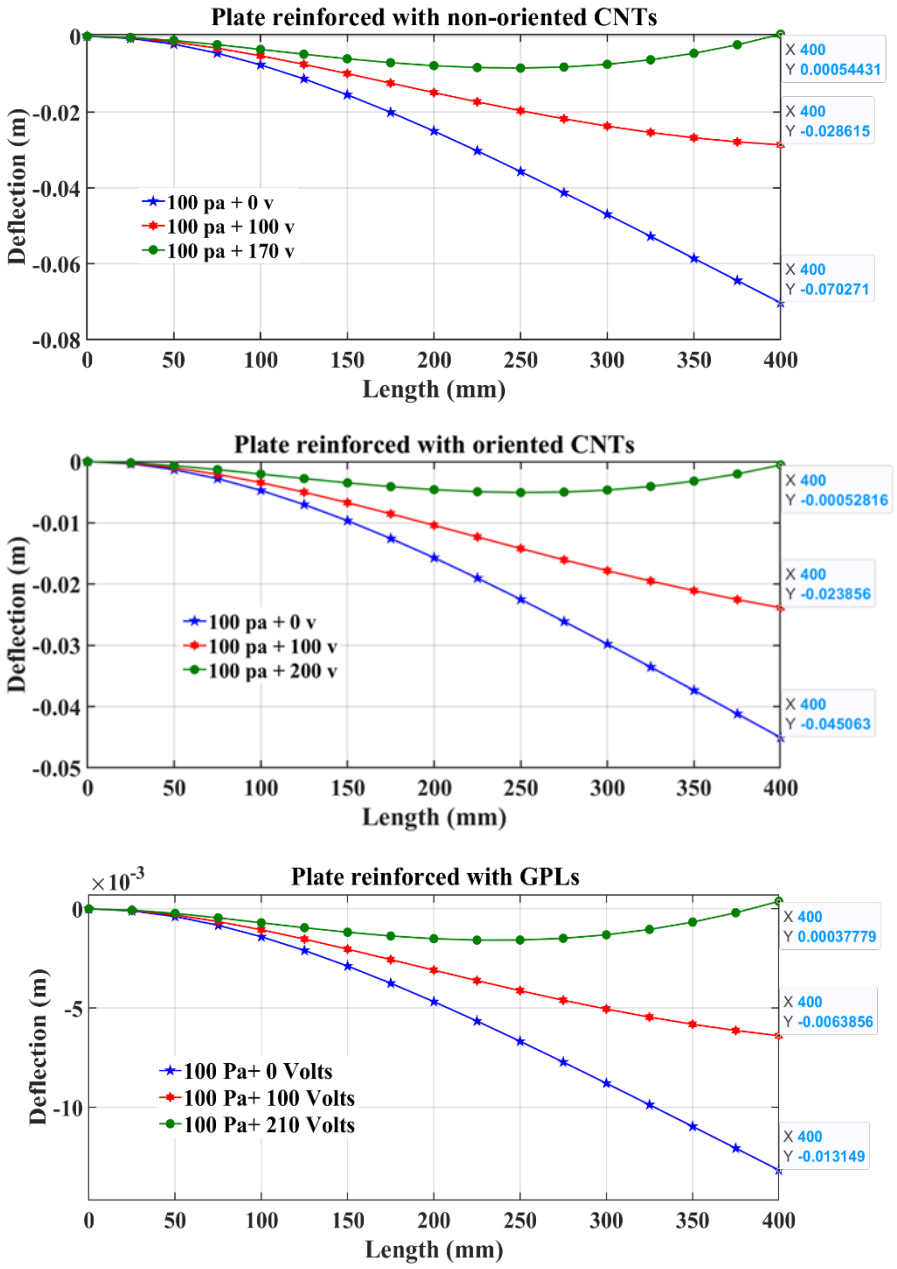


difference between reinforcements, the effect of stacking sequences, and the function that distribute nanofillers (expo law).

**Figure 5.9:** Deflection of CFFF plates reinforced with $(0°)_{20}$, $(-45°/45°)_{20}$ oriented CNTs and GPLs.

The Figure 5.10 present the plate deflection under SSSS boundary conditions. The applied electrical potential that needs the plate to be in horizontal position looks small compared to the electrical potential applied in previous this is due to the type of boundary conditions. The

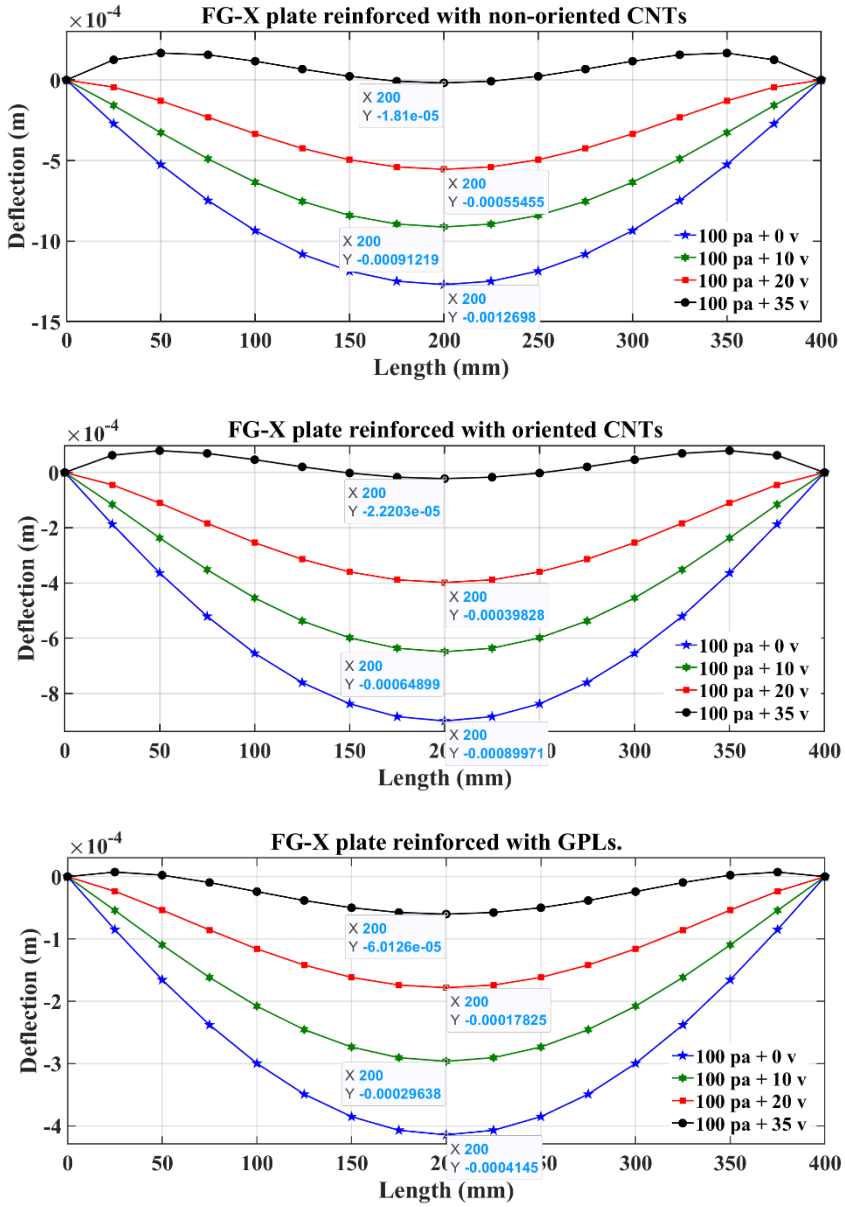


plate reinforced with GPLs and FG-X distribution looks still needs high electrical potential to turn back to the horizontal position which explain the stiffness of the plate (more than 35 v).

**Figure 5.10:** Deflection of the centerline of the SSSS plates reinforced with non-oriented CNTs, oriented CNTs and GPLs.

## 5.5. Dynamic analysis of piezoelectric sandwich plate

### 5.5.1. Validation study

To validate the effectiveness of our vibration control code, a comparative study was carried out to prove its ability to produce accurate results. For this purpose, we use the data provided by Yu and al [53], which used to analyze the vibration of a square sandwich plate 400 × 400 *mm*, with $h_c$ = 5 *mm*, and $h_p$ = 0.1 *mm*. The top and bottom layers are made of G1195-N piezoelectric material, while the core is a functionally graded composite reinforced with CNTs. Figure 5.11 presents the vibration control of the proposed sandwich, using the velocity control gain $G_v$. After comparing our present results with those of Yu and al [53],

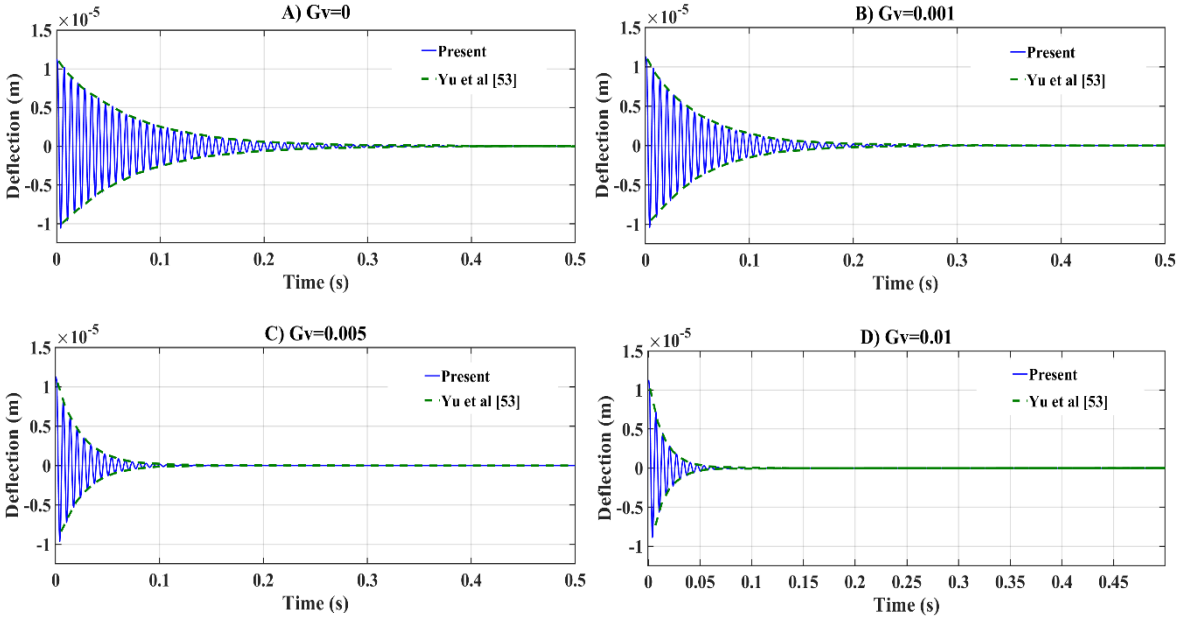


one can observe that there is an excellent concordance between results.

**Figure 5.11:** Vibration control of piezoelectric composite plate reinforced with CNTs and FG-X configuration using control gain: $G_v$ = 0, 0.001, 0.005, and 0.01.

### 5.5.2. Uncontrolled sandwich plate

For the present application, we will study the dynamic behavior of the same plate used in previous work, with simply supported edges, reinforced using the FG-X configuration and the exponential law for the distribution of oriented, non-oriented CNTs, and GPLs. The two points of interest *A* and *B* will be analyzed as explained in Figure 5.12. The plate was supposed to be initially excited by a load of 100 Pa, after which it would be free. The deflection at point A, situated in the center of the plate, is shown in Figure 5.13.

The results obtained show that the vibrations are attenuated for the plate with non-oriented CNTs after approximately 0.45s, and 0.3s for the plate reinforced with oriented CNTs $(-45°/45°)_{20}$, and less than 0.25s for the plate with GPLs. This is due to the stiffness of each of these plates. Furthermore, the plate with GPLs has a less bending about $3.4\times10^{-6}m$ compared to the other plates, which makes her the stiffest one.

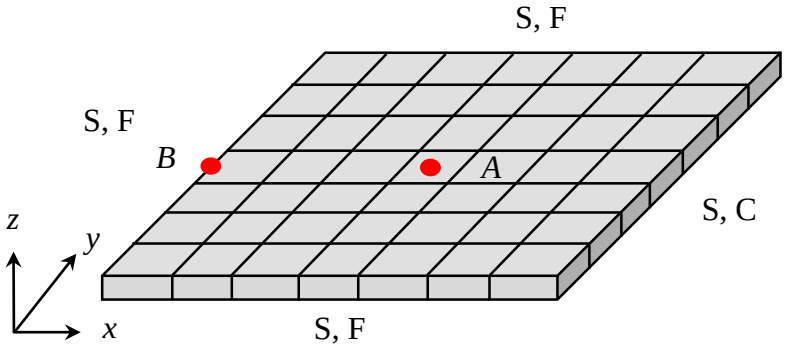


**Figure 5.12:** position of the two points studied.

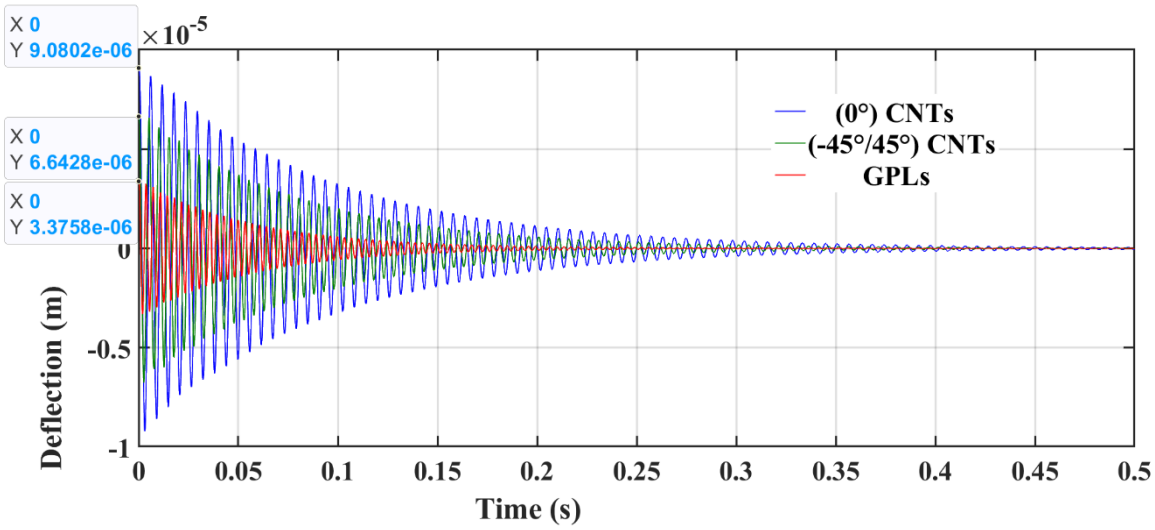


**Figure 5.13:** Deflection of the middle point situated at (x = 0.2 *m*, y = 0.2 *m*).

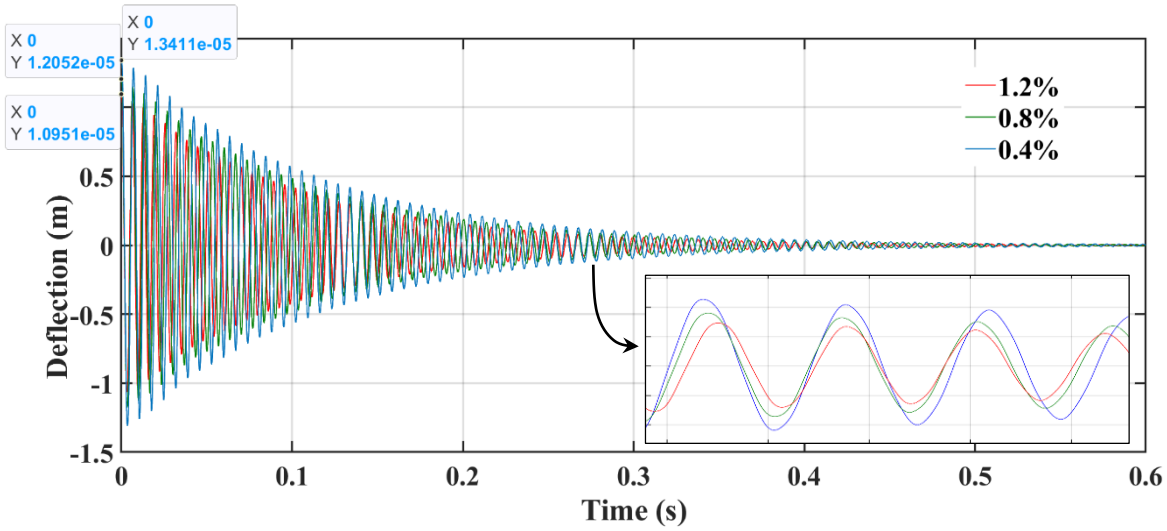


**Figure 5.14:** Effect of increasing the volume fraction of GPLs on vibration amplitudes.

In the following, we studied the effect of varying the volume fraction of GPLs on the deflection of the plate and the time needed to attenuate vibrations. Figure 5.14 presents the obtained signal. It can be seen that when increasing the volume fraction from 0.4% to 1.2%, one notices a decrease in vibrations and this is normal because when we add more reinforcement, the vibrations are decreased and the time is reduced.

In Figure 5.15 we present the vibration of plates reinforced using the four configurations: UD, FG-X, FG-O, and FG-A of distribution.

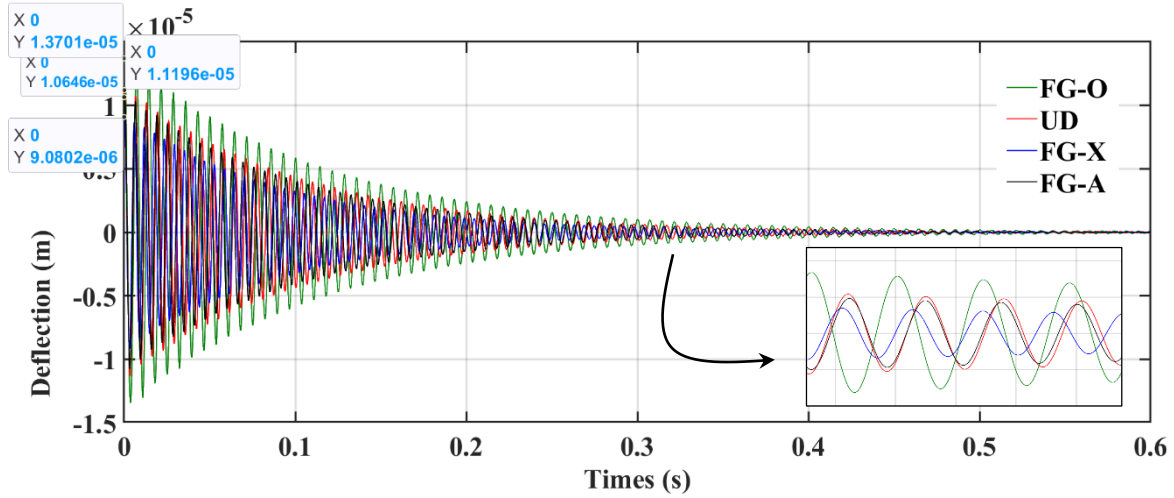


**Figure 5.15:** Vibration control of a simply supported composite plate reinforced with UD, FG-X, FG-O, and FG-A distributions of CNTs.

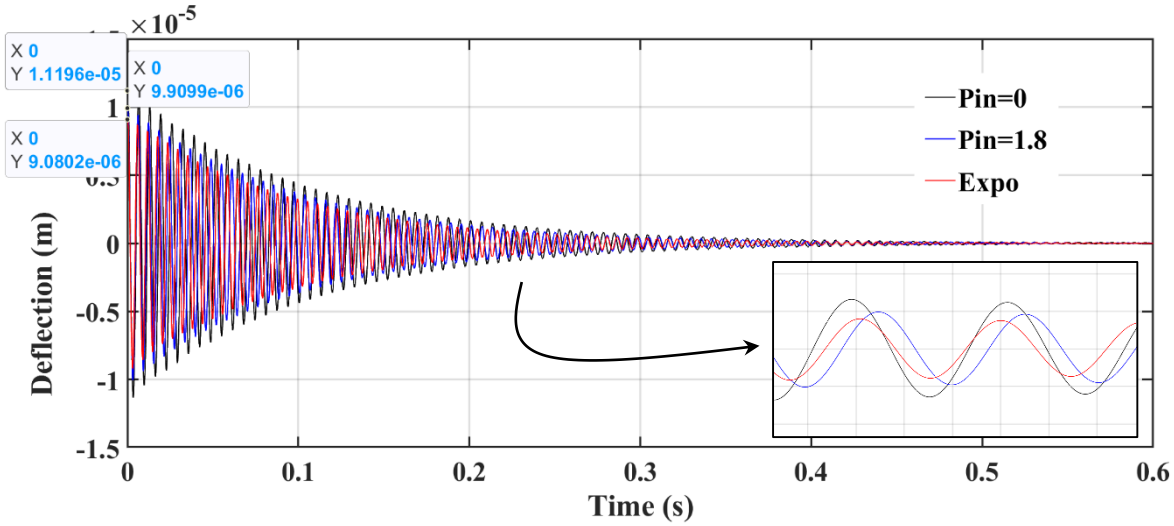


**Figure 5.16:** Vibration control of SSSS Composite plate reinforced with CNTs nonlinear FG-X distribution using $P_{in}$ = 0, 1.8 and Expo.

The objective of this part of the study is to determine the stiffest plate configuration and identify which distribution of carbon nanotubes (CNTs) offers the highest performance in terms of vibration control. Further efforts were made to evaluate the effect of increasing the $P_{in}$ index of the power law distribution and the use of exponential distribution on the vibration behavior of the plate reinforced with the stiffest configuration, identified as the FG-X configuration. The results presented in Figure (5.16) indicate that increasing the $P_{in}$ index of the power law distribution help reduce vibrations, but the exponential distribution help more.

Controlled sandwich plate

In this section, we act the bottom piezoelectric layer as a sensor layer to convert the deformation response into an electrical signal, and the top piezoelectric layer as the actuator. Our sandwich plate is supposed to be simply supported at its four edges. The plate is considered to support a uniform load of 3000 Pa. The Rayleigh damping coefficients $\alpha_R$ and $\beta_R$ are calculated [103] using the design value for the damping ratio (0.8%), the $i^{th}$ natural frequency and the number of modes ($N$) used to estimate Rayleigh's coefficients. For our application, these parameters are taken as $\psi$ = 0.8%, $i^{th}$ = 10 and $N$ = 10, respectively. The parameters in the Newmark method are taken as $\beta$ = 0.25 and $\gamma$ = 0.5, respectively. The goal of this study is to identify the configuration and control parameters that produces the least deflection.

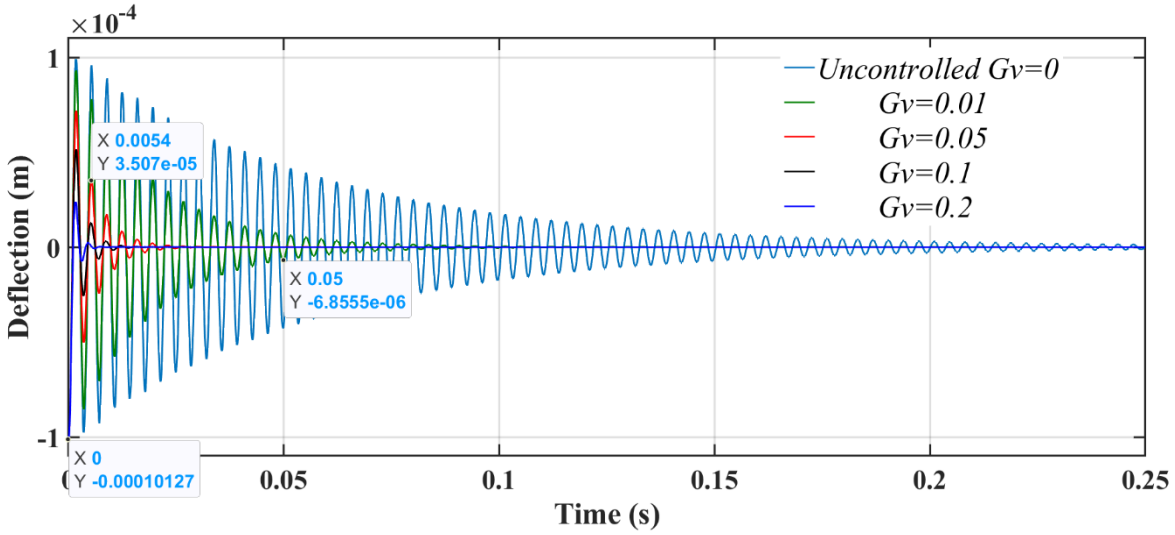


**Figure 5.17:** Dynamic transient response for the observing point *A* of the SSSS square piezoelectric X-GPL sandwich plate using the exponential distribution and velocity control gain ($G_v$ = 0, 0.01, 0.05, 0.1 and 0.2).

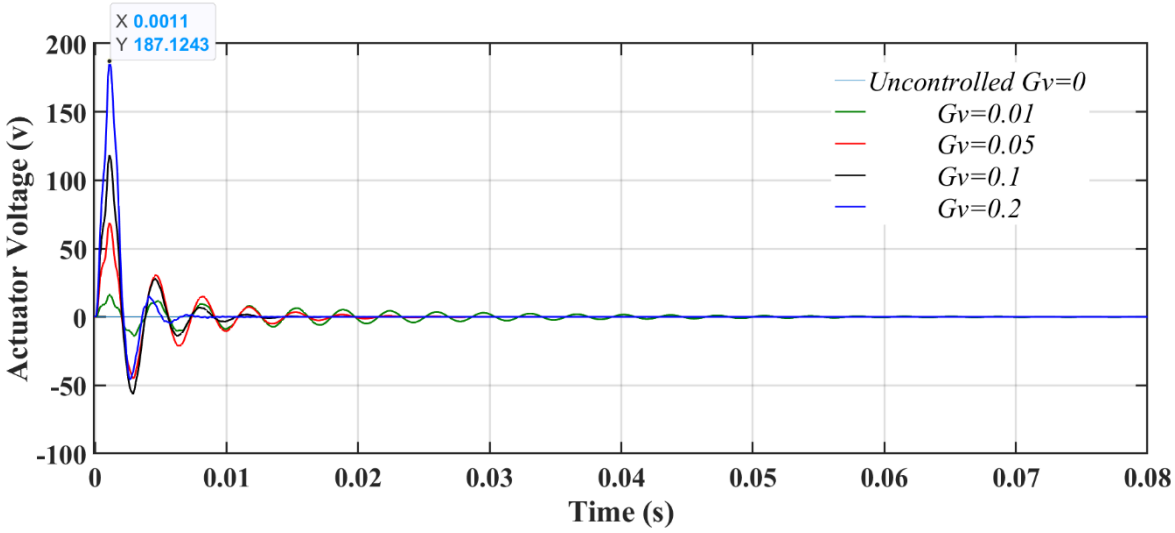


**Figure 5.18:** The applied voltage to the center point of the actuator layer of the SSSS square piezoelectric X-GPL plate.

Figures 5.17, 5.18 and 5.19 explore the impact of the velocity control gain $G_v$ on the dynamic transient response of deflection, actuator and sensor at the observation point A for SSSS plate. As first see, it is noted that the form of the sensor signal is the same as deflection but in term of tension, while the actuator signal differ completely. From figure 5.17 on see clearly that the vibrations are attenuated completely at more than 0.25s for the uncontrolled plate ($G_v$ = 0), at 0.1s when using $G_v$ = 0.01, 0.025s when using $G_v$ = 0.05, less than 0.02s when using $G_v$ = 0.1, and 0.01s when using $G_v$ = 0.2. Another remark, when increasing in the velocity gain, the actuator layer receive a high voltage from controller to attenuate vibration at the first part of the second (0.1s).

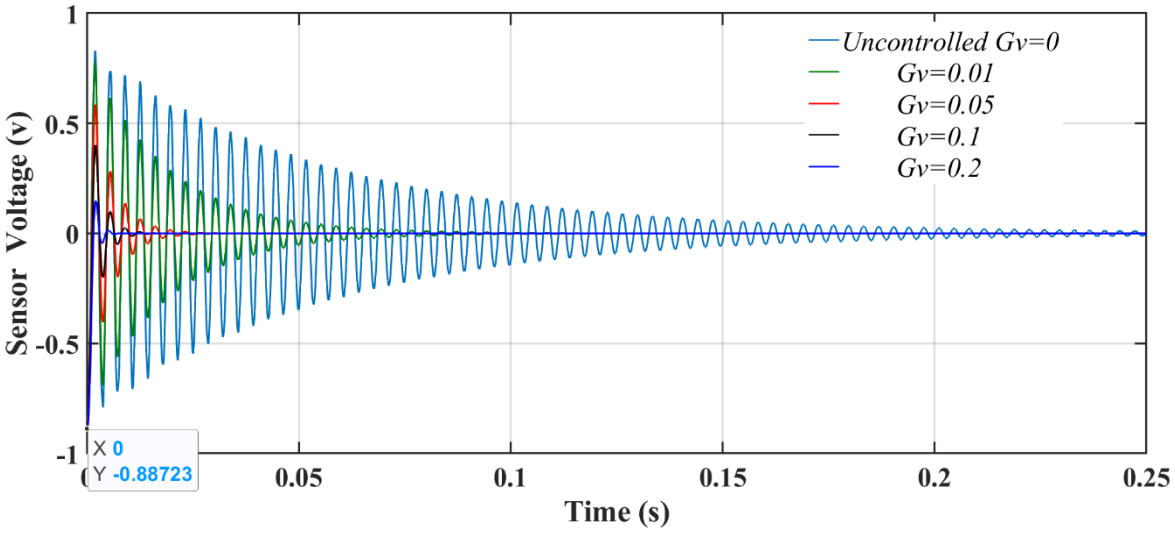


**Figure 5.19:** The generated voltage in the center point of the sensor layer of the SSSS square piezoelectric X-GPL plate.

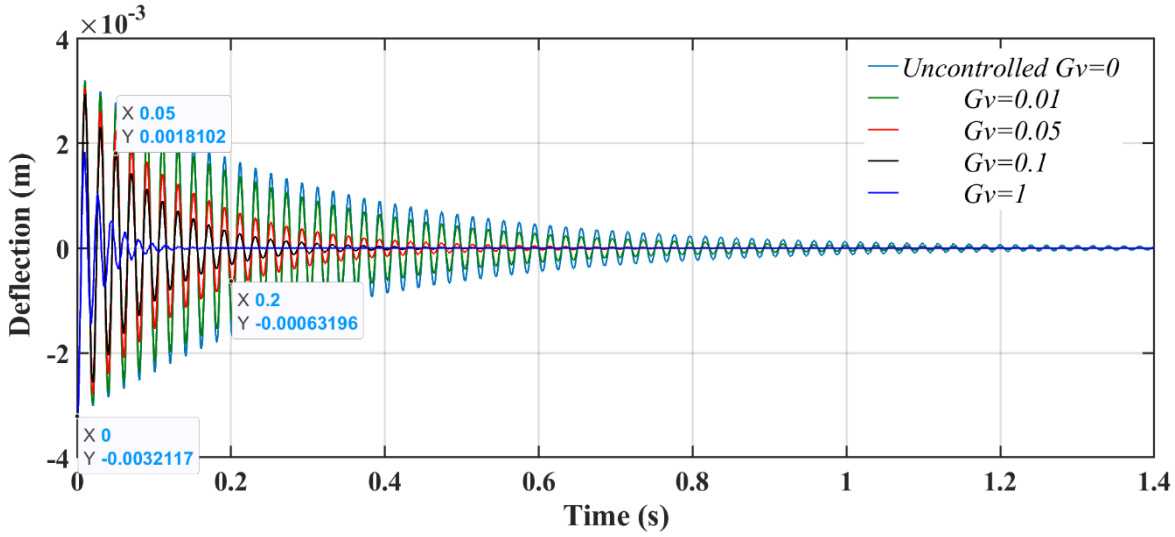


**Figure 5.20**: Dynamic transient response for the observing point *B* of the CFFF square

piezoelectric X-GPL sandwich plate using the exponential distribution and velocity control gain ($G_v$ = 0, 0.01, 0.05, 0.1, and 1).

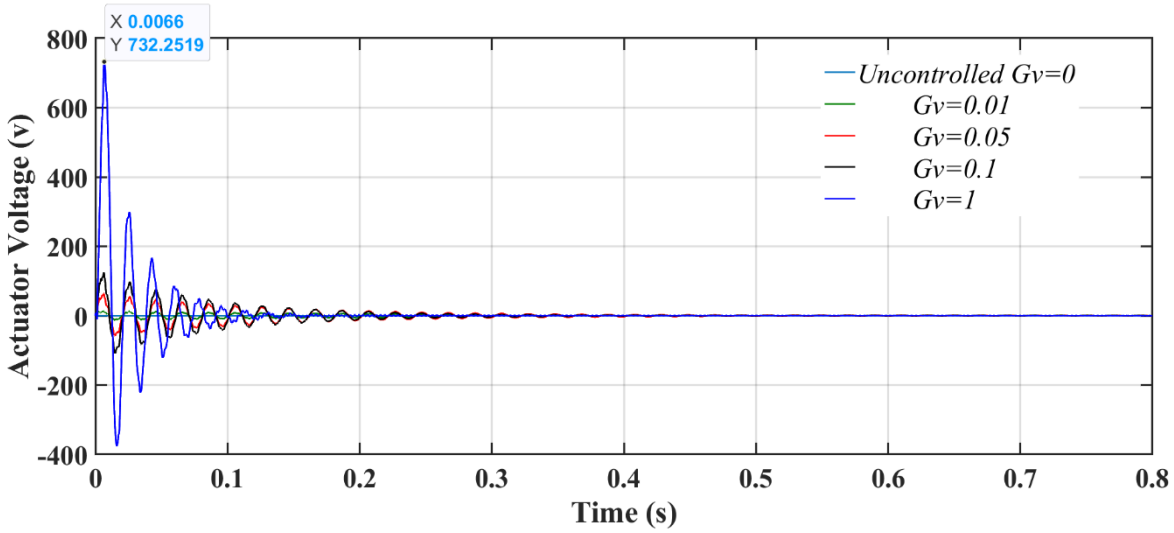


**Figure 5.21:** The applied voltage to the center point of the actuator layer of the CFFF square piezoelectric X-GPL plate.

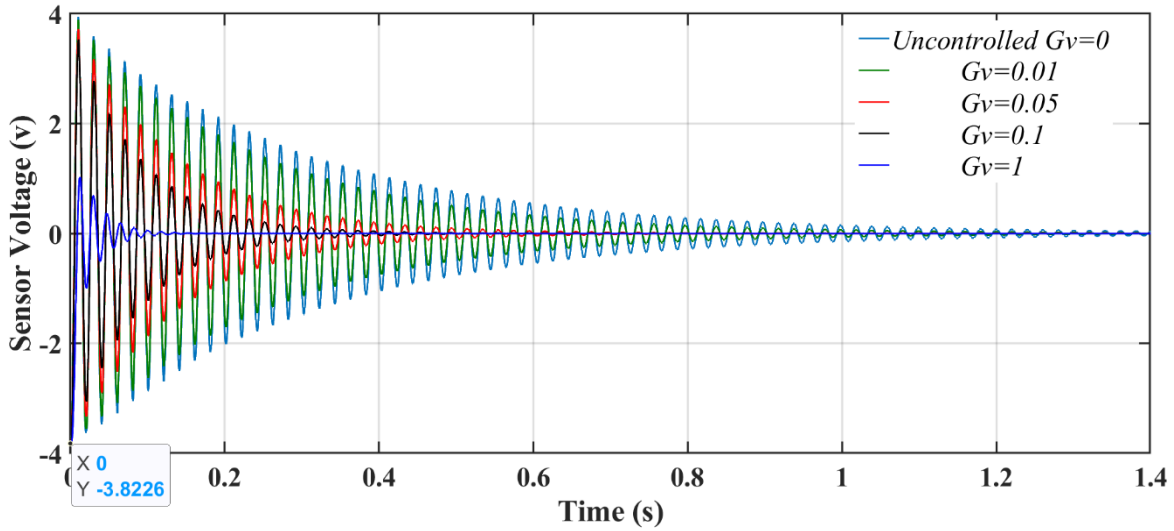


**Figure 5.22:** The generated voltage in the center point of the sensor layer of the CFFF square piezoelectric X-GPL plate.

Figures 5.20, 5.21 and 5.22 explore the impact of the velocity control gain $G_v$ on the dynamic transient response of deflection, actuator and sensor at the observation point B for CFFF plate. From figure 5.20, which represent the vibrations of CFFF plate, the vibrations lock's attenuated completely at 1.6s for the uncontrolled CFFF plate, at 1.2s for the controlled plate using $G_v$ = 0.01, less than 0.8s when using $G_v$ = 0.05, 0.4s when using $G_v$ = 0.1, and 0.15s when using $G_v$ = 1. For the CFFF, the plate vibration locks not completely attenuated which

means that we needs to generate high value of $G_v$ (more than 0.5) to attenuate plate vibrations. Moreover, after comparison between SSSS and CFFF plate vibration it is noted that the SSSS plate vibrations needs low velocity control gain to attenuate vibration in short period, oppositely to the CFFF plate, which need high $G_v$.

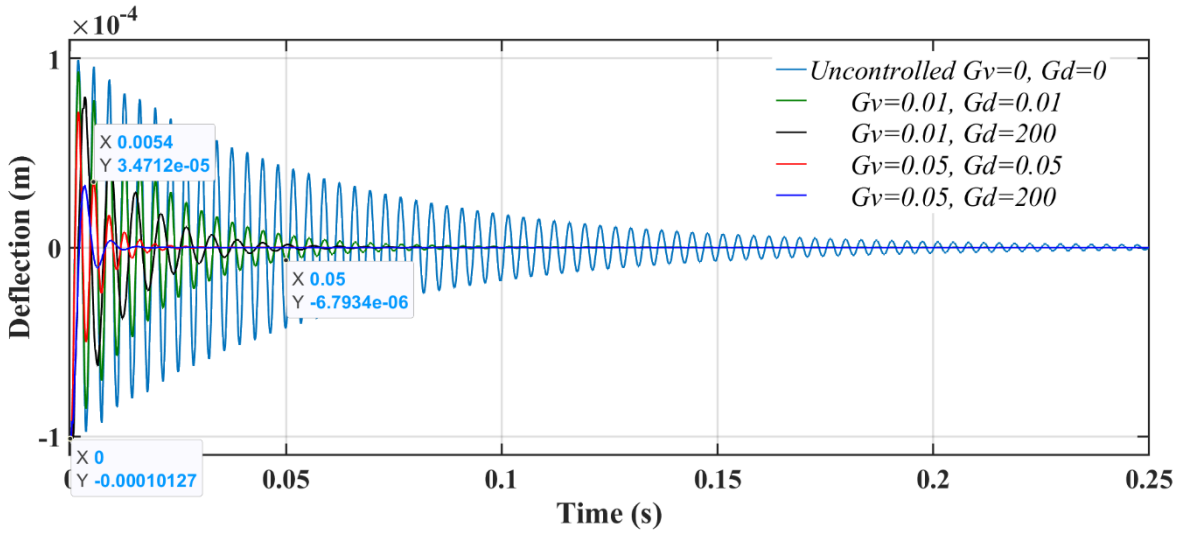


**Figure 5.23:** Dynamic transient response for the observing point *A* of the SSSS square piezoelectric X-GPL sandwich plate using the exponential distribution, the proportional and velocity control gain ($G_v$ and $G_d$).

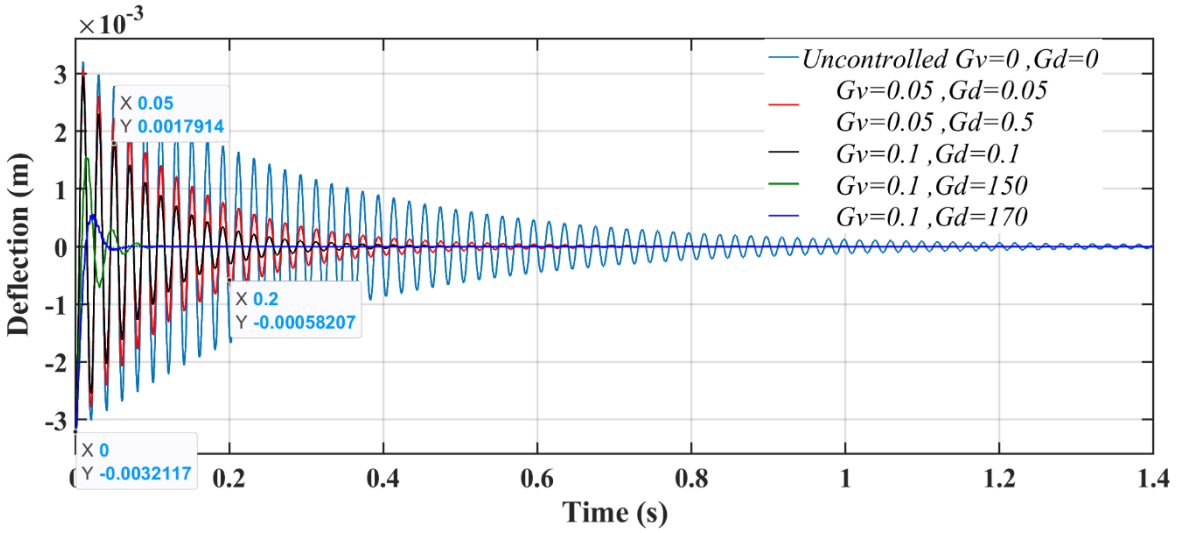


**Figure 5.24:** Dynamic transient response for the observing point *B* of the CFFF square piezoelectric X-GPL sandwich plate using the exponential distribution, the proportional and velocity control gain ($G_v$ and $G_d$).

Figure 5.23 and 5.24 show the effect of increasing the proportional gain $G_d$ on the deflection of the considered square plate. As can be seen, the results indicate that $G_d$ does not affect the

vibrations for low values, but the increase of this to high values is followed by a decrease in plate vibrations. The physical explanation for the use of high $G_d$ values is that this plate exhibit high structural damping $[C_{uu}]_{sandwich}$ than the stiffness $\left[K_{eff}\right]_{sandwich}$.

In another phase of the study, which tests the strength and validates the stiffness of the chosen plate, the plate is considered to keep supporting the uniform load ($F_0 = 3000$ Pa), and is subjected to step or sinusoidal loads. The total exerted force is expressed below:

$$F_{Total} = F_0 . f_1(t) + F(t) . f_2(t) \tag{5.1}$$

SSSS: $$F(t) = F_0 . \sin(\pi . x_A / a) . Sin(\pi . y_A / b) \tag{5.2}$$

CFFF: $$F(t) = F_0 . \cos(\pi . x_B / a) . Sin(\pi . y_B / b) \tag{5.3}$$

With: Step load:

$$\begin{cases} f_1(t) = \begin{cases} 1 & if \quad 0 \le t \le t_1 \\ 0 & if \quad t > t_1 \end{cases} \\ f_2(t) = \begin{cases} 1 & if \quad t = 0 \\ 0 & if \quad t > 0 \end{cases} \end{cases} \tag{5.4}$$

Sinusoidal load:

$$\begin{cases} f_1(t) = \{ \quad 0 \quad if \quad 0 \le t \le +\infty \\ f_2(t) = \begin{cases} Sin\left(\pi . \dfrac{t}{t_1}\right) & if \quad 0 \le t \le t_1 \\ 0 & if \quad t > t_1 \end{cases} \end{cases} \tag{5.5}$$

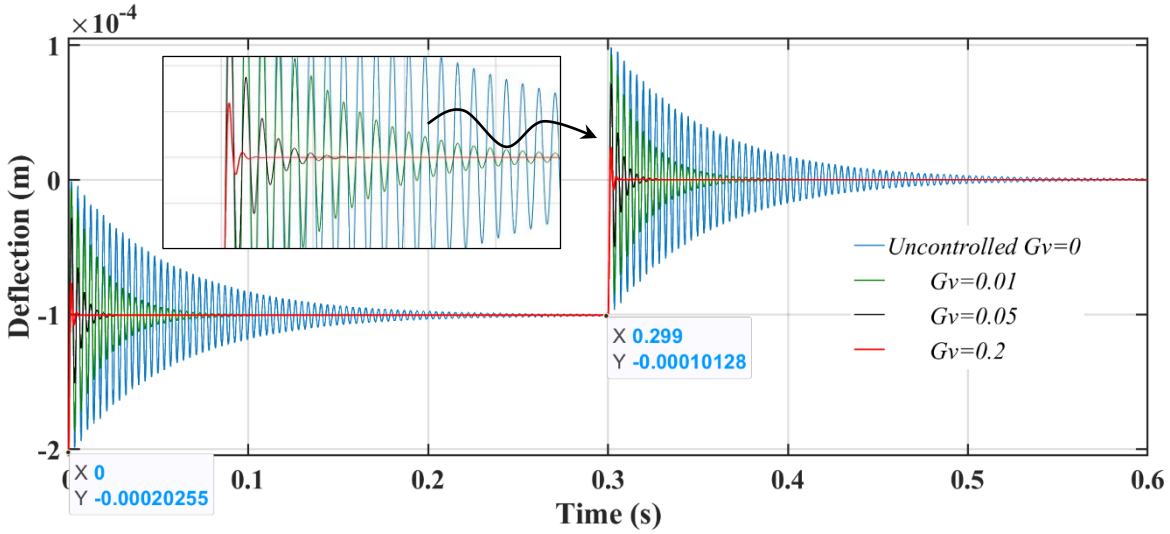


**Figure 5.25:** Dynamic transient response for the observing point *A* of the forced SSSS square piezoelectric X-GPL sandwich plate using step load, the exponential function in distribution, and velocity control gain ($G_v$ = 0, 0.01, 0.05, and 0.2).

Where the x and y are the coordinates of the middle point $A$ ($x_A = 0.2m$, $y_A = 0.2m$) of the plate for the SSSS configuration, and the end point $B$ ($x_B = 0m$, $y_B = 0.2m$) of the plate for the CFFF configuration. a and b are the length and width of the plate (a = $0.4m$, b = $0.4m$).

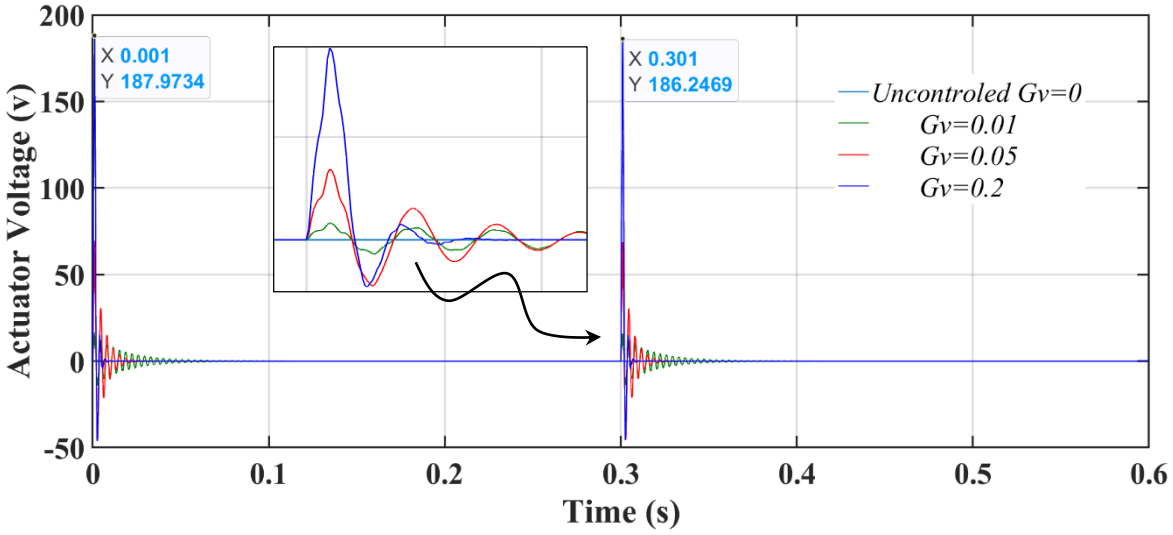


**Figure 5.26:** The applied voltage to the center point of the actuator layer of the forced SSSS square piezoelectric X-GPL plate using step load.

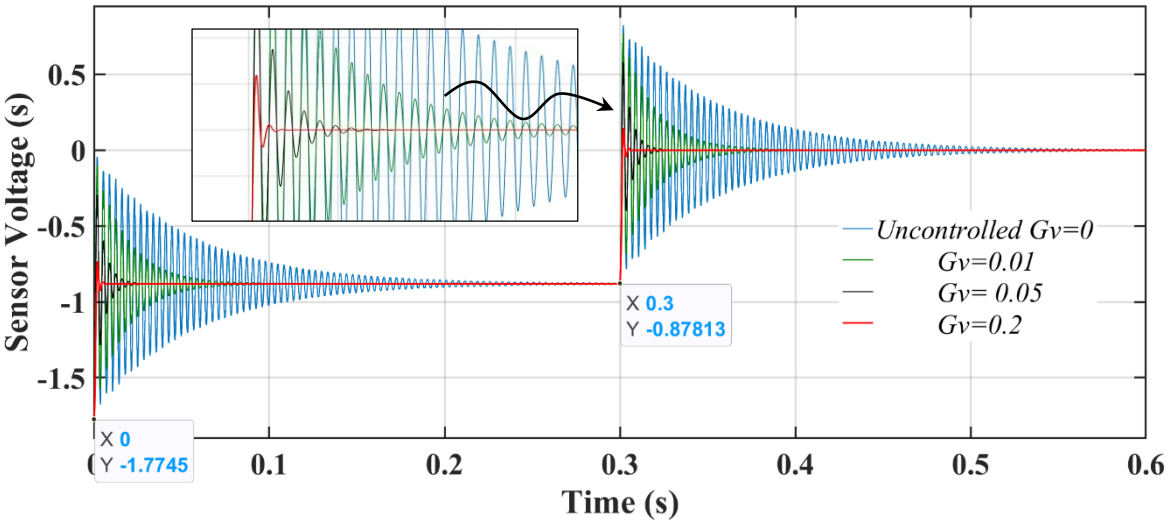


**Figure 5.27:** The generated voltage in the center point of the sensor layer of the forced SSSS square piezoelectric X-GPL plate using step load.

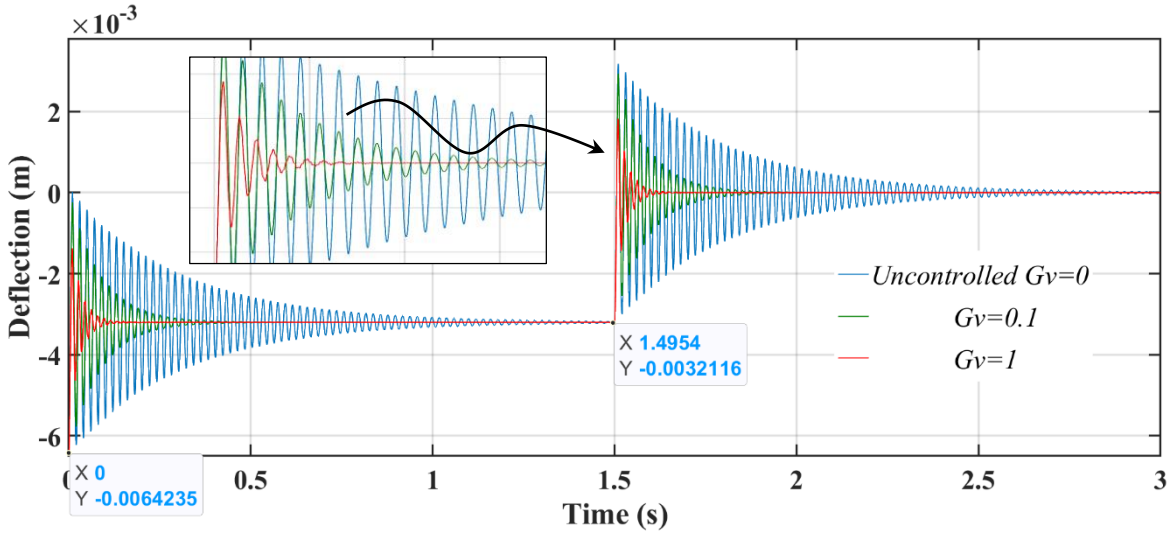


**Figure 5.28:** Dynamic transient response for the observing point *B* of the forced CFFF square piezoelectric X-GPL sandwich plate using step load, the exponential function in distribution, and velocity control gain ($G_v$ = 0, 0.1 and 1).

Figures 5.25, 5.26, and 5.27 present the deflection, actuator, and sensor response, respectively of a SSSS plate, while figures 5.28, 5.29, and 5.30 present the deflection, actuator, and sensor response, respectively of a CFFF plate, under the application of a step load explained in equations 5.1, 5.2, 5.3, and 5.4 during the time interval [0s , 0.3s] and [0s , 1.5s ] respectively. After picking up the $F(t)$ load at t > 0s both SSSS and CFFF plate signal looks on the same staircase compared to the deflection and sensor signals, which have the stairs form.

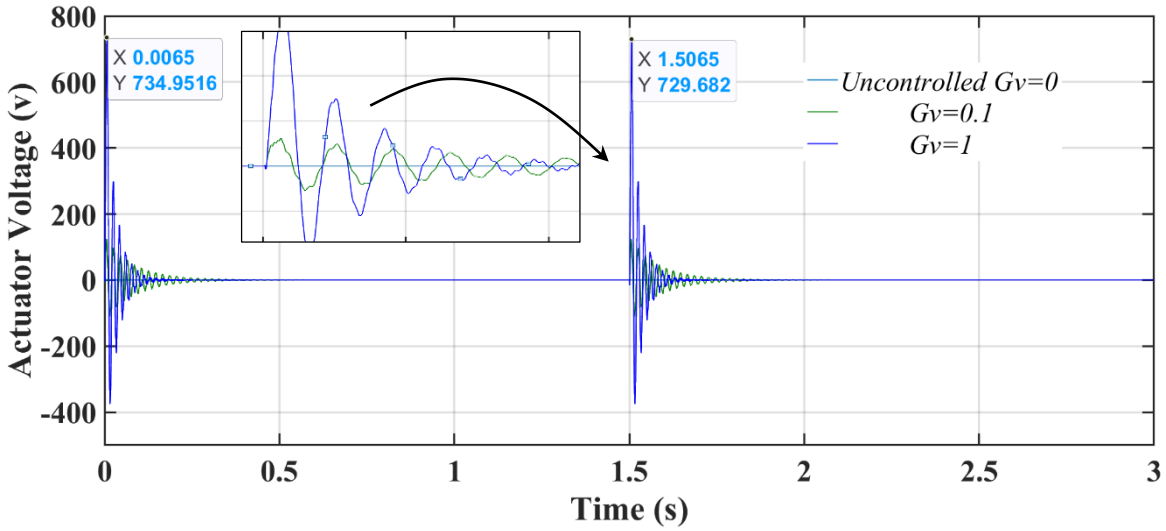


**Figure 5.29:** The applied voltage to the center point of the actuator layer of the forced CFFF square piezoelectric X-GPL plate using step load.

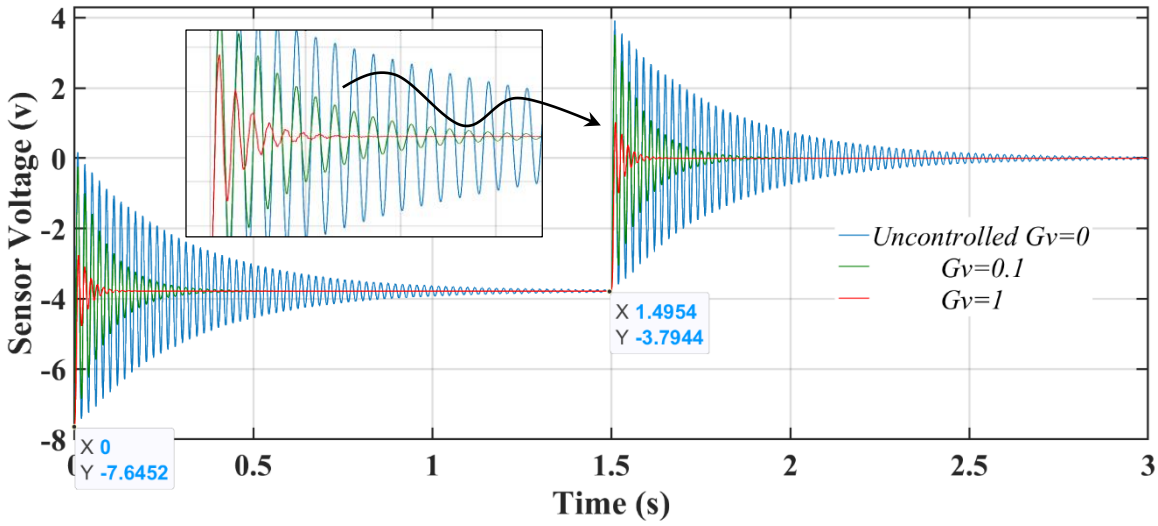


**Figure 5.30:** The generated voltage in the center point of the sensor layer of the forced CFFF square piezoelectric X-GPL plate using step load.

Figures 5.31, 5.32, and 5.33 present the deflection, actuator, and sensor response, oscillate, till they will stabilizes in the bending position obtained in figure 5.17 and 5.20 respectively. Then all the forces are picked up (after 0.3s for SSSS, and 1.5s for CFFF plate respectively). The bending of plate goes to zero. Another observation is that the actuator respectively, of an SSSS plate, while figures 5.34, 5.35, and 5.36 present the deflection, actuator, and sensor response, respectively of a CFFF plate, under the application of a sinusoidal load explained in equations 5.1, 5.2, 5.3, and 5.5 during the time interval [0s 0.3s] and [0s 1.5s ] respectively.

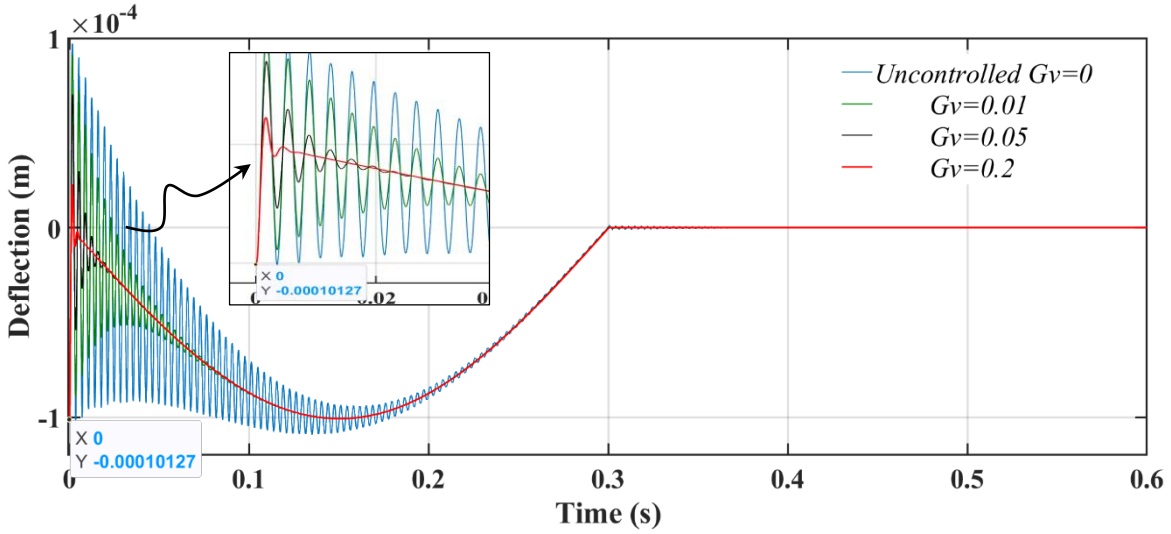


**Figure 5.31:** Dynamic transient response for the observing point *A* of the forced SSSS square piezoelectric X-GPL sandwich plate using sinusoidal load, the exponential function in distribution, and velocity control gain ($G_v$ = 0, 0.01, 0.05 and 0.2).

As we see, the response obtained in deflections of both SSSS and CFFF are transient and permanent response. The increase in the derivative gain leads to the attenuation of vibration in transient response.

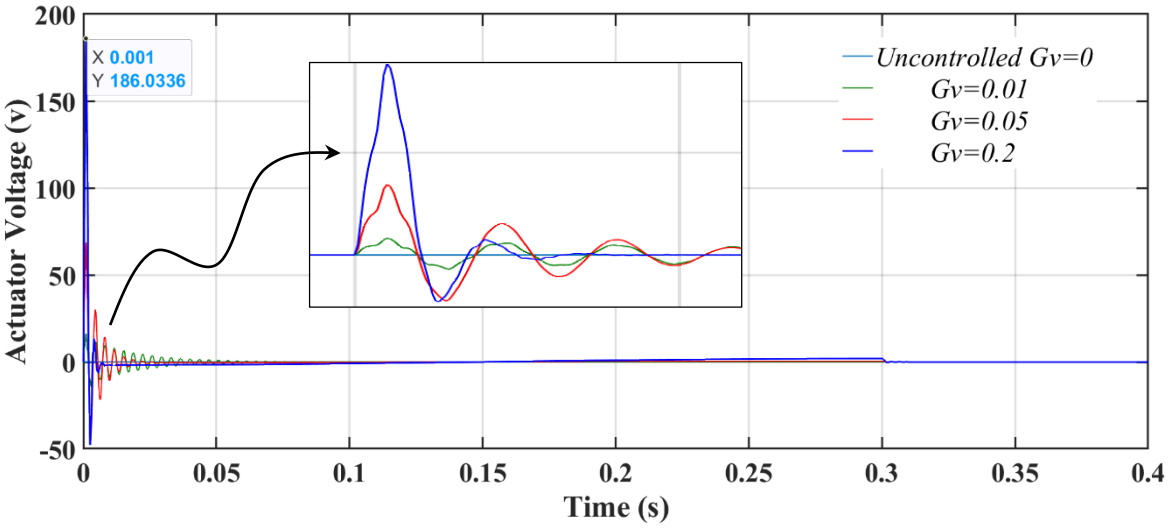


**Figure 5.32:** The applied voltage to the center point of the actuator layer of the forced SSSS square piezoelectric X-GPL plate using sinusoidal load.

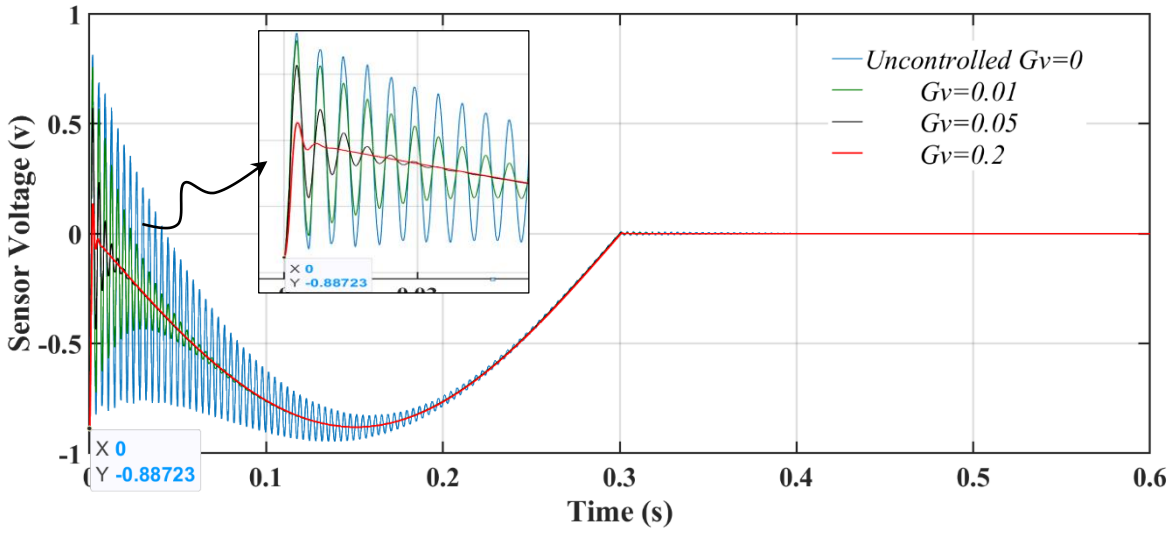


**Figure 5.33:** The generated voltage in the center point of the sensor layer of the forced SSSS square piezoelectric X-GPL plate using sinusoidal load.

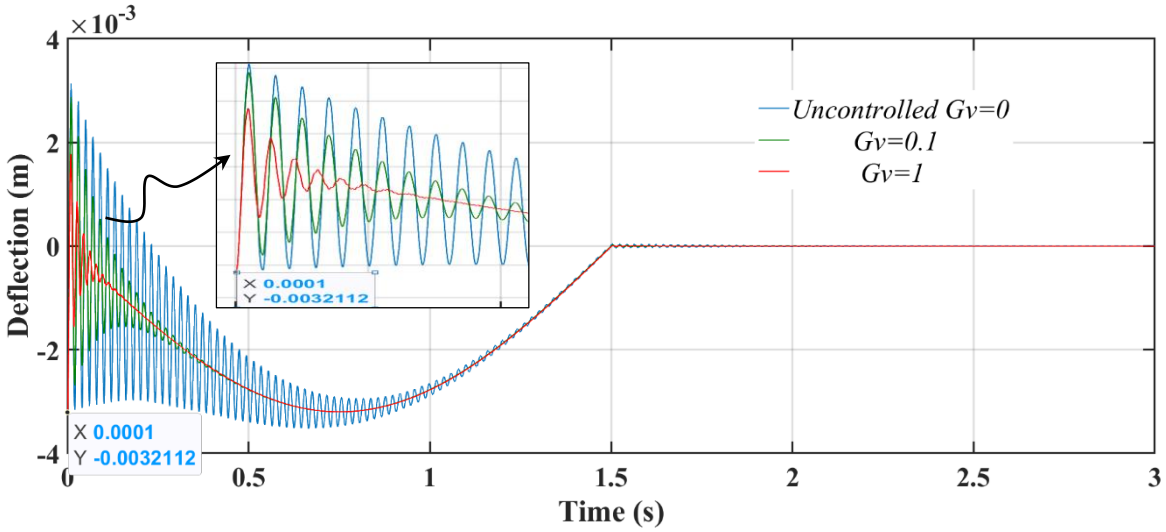


**Figure 5.34:** Dynamic transient response for the observing point *A* of the forced CFFF square piezoelectric X-GPL sandwich plate using sinusoidal load, the exponential function in distribution, and velocity control gain ($G_v$ = 0, 0.1, and 1).

In the CFFF plate, the vibrations do not look completely attenuated, which is due to the boundary conditions that play an essential role in the shrinking and elongation of the piezoelectric actuator layer.

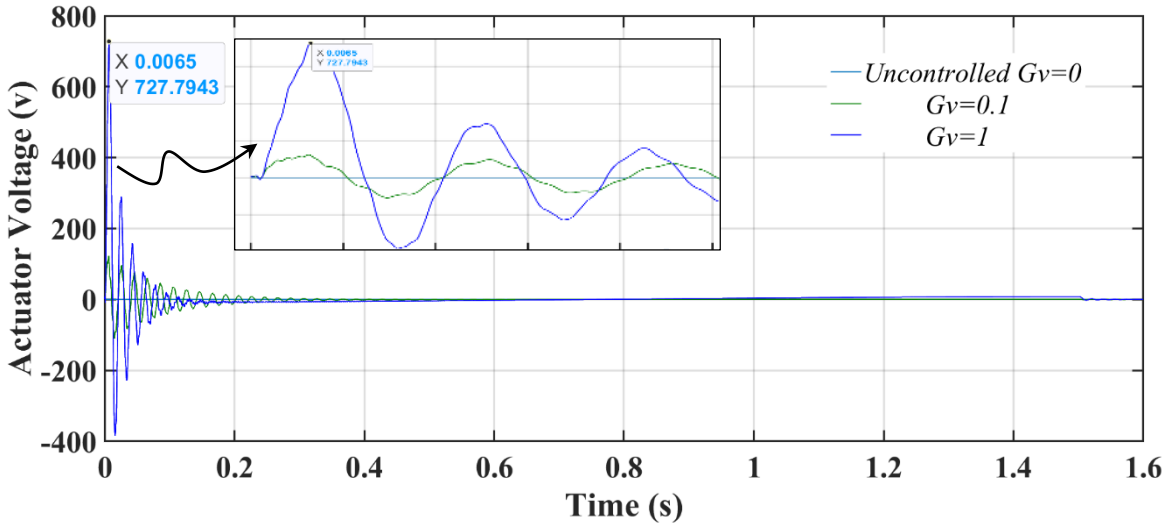


**Figure 5.35:** The applied voltage to the center point of the actuator layer of the forced CFFF square piezoelectric X-GPL plate using sinusoidal load.

.

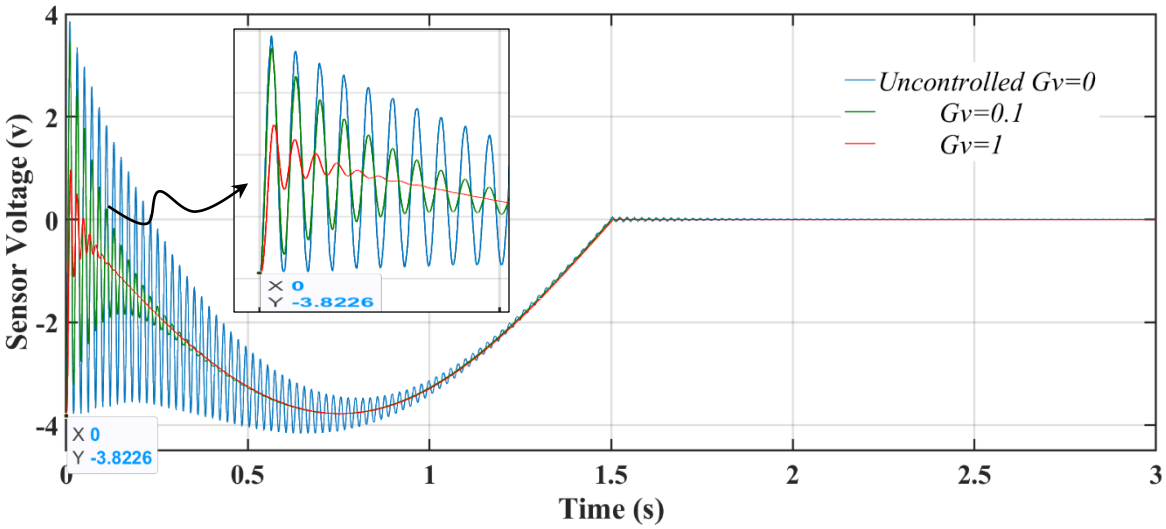


**Figure 5.36:** The generated voltage in the center point of the sensor layer of the forced CFFF square piezoelectric X-GPL plate using sinusoidal load.

# Conclusion

In this thesis, the objective of active vibration control in a sandwich plate, fabricated from a multilayer nanocomposite reinforced with carbon nanotubes or graphene nanoplatelets and utilizing piezoelectric layers as both actuators and sensors, has been achieved. To establish a strong foundation, existing literature on carbon nanotube and graphene nano-platelet-reinforced structures, with a focus on research conducted within the last ten years, is delved into in Chapter one.

The generation of vibrations in various domains where control can be applied, as well as the direct and inverse phenomena of piezoelectricity, are explained in the second chapter. The mechanism of piezoelectric actuator layers in a beam structure is also covered. Subsequently, the nano-fillers considered as reinforcement for the studied composite plates are presented, along with the functions that distribute the nano-fillers inside the composite material. These functions are inspired by the Power and Exponential functionally graded material concept (P-FGM and E-FGM, respectively).

The third chapter successfully presents the first-order shear deformation theory, along with the necessary formulations for kinetic and potential energy and the work done by the external forces of a piezoelectric sandwich plate.

Chapter four focuses on the analysis of the behavior of a square plate subjected to various boundary conditions, using the finite element method (FEM). The main objective is to deduce the stiffness and mass matrices of the plate from the expressions for kinetic and potential energy in the discretized model.

Chapter five presents the main results obtained. It begins with a comparison of the stiffness of two composite plates reinforced with CNTs or GPLs, using power and exponential laws in their distribution. The effect of increasing the volume fraction and the Pin index on the high vibration amplitude is also studied. Subsequently, the plate vibrations were controlled, and their performance was proven. The following important points are derived from the analysis:

- The highest frequencies are exhibited by a plate with concentrated CNTs on the top and bottom surfaces of an FG-X configuration.
- As the volume fraction of CNTs or GPLs rises, so do the natural frequencies.
- Frequencies are increased exponentially, exceeding those predicted by the power law.
- An investigation into the amount of carbon fiber needed in a conventional composite to match the stiffness of a composite containing 11% of CNTs is required.

- Among the three plates reinforced with graphene platelets (GPLs), carbon nanotubes (CNTs), and oriented CNTs, the highest stiffness is exhibited by the GPL-reinforced plate, due to the geometrical characteristics of the nanoplatelets.
- The transient behavior (time history response) observed at the point of interest is not affected by the use of low values for the proportional control gain. However, a significant impact on the response is seen with the derivative control gain.
- As the derivative control gain increases, the time history response at the observation point settles faster, resulting in reduced overshoot.
- An increase in the derivative control gain value leads to a decrease in the generated voltage at the center of the sensor layer, an increase in the applied voltage at the center of the actuator layer, and an attenuation in vibration at the first part of the second.
- In the FG-X configuration, strengthening of the structure and a potential reduction in vibrations are achieved by condensing nano-fillers on the top and bottom layers of the plate.
- The piezoelectric layer, considered as an actuator, is left acting hard on the structure by the use of SSSS boundary conditions. Conversely, the piezoelectric layer is left acting weakly on the structure by the CFFF boundary conditions.

**Perspectives**

In the end, our mind did not stop thinking here, and proposed to explore the active vibration control of the previously studied plate under the influence of external factors like temperature and humidity, and internal factors such as cracks.

Additionally, we propose investigating active vibration control of these plates using electromagnetic attraction and repulsion and doing the comparison with previous control method witch use the piezoelectric material.

## REFERENCES


[1] Iijima, Sumio. 19 9 1 Nature Publishing Group. *Nature*, 1991, vol. 354, no 6348, p. 56-58.

[2] Shen, Hui-Shen. Nonlinear bending of functionally graded carbon nanotube-reinforced composite plates in thermal environments. *Composite Structures*, 2009, vol. 91, no 1, p. 9-19.

[3] Kim, Myungsoo, Park, Young-Bin, Okoli, Okenwa I., *et al.* Processing, characterization, and modeling of carbon nanotube-reinforced multiscale composites. *Composites Science and Technology*, 2009, vol. 69, no 3-4, p. 335-342.

[4] Faulkner, Susan D., Kwon, Young W., Barttlet, S., *et al.* Study of composite joint strength with carbon nanotube reinforcement. *Journal of materials science*, 2009, vol. 44, p. 2858-2864.

[5] Shao, L. H., Luo, R. Y., Bai, S. L, *et al.* Prediction of effective moduli of carbon nanotube–reinforced composites with waviness and debonding. *Composite structures*, 2009, vol. 87, no 3, p. 274-281.

[6] Karappapas, P., Vavoliotis, A., Tsotra, P., *et al.* Enhanced fracture properties of carbon reinforced composites by the addition of multi-wall carbon nanotubes. *Journal of Composite Materials*, 2009, vol. 43, no 9, p. 977-985.

[7] Choi, Hyunjoo, Shin, Jaehyuck, Min, Byungho, *et al.* Reinforcing effects of carbon nanotubes in structural aluminum matrix nanocomposites. *Journal of Materials Research*, 2009, vol. 24, no 8, p. 2610-2616.

[8] Formica, Giovanni, Lacarbonar, Walter, et Alessi, Roberto. Vibrations of carbon nanotube-reinforced composites. *Journal of sound and vibration*, 2010, vol. 329, no 10, p. 1875-1889.

[9] Konsta-Gdoutos M. S. , Z. S. Metaxa, and S. P. Shah, “Highly dispersed carbon nanotube reinforced cement based materials,” *Cem. Concr. Res.*, vol. 40, no. 7, pp. 1052–1059, 2010.

[10] Liu S. Y. , F. P. Gao, Q. Y. Zhang, X. Zhu, and W. Z. Li, “Fabrication of carbon nanotubes reinforced AZ91D composites by ultrasonic processing,” *Trans. Nonferrous Met. Soc. China (English Ed.*, vol. 20, no. 7, pp. 1222–1227, 2010.

[11] Kwon, Hansang, Bradbury, Christopher R., et LEPAROUX, Marc. Fabrication of functionally graded carbon nanotube-reinforced aluminum matrix composite. *Advanced engineering materials*, 2011, vol. 13, no 4, p. 325-329.

[12] Burkholder, Garrett L., Kwon, Young W., et Pollak, Randall D. Effect of carbon nanotube reinforcement on fracture strength of composite adhesive joints. *Journal of materials science*, 2011, vol. 46, p. 3370-3377.

[13] Ayatoulahi, M. R., Shadlou, S., et Shokrieh, M. M. Multiscale modeling for mechanical properties of carbon nanotube reinforced nanocomposites subjected to different types of loading. *Composite Structures*, 2011, vol. 93, no 9, p. 2250-2259.

[14] Yang, Xudong, SHI, Chunsheng, HE, Chunnian, *et al.* Synthesis of uniformly dispersed carbon nanotube reinforcement in Al powder for preparing reinforced Al composites. *Composites Part A: Applied Science and Manufacturing*, 2011, vol. 42, no 11, p. 1833-1839.

[15] Savvas, D. N, Papadoppoulos, V, et Papadrakakis, M. The effect of interfacial shear strength on damping behavior of carbon nanotube reinforced composites. *International Journal of Solids and Structures*, 2012, vol. 49, no 26, p. 3823-3837.

[16] Mehrabadi, S. Jafari, ARAGH, B. Sobhani, Khoshkhahesh, V., *et al.* Mechanical buckling of nanocomposite rectangular plate reinforced by aligned and straight single-walled carbon nanotubes. *Composites Part B: Engineering*, 2012, vol. 43, no 4, p. 2031-2040.

[17] LEI, Z. X., LIEW, K. M., et YU, J. L. Free vibration analysis of functionally graded carbon nanotube-reinforced composite plates using the element-free kp-Ritz method in thermal environment. *Composite Structures*, 2013, vol. 106, p. 128-138.

[18] Rafiee, Mohammad, Yang, Jie, et Kitiporenshai, Sritawat. Large amplitude vibration of carbon nanotube reinforced functionally graded composite beams with piezoelectric layers. *Composite Structures*, 2013, vol. 96, p. 716-725.

[19] Wattenasakulpong, Nuttawit et Ungbhakorn, Variddhi. Analytical solutions for bending, buckling and vibration responses of carbon nanotube-reinforced composite beams resting on elastic foundation. *Computational Materials Science*, 2013, vol. 71, p. 201-208.

[20] Ke, Liao-Liang, Yang, Jie, et Kitiporenshai, Sritawat. Dynamic stability of functionally graded carbon nanotube-reinforced composite beams. *Mechanics of Advanced Materials and Structures*, 2013, vol. 20, no 1, p. 28-37.

[21] Alibeigloo, A. Static analysis of functionally graded carbon nanotube-reinforced composite plate embedded in piezoelectric layers by using theory of elasticity. *Composite Structures*, 2013, vol. 95, p. 612-622.

[22] Devalve, C. et Pitchumani, R. Experimental investigation of the damping enhancement in fiber-reinforced composites with carbon nanotubes. *Carbon*, 2013, vol. 63, p. 71-83.

[23] Malekzadeh, P. et Shojaee, M. Buckling analysis of quadrilateral laminated plates with carbon nanotubes reinforced composite layers. *Thin-Walled Structures*, 2013, vol. 71, p. 108-118.

[24] Shahrbabaki, E. Abdollahzadeh et Alibeigloo, A. Three-dimensional free vibration of carbon nanotube-reinforced composite plates with various boundary conditions using Ritz method. *Composite Structures*, 2014, vol. 111, p. 362-370.

[25] Ansari, R., Shojaei, M. Faghih, Mohammadi, V., *et al.* Nonlinear forced vibration analysis of functionally graded carbon nanotube-reinforced composite Timoshenko beams. *Composite Structures*, 2014, vol. 113, p. 316-327.

[26] Malekzadeh, P. et Zarei, A. R. Free vibration of quadrilateral laminated plates with carbon nanotube reinforced composite layers. *Thin-Walled Structures*, 2014, vol. 82, p. 221-232.

[27] Lin, Feng et Xiang, Yang. Numerical analysis on nonlinear free vibration of carbon nanotube reinforced composite beams. *International Journal of Structural Stability and Dynamics*, 2014, vol. 14, no 01, p. 1350056.

[28] Heydarpour, Y., Aghdam, M. M., et Malekzadeh, P. Free vibration analysis of rotating functionally graded carbon nanotube-reinforced composite truncated conical shells. *Composite Structures*, 2014, vol. 117, p. 187-200.

[29] Natarajan, Sundararajan, Haboussi, Mohamed, et Manickam, Ganapathi. Application of higher-order structural theory to bending and free vibration analysis of sandwich plates with CNT reinforced composite facesheets. *Composite Structures*, 2014, vol. 113, p. 197-207.

[30] FAN, Yin et Wang, Hai. Nonlinear vibration of matrix cracked laminated beams containing carbon nanotube reinforced composite layers in thermal environments. *Composite Structures*, 2015, vol. 124, p. 35-43.

[31] Wattanasakulpong, Nuttawit et Chaikittiratana, Arisara. Exact solutions for static and dynamic analyses of carbon nanotube-reinforced composite plates with Pasternak elastic foundation. *Applied Mathematical Modelling*, 2015, vol. 39, no 18, p. 5459-5472.

[32] Ravari, MR Karamooz, Zeighampour, H. *et al.* Vibration analysis of functionally graded carbon nanotube-reinforced composite nanoplates using Mindlin's strain gradient theory. *Composite Structures*, 2015, vol. 134, p. 1036-1043.

[33] Thomas, Benedict et Roy, Tarapada. Vibration analysis of functionally graded carbon nanotube-reinforced composite shell structures. *Acta Mechanica*, 2016, vol. 227, no 2, p. 581-599.

[34] Wang, Miao, LI, Zhi-Min, et Qiao, Pizhong. Semi-analytical solutions to buckling and free vibration analysis of carbon nanotube-reinforced composite thin plates. *Composite Structures*, 2016, vol. 144, p. 33-43.

[35] Mirzai, M. et Kiani, Y. Free vibration of functionally graded carbon nanotube reinforced composite cylindrical panels. *Composite Structures*, 2016, vol. 142, p. 45-56.

[36] Kamarian, Saeed, Salim, Mostafa, Dimitri, Rossana, *et al.* Free vibration analysis of conical shells reinforced with agglomerated Carbon Nanotubes. *International Journal of Mechanical Sciences*, 2016, vol. 108, p. 157-165.

[37] Setoodeh, A. R. et Shojafee, M. Application of TW-DQ method to nonlinear free vibration analysis of FG carbon nanotube-reinforced composite quadrilateral plates. *Thin-Walled Structures*, 2016, vol. 108, p. 1-11.

[38] Fu, Yiming, Zhong, Jun, Shao, Xuefei, *et al.* Analysis of nonlinear dynamic stability for carbon nanotube-reinforced composite plates resting on elastic foundations. *Mechanics of Advanced Materials and Structures*, 2016, vol. 23,

no 11, p. 1284-1289.

[39] Wu, H. L., Yang, Jie, et Kitiporanshai, Sritawat. Nonlinear vibration of functionally graded carbon nanotube-reinforced composite beams with geometric imperfections. *Composites Part B: Engineering*, 2016, vol. 90, p. 86-96.

[40] Garciz-Macias, Enrique, Rodreguez-Tembleque, Luis, et SÁEZ, Andrés. Bending and free vibration analysis of functionally graded graphene vs. carbon nanotube reinforced composite plates. *Composite Structures*, 2018, vol. 186, p. 123-138.

[41] Song, Mitao, Yang, Jie, Kitiporenshai, Sritawat, *et al.* Buckling and postbuckling of biaxially compressed functionally graded multilayer graphene nanoplatelet-reinforced polymer composite plates. *International Journal of Mechanical Sciences*, 2017, vol. 131, p. 345-355.

[42] Lin, H. G., CAO, D. Q., et XU, Y. Q. Vibration, buckling and aeroelastic analyses of functionally graded multilayer graphene-nanoplatelets-reinforced composite plates embedded in piezoelectric layers. *International Journal of Applied Mechanics*, 2018, vol. 10, no 03, p. 1850023.

[43] Arefi, Mohammad, Bidgoli, Elyas Mohammad-Rezaei, Dimitri, Rossana, *et al.* Free vibrations of functionally graded polymer composite nanoplates reinforced with graphene nanoplatelets. *Aerospace Science and Technology*, 2018, vol. 81, p. 108-117.

[44] Wang, Aiwen, Chen, Hongyan, Hao, Yuxin, *et al.* Vibration and bending behavior of functionally graded nanocomposite doubly-curved shallow shells reinforced by graphene nanoplatelets. *Results in Physics*, 2018, vol. 9, p. 550-559.

[45] Selim, B. A., Liu, Zishun, et Liew, K. M. Active vibration control of functionally graded graphene nanoplatelets reinforced composite plates integrated with piezoelectric layers. *Thin-Walled Structures*, 2019, vol. 145, p. 106372.

[46] Nguyen, Nam V., Lee, Jaehong, et Nguyen-Xuan, H. Active vibration control of GPLs-reinforced FG metal foam plates with piezoelectric sensor and actuator layers. *Composites Part B: Engineering*, 2019, vol. 172, p. 769-784.

[47] Mirjavadi, Seyed Sajad, Forsat, Masoud, Hamouda, A. M. S., *et al.* Dynamic response of functionally graded graphene nanoplatelet reinforced shells with porosity distributions under transverse dynamic loads. *Materials Research Express*, 2019, vol. 6, no 7, p. 075045.

[48] Karami, Behrouz, Shahsavari, Davood, Janghorban, Maziar, *et al.* Resonance behavior of functionally graded polymer composite nanoplates reinforced with graphene nanoplatelets. *International Journal of Mechanical Sciences*, 2019, vol. 156, p. 94-105.

[49] Ma, Lianghua, Liu, Xiaoliang, et Shavalipour, Aghil. Active vibration control responses of a smart microshell reinforced with graphene nanoplatelets and subjected to external force. *Mechanics Based Design of Structures and Machines*, 2022, vol. 50, no 11, p. 3701-3721.

[50] Dong, Youheng, Li, Yinghui, LI, Xiangyu, *et al.* Active control of dynamic behaviors of graded graphene reinforced cylindrical shells with piezoelectric actuator/sensor layers. *Applied Mathematical Modelling*, 2020, vol. 82, p. 252-270.

[51] Fadaee, Mohammad et Talebitooti, Mostafa. Active vibration control of carbon nanotube-reinforced composite beam submerged in fluid using magnetostrictive layers. *Mechanics Based Design of Structures and Machines*, 2022, vol. 50, no 3, p. 799-816.

[52] She, Gui-Lin, Liu, Hai-Bo, et Karami, Behrouz. Resonance analysis of composite curved microbeams reinforced with graphene nanoplatelets. *Thin-Walled Structures*, 2021, vol. 160, p. 107407.

[53] Yu, X. L., Zhang, X. H., et Wang, J. F. Active vibration control of functionally graded carbon nanotube reinforced composite plate with coupled electromechanical actuation. *Frontiers in Materials*, 2022, vol. 9, p. 861388.

[54] Liu, Siyu, Wang, Aiwen, LI, Wei, *et al.* Nonlinear transient dynamics of graphene nanoplatelets reinforced pipes conveying fluid under blast loads and thermal environment. *Mathematics*, 2022, vol. 10, no 13, p. 2349.

[55] Ly, Duy-Khuong, Truong, Tam T., Nguyen, Sy-Ngoc, *et al.* A smoothed finite element formulation using zig-zag theory for hybrid damping vibration control of laminated functionally graded carbon nanotube reinforced composite plates. *Engineering Analysis with Boundary Elements*, 2022, vol. 144, p. 456-474.

[56] Alnujaie, Ali, Alshahrani, Mohammad Yahya, Ibrahim, Wessim Salahaddin, *et al.* Dynamic analysis of thick plates reinforced with agglomerated GNPs. *Heliyon*, 2023, vol. 9, no 9.

[57] Ezzraimi, Madjid, Lazar, Mohammed Essedik, Tiberkak, Rachid, *et al.* Piezoelectric patches for deflection control of functionally graded carbon nanotube-reinforced composite plates. *Applied Mechanics and Materials*, 2023, vol. 913, p. 3-14.

[58] Chiker, Yasser, Bachene, Mourad, Guemana, Mouloud, *et al.* Free vibration analysis of multilayer functionally graded polymer nanocomposite plates reinforced with nonlinearly distributed carbon-based nanofillers using a layer-wise formulation model. *Aerospace Science and Technology*, 2020, vol. 104, p. 105913.

[59] Chiker, Yasser, Bachene, Mourad, Bouaziz, Slim, *et al.* Free vibration analysis of hybrid laminated plates containing multilayer functionally graded carbon nanotube-reinforced composite plies using a layer-wise formulation. *Archive of Applied Mechanics*, 2021, vol. 91, p. 463-485.

[60] Lazar, Mohamed Essedik, Ezzraimi, Madjid, Tiberkak, Rachid, *et al.* Vibration analysis of composite plates reinforced CNTs using an exponential function approach. *Materials Science and Technology*, 2023, vol. 39, no 17, p. 2680-2689.

[61] R. V. P. Mehrdad R. Kermani, Mehrdad Moallem, *Optimal Real-time Control of Sewer Networks Process Modelling for Control Benoît Codrons Computational*

*Intelligence in Time Series Forecasting Ajoy K. Palit and Dobrivoje Popovic Modelling and Control of mini-Flying Machines*. 2006.

[62] R. V. P. Mehrdad R. Kermani, Mehrdad Moallem, "Applied Vibration Suppression Using Piezoelectric Materials," 2008, [Online].

[63] Washing machine vibration Isolators, "https://www.daraz.com.np/products/anti-vibration-pads-for-washing-machine4pc-stackable-shock-noise-cancelling-washer-dryer-isolation-pad-anti-walk-washer-support-feet-stabilizer-mat-i124606795.html", [Online].

[64] Damping acoustic in car Doors, "https://www.theautomotiveindia.com/forums/threads/detailed-guide-door-damping-and-diy.17519/ ", [Online].

[65] Building vibration Dampers, "https://www.researchgate.net/publication/281893247_A_critical_review_on_enhancing_the_seismic_response_of_buildings_with_energy_dissipation_methods", [Online].

[66] Jim Moore, "REAL-TIME WING FLUTTER ANALYSIS A FIRST," 2012. https://www.aopa.org/news-and-media/all-news/2018/october/17/flutter-analysis-a-first#

[67] Crack in a pillar of a Bridge, "https://www.alamy.com/stock-photo-a-crack-in-a-support-column-of-the-west-seattle-freeway-bridge-seattle-24009903.html?imageid=1D104974-575B-47BB-B704-301F1FE383F7&p=53807&pn=1&searchId=dfd0783241e8cc2ec24e027d66b4191b&searchtype=0", [Online].

[68] Crack in a Pillarof a bridge. Ail, "https://www.reddit.com/r/aviation/comments/v5l4ct/is_this_normal_for_a_flap_on_a_737ng/?rdt=63193", [Online].

[69] Crack in House Wall, "https://dedant.com.au/2020/09/03/when-do-you-need-to-worry-about-cracking-in-houses/", [Online].

[70] Y. Chiker, "Comportement mecanique des plaques composites hybrides renforcées avec des plis en nanotubes de carbon mono- feillées," thèse de doctorat 2021.

[71] Rodreges, Peter (ed.). *Nanoscience and technology: a collection of reviews from nature journals*. World Scientific, 2009.

[72] Monthioux, Marc. *Carbon meta-nanotubes: Synthesis, properties and applications*. John Wiley & Sons, 2011.

[73] Chi, Shyang-Ho et Chung, Yen-Ling. Mechanical behavior of functionally graded material plates under transverse load—Part I: Analysis. *International Journal of Solids and Structures*, 2006, vol. 43, no 13, p. 3657-3674.

[74] Elishakoff, Isaac E., Pentaras, Demetris, et Gentilini, Cristina. *Mechanics of functionally graded material structures*. World scientific, 2015.

[75] Chakraverty, S. et Pradhan, K. K. Free vibration of exponential functionally graded rectangular plates in thermal environment with general boundary conditions. *Aerospace Science and Technology*, 2014, vol. 36, p. 132-156.

[76] Ebrahimi, Farzad et Dabbagh, Ali. *Mechanics of nanocomposites: homogenization and analysis*. CRC Press, 2020.

[77] O. O. Ochoa and J. N. Reddy, "Finite-Element Analysis of Composites Laminates.," *Advanced Materials and Processes,* vol. 132, no. 5. pp. 36–43, 1987.

[78] M. Ezzraimi, "Contrôle actif des vibrations de plaque composites multicouches," *theses,* 2019.

[79] Carrera, Erasmo, Brischetto, Salvatore, et Nali, Pietro. *Plates and shells for smart structures: classical and advanced theories for modeling and analysis*. John Wiley & Sons, 2011.

[80] Berthelot, Jean-Marie. Fracture Mechanisms and Damage of Composite Materials. In : *Composite Materials*. Springer, New York, NY, 1999. p. 228-264.

[81] Reddy, Junuthula Narasimha. *Mechanics of laminated composite plates and shells: theory and analysis*. CRC press, 2003.

[82] Hwu, Chyanbin. *Anisotropic elastic plates*. Springer Science & Business Media, 2010.

[83] Altenbach, Holm, Altenbach, Johannes, Kissing, Wolfgang, *et al. Mechanics of composite structural elements*. Berlin : Springer-Verlag, 2004.

[84] Birman, Victor. Introduction and Basic Concepts. In : *Plate Structures*. Dordrecht : Springer Netherlands, 2011. p. 1-51.

[85] Whitney. J. M, "Structural Analysis Of Laminated Anisotropic Plates.," pp. 7823–7830. Book.

[86] Kollar, Laszlo P. et Springer, George S. *Mechanics of composite structures*. Cambridge university press, 2003.

[87] Qatu, Mohamad Subhi. *Vibration of laminated shells and plates*. Elsevier, 2004.

[88] Vasques, C. M. A. et Rodregues, J. Dias (ed.). Vibration and structural acoustics analysis: Current research and related technologies. 2011.

[89] Varadan, Vijay K., Vinoy, Kalarickaparambil Joseph, et Gopalakrishnan, Srinivasan. *Smart material systems and MEMS: design and development methodologies*. John Wiley & Sons, 2006.

[90] Morris. A. J, *Introduction to finite element vibration analysis*, vol. 153, no. 3. 1992.

[91] Lakshmininarayana. H, "Finite Elements Analysis: Procedures in Engineering," Book, 2004.

[92] Tzou, Hornsen HS. *Piezoelectric Shells: Sensing, Energy Harvesting, and Distributed Control—Second Edition*. Springer, 2018.

[93] Yang, Jiashi. *Analysis of piezoelectric devices*. World Scientific, 2006.

[94] Fang, Daining, Wang, Ji, Chen, Weiqiu, *et al.* (ed.). *Analysis of piezoelectric structures and devices*. de Gruyter, 2013.

[95] Chen. S. E *et al.*, *Nonlinear Analysis of Thin-Walled Smart Structures*, vol. 21, no. 1. 2021.

[96] Zorbit. G. w, "intelligent systems and robotics," 2000.

[97] Allard, Jean et Atalla, Noureddine. *Propagation of sound in porous media: modelling sound absorbing materials*. John Wiley & Sons, 2009.

[98] Vepa, Ranjan. *Dynamics of smart structures*. John Wiley & Sons, 2010.

[99] Liu, Gui-Rong et Quek, Siu Sin. *The finite element method: a practical course*. Butterworth-Heinemann, 2013.

[100] Kenneth. T. G. B, H. Huebner, Donald L. Dewhirst, Douglas E. Smith, "The finite element method for enginee,rs," *Choice Reviews Online*, vol. 32, no. 10. pp. 32-5680-32–5680, 1995.

[101] Heinrich. J. C. , 7. The Finite Element Method. Book, 2006.

[102] Dhatt. G, Touzot. G, and Lefrançois. E, "Numerical Methods Series - Finite Element Method," *Statewide Agricultural Land Use Baseline 2015*, vol. 1, no. 5. pp. 561–563, 2015.

[103] Abbaspour, Fatemeh, Arvin, Hadi, et Shahriarri-Kahkeshi, Maryam. Active control of vibrations of piezoelectric rectangular nanocomposite micro plates reinforced with graphene platelet in thermal ambient considering the structural damping. *International Journal for Computational Methods in Engineering Science and Mechanics*, 2022, vol. 23, no 3, p. 243-262.

[104] Hughes, Thomas JR. *The finite element method: linear static and dynamic finite element analysis*. Courier Corporation, 2003.

[105] Zhu, Ping, Lei, Z. X., et Liew, Kim Meow. Static and free vibration analyses of carbon nanotube-reinforced composite plates using finite element method with first order shear deformation plate theory. *Composite Structures*, 2012, vol. 94, no 4, p. 1450-1460.

[106] Song, Mitao, Kitiporenshai, Sritawat, et Yang, Jie. Free and forced vibrations of functionally graded polymer composite plates reinforced with graphene nanoplatelets. *Composite Structures*, 2017, vol. 159, p. 579-588.

[107] Reddy, R. Muni Rami, Karunasena, W., et Lokuge, W. Free vibration of functionally graded-GPL reinforced composite plates with different boundary conditions. *Aerospace Science and Technology*, 2018, vol. 78, p. 147-156.

[108] Kiani, Yaser. Free vibration of functionally graded carbon nanotube reinforced composite plates integrated with piezoelectric layers. *Computers & Mathematics with Applications*, 2016, vol. 72, no 9, p. 2433-2449.